APPENDIX H7.3

Spencer Gulf modelling assessments (200 ML/day desalination plant)

BMT WBM

Spencer Gulf Modelling Assessments (200 ML/Day Desalination Plant) Final Report

R.B17748.002.03.Assessments.doc
October 2010

Spencer Gulf Modelling Assessments (200 ML/Day Desalination Plant) Final Report

Prepared For:	BHP Billiton
Prepared By:	BMT WBM Pty Ltd (Member of the BMT group of companies)

Offices

Brisbane
Denver
Mackay
Melbourne
Newcastle
Perth
Sydney
Vancouver

CONTENTS

1 INTRODUCTION

BHP Billiton is proposing to expand its mining operations at Olympic Dam, South Australia. Part of this proposal includes construction and operation of a desalination plant at Point Lowly on the coastline of Northern Spencer Gulf (Figure 1-1 and Figure 1-2). This plant would provide water to the proposed mine if approved.

BHP Billiton (2009) released the Olympic Dam Expansion Draft Environmental Impact Statement (hereafter DEIS) document with respect to the proposed expansion and desalination plant in May 2009. Part of this Draft EIS described numerical modelling undertaken to better understand the behaviour of return water discharged from the proposed desalination plant. BMT WBM and The Centre for Water Research (CWR) of The University of Western Australia undertook this numerical modelling on behalf of BHP Billiton, and details have been provided in a series of peer reviewed reports contained in the DEIS (see Appendices O11.2, O11.3, O11.4). Similar studies have been undertaken in the Australian context, and the reader is referred to these contextually relevant studies for further information (Okely et al. 2007a, 2007b; SA Water 2008, 2009; DSE 2008)

Since the release of the DEIS, BHP Billiton has commissioned BMT BWM to upgrade all modelling tools used in that study so that the quality of assessments is able to keep pace with industry best practise and to ensure the ongoing delivery of robust and rigorous modelling outcomes. This has included execution of a targeted and comprehensive supporting field data collection program in 2009. The upgraded modelling tools and field data are described in Appendix 17.5.2 of the Supplementary Environmental Impact Statement (hereafter SEIS).

This report presents the methodology and outcomes of a series of analyses that have used these upgraded modelling tools to support preparation of the SEIS. Each analysis is presented in a separate chapter, with linkages between assessments and techniques noted as required.

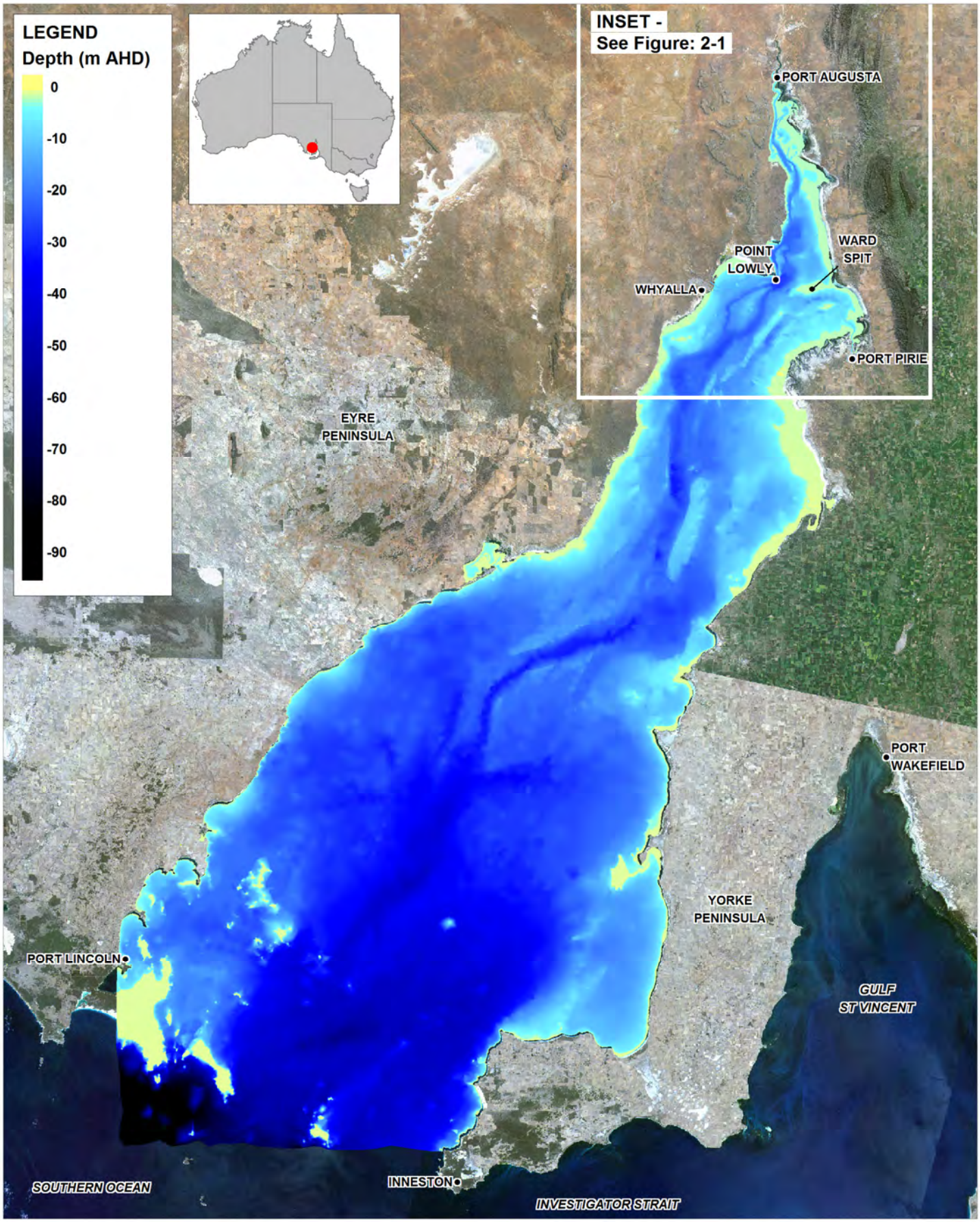

Title:

Spencer Gulf
Location and Bathymetry

Figure: 1-1

Rev: A

N

0 30 60km

Approx. Scale

BMT WBM

www.bmtwbm.com.au

Filepath :

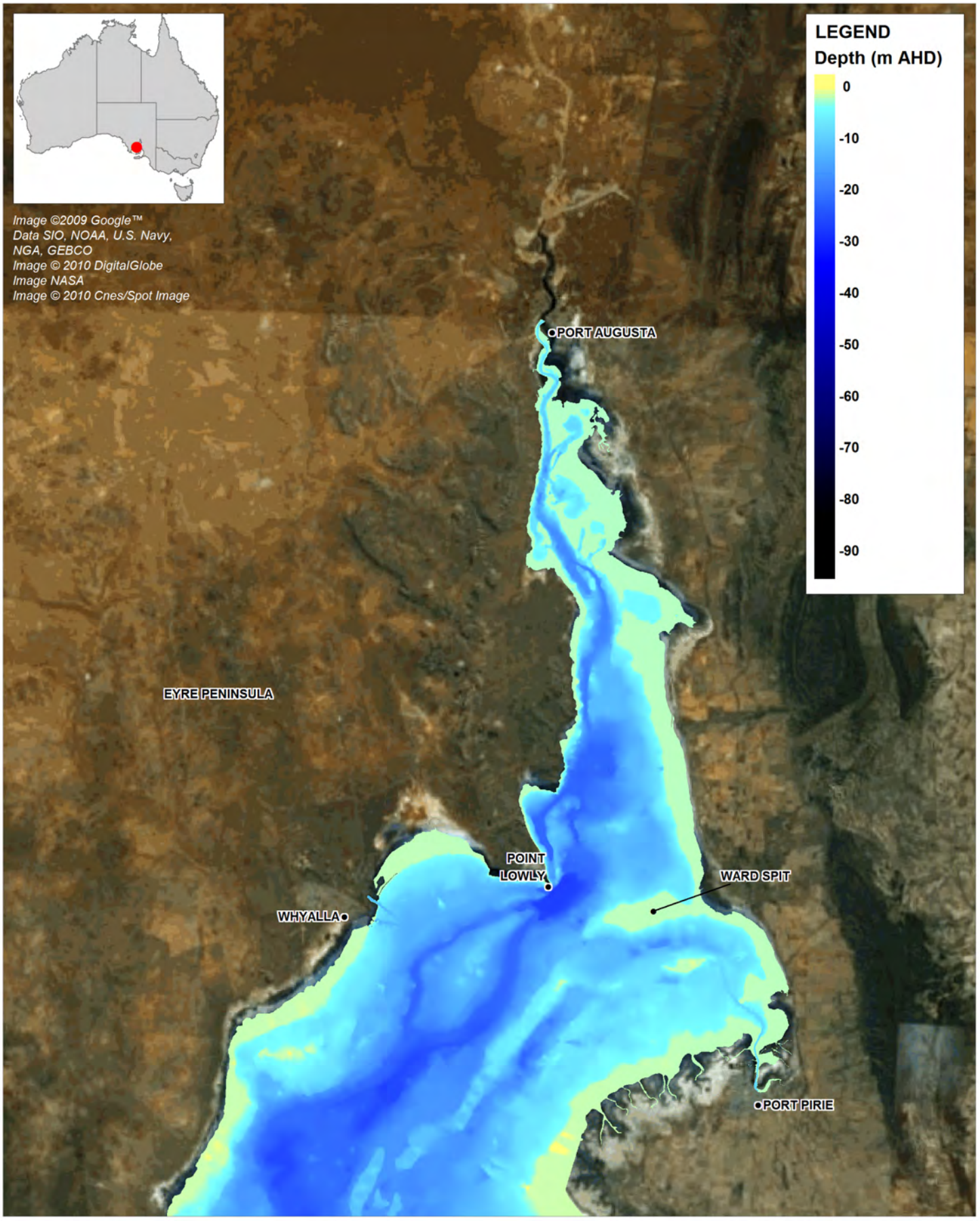

Title:

Northern Spencer Gulf
Location and Bathymetry

Figure: 1-2

Rev: A

N

0 10 20km

Approx. Scale

BMT WBM

www.bmtwbm.com.au

Filepath :

2 COMPUTATIONAL FLUID DYNAMICS: DETAILED DIFFUSER SIMULATION

Following completion of the diffuser optimisation study (see Appendix 17.6.1), it was determined that more advanced tools were required to adequately support design of the proposed return water diffuser arrangement. This section describes such a Computational Fluid Dynamics (CFD) tool and its application to the current study.

2.1 Computational Fluid Dynamics

CFD has evolved over the last three decades to become a highly advanced, and relied upon, tool for studying fluid flows. Most available CFD packages offer the ability to:

- Solve on an arbitrary mesh constructed around specified geometry;
- Solve for compressible and incompressible fluid flows;
- Solve for steady state and transient problems; and
- Choose from a wide selection of turbulence models.

The equations solved are typically a reduced set of the Navier-Stokes Equations, depending on assumptions made regarding the flow.

2.2 OpenFOAM

There are a number of commercially available CFD packages, however there is an open source alternative which offers many advantages. OpenFOAM is developed by Open CFD Ltd (based in the UK) and is used by Shell, Audi, and motor racing teams. Three significant advantages of using OpenFOAM are:

- Transparency of code. The user is able interrogate any aspect of the source code to determine exactly which equations are being used.
- Extension of code. The user is able to write tailored conditions, modify equations, and even create new solvers for specific problems.
- Parallel computation. As the software is licensed under a GNU license, a multi-CPU computer cluster may be used to solve large problems without incurring license fees.

BMT WBM has been using OpenFOAM for a significant portion of its CFD work for many years. Projects include reacting chemistry in smelting furnaces, coal dust combustion and explosion modelling, RAAF engine test bunker airflow modelling, tidal turbine hydrodynamics, and other diffuser outfall models.

2.3 CFD Model Setup

2.3.1 Domain and Mesh

The model domain for this study was a Cartesian box aligned with the diffuser, spanning 160m either side of the centre of the diffuser in both directions. The top surface of the model was the z = 0 mAHD plane and the bottom surface was fitted to DEM data from the ELCOM model. For the majority of the domain this was approximately z = -26.5 m AHD, save for the most western corner which rose a little in elevation.

Approximately cubic cells were required within the immediate vicinity of the diffuser for the automatic mesh generation to refine the mesh around the stand pipes. These were set at 0.5 m edge length before refinement. However, to use 0.5 m cells in the remainder of the domain would produce a 5 million cell mesh even before refinement around the diffuser, so a grading system was adopted such that horizontal spacing of the cells was increased in steps to 4 m in outer regions of the domain, which is acceptable since the vertical component of the flow at those locations is not significant. Figure 2-1 provides an illustration of this.

The mesh was then refined around the diffuser stand pipes as shown in Figure 2-2. This process refined the mesh down to 15 mm cells immediately adjacent to the pipe exits.

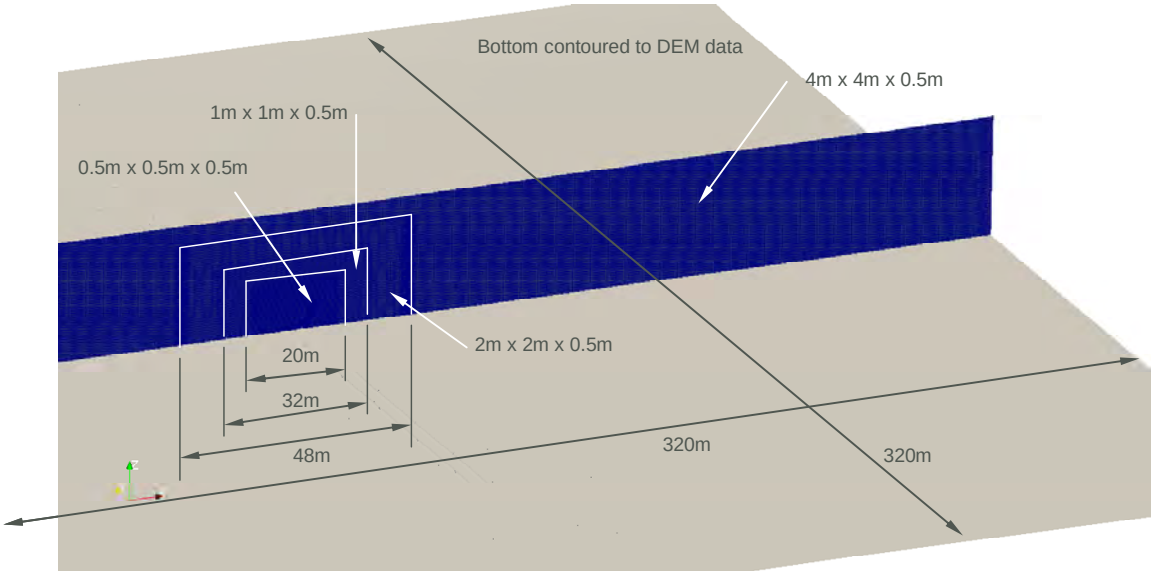

Figure 2-1 Domain and initial mesh

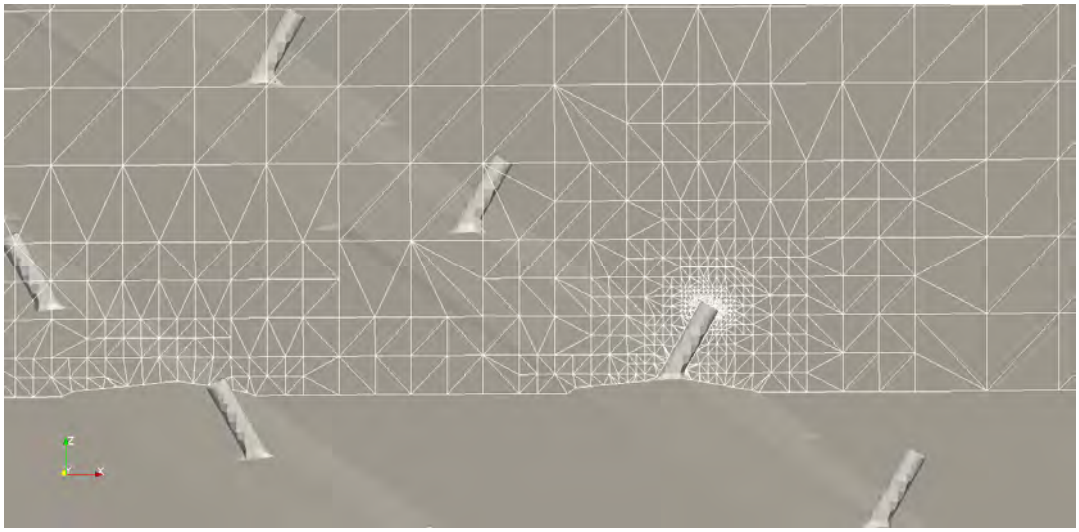

Figure 2-2 Standpipe mesh

2.3.2 Equations

The equations solved are listed below, where α is the mixing fraction of outfall fluid to background fluid (it is the reciprocal of dilution), ϕ is the mass flux vector, U the mean velocity vector, υ_t the turbulent contribution to kinematic viscosity, ρ the fluid density and p_d a modified pressure field.

$$\nabla \bullet [\phi\alpha] - \nabla^2\left[\left(D + \tfrac{\upsilon_t}{Sc_t}\right)\alpha\right] = 0$$

$$\rho = \alpha\rho_1 + (1-\alpha)\rho_2$$

$$\phi = \rho U$$

$$\nabla \bullet [\phi U] - \nabla^2[\mu_{eff} U] - \nabla U \bullet \nabla \mu_{eff} = -(gh\nabla\rho + p_d)$$

$$p_d = p - \rho g h$$

$$\mu_{eff} = \rho\upsilon_{eff} = \rho(\upsilon + \upsilon_t)$$

The model constants are listed in Table 2-1.

Table 2-1 Model constants

Parameter	Description	Value
D	Molecular diffusion constant for salt in water	2e-9 m^2/s
Sc_t	Turbulent Schmidt number	0.71
υ	Laminar kinematic viscosity	1e-6 m^2/s
g	Gravity vector	(0 0 -9.81) m/s2

2.3.3 Turbulence Model

The turbulent contribution to the viscosity υ_t is calculated by a turbulence model which estimates the energy and length scales of the random fluctuations in the flow field. This variable influences the rate

of dispersion/diffusion of the plume, in terms of both momentum and brine concentration. As the Reynolds numbers of the plumes are of the order of 1,000,000 both of the k-Epsilon or k-Omega turbulence models are appropriate choices. The k-Omega model was selected due to its greater stability and reduced sensitivity to initial conditions. Standard model constants were used.

2.3.4 Boundary Conditions

The bottom surface of the model (including stand pipes) was defined as a wall (velocity = 0 vector), against which standard wall functions were used in the turbulence model. The top surface of the model was defined as a 'slip wall' which has no friction but constrains the flow to be parallel to the surface. The remaining field variables were defined as zero-gradient against the top and bottom boundaries. The change in model depth with tide cycle is not taken into account in the CFD model.

For the steady state studies involving zero background velocity, the four vertical boundaries of the model were defined to be 'zero gradient' in all variables except for alpha, and thus they allowed inflow and outflow such that total volume flux in and out of the domain was conserved. As the brine outfall is negatively buoyant, the resulting velocity fields flow radially (in an oval sense) away from the diffuser in the bottom layers, and toward the diffuser in the top layers, with a meta-stable convergence zone formed above the diffuser. The boundary condition for alpha was such that any inflows on the model boundaries were defined as being zero in alpha, and outflows were defined as zero-gradient.

For the studies involving background velocities, the two vertical boundaries with influx were constrained to have the specified velocity profile (magnitude and direction) as a function of depth that had been extracted from the recorded ADCP data. The other two vertical boundaries were unconstrained in velocity except that total volume flux in and out of the domain was conserved. Again the boundary condition for alpha was such that any inflows on the model boundaries were defined as zero in alpha, and outflows were defined as zero-gradient. The remaining variables were defined as zero gradient.

The background velocity profiles for all steady state and transient simulations were obtained by calculating a depth averaged velocity from the ADCP data and ranking these from maximum flood through to maximum ebb flow. Velocity profiles were then selected to represent 10%, 30%, 50%, 70%, and 90% flood flow based on time, and similar for ebb flow. Figure 2-3 below illustrates the 50% ebb and flood profiles chosen as an example.

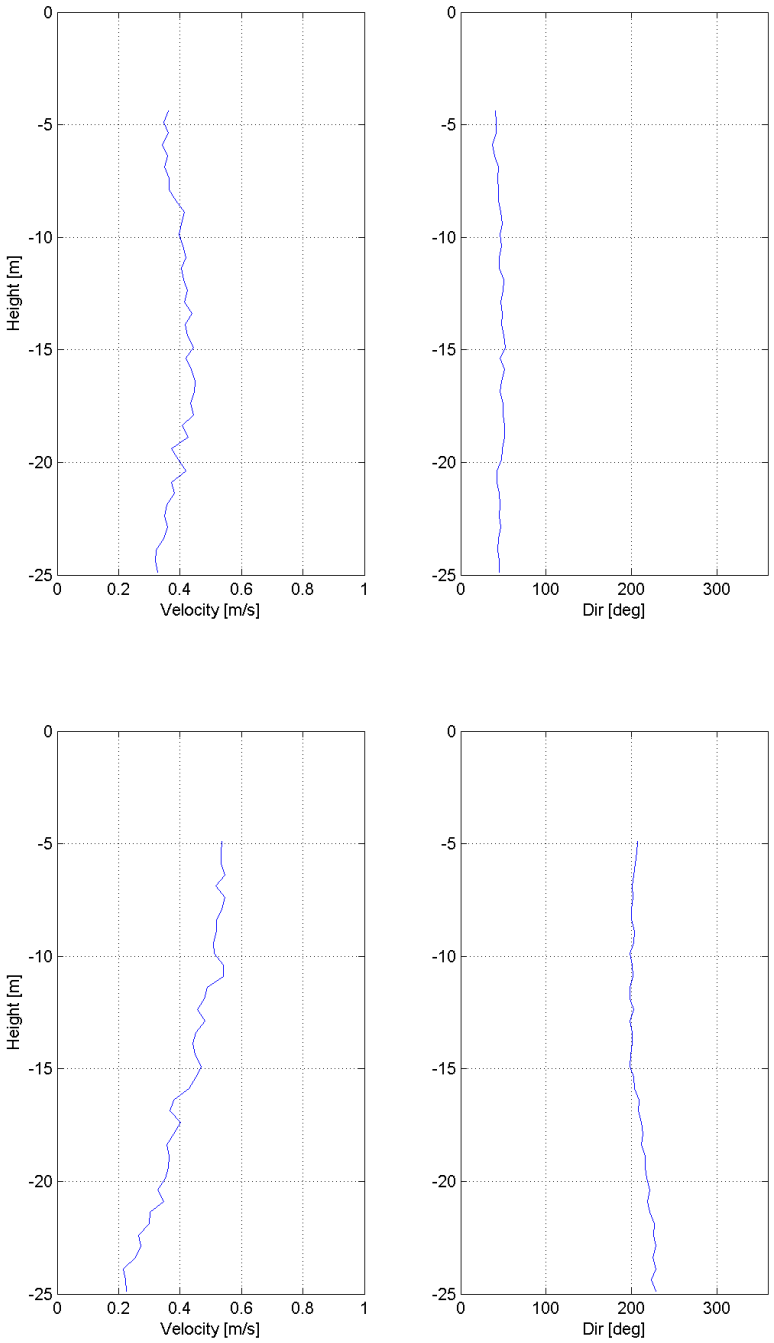

Figure 2-3 Representative 50% ebb flow profile (top) and 50% flood flow profile (bottom)

2.3.5 Initial Conditions

For steady state runs initial conditions are not relevant. Transient simulation initialisation is described in subsequent sections.

2.3.6 Adaptive Mesh Refinement

Accurately calculating the evolution of the plumes is the most essential aspect of the CFD work. This requires a fine mesh around the boundaries of the plumes (where spatial gradients in velocity and

concentration are high). However utilising such a fine mesh through the entire model domain is not tractable. The mesh needs to be refined around the plume boundaries, but the exact location of these are not known a-priori as the plumes depend on the configuration being modelled and the background velocity.

The remedy to this problem is to calculate a first pass solution, refine the mesh in the regions where spatial gradients exceed a pre-defined threshold, and repeat this process until the results converge. Figure 2-4 shows a cross section of the mesh (coloured by velocity) through the stand pipe at each stage of mesh refinement.

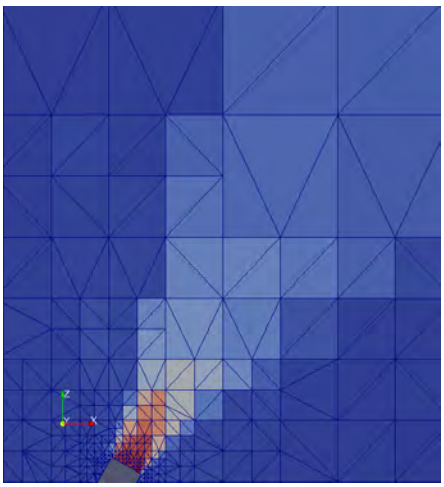

(a) Solution step 1, 1346124 cells

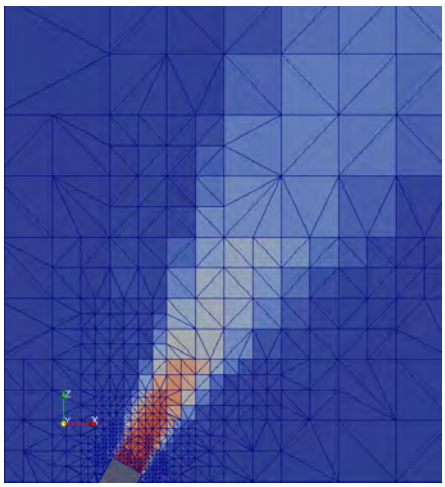

(b) Solution step 2, 1425091 cells

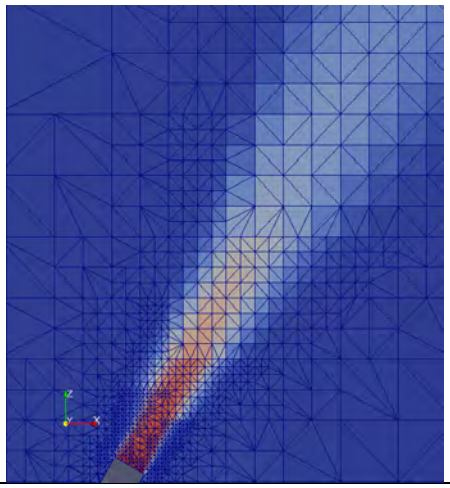

(c) Solution step 3, 1594169 cells

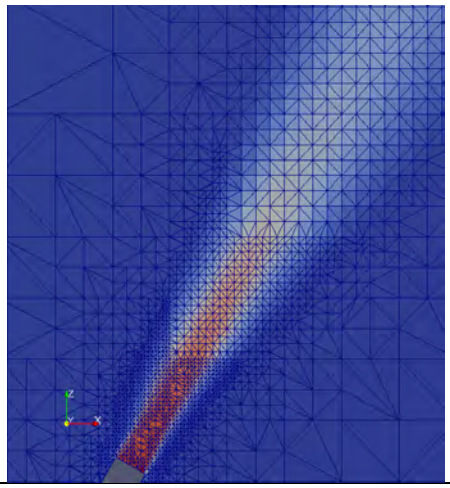

(d) Solution step 4, 1942531 cells

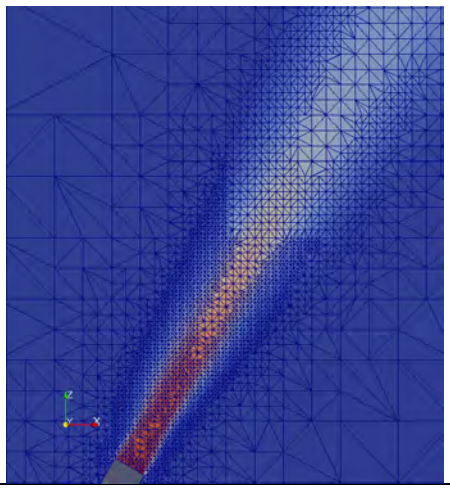

(e) Solution step 5, 2553071 cells

Figure 2-4 Adaptive mesh refinement

2.4 Validation

The primary goal for the CFD modelling was to provide best estimates for outfall dilutions in the near vicinity of the diffuser for subsequent seeding of the ELCOM models (see discussion in Section 3 of this Appendix report). As such, the CFD predictions were benchmarked to previous studies where possible to ensure robustness of predictions.

Whilst acknowledging the work of Petersen and Larsen (1997) and Cipollina *et al.* (2004), currently the three most commonly used tools for estimating the behaviour of *single* negatively buoyant outfall plumes are those developed by Roberts *et al.* (1997), Roberts and Toms (1987) (which were both experimental studies) and the CORMIX model. For simplicity, the former two studies are referred to herein as Roberts 97 and Roberts 87, respectively. It has been documented in the literature that Roberts 97 predicts greater dilution ratios than Roberts 87 for the same jet-densimetric Froude number by some margin, with some supporting explanation for same. In contrast to these Roberts studies, however, it is noted that extensive experimental data that accounts for *multiport* dense plume overlap and outfall re-entrainment is not known at this point, hence the motivation to use computational fluid dynamics as applied to the proposed multiport diffuser, and to validate the CFD predictions against historical studies.

To do so, the CFD predictions were sequentially compared with Roberts experiments, CORMIX predictions and field measurements. These comparisons are presented below.

2.4.1 Comparison with Roberts Predictions

Given the above, it was deemed appropriate to compare CFD predictions with Roberts 97 and Roberts 87 for one of the test cases published in Roberts 97 where the densimetric Froude number was 27.6 (although it is noted that not all the information required to exactly replicate the Roberts 97 setup was published, so some assumptions have been made regarding tank configuration in the CFD modelling). Table 2-2 below summarises the parameters used for the steady state comparison.

Table 2-2 CFD Validation case parameters

Parameter	Description	Value
ρ_1	Outfall density	1015.7 kg/m^3
ρ_2	Background density	998.2 kg/m^3
d	Port diameter	4.29 mm
Q	Flow rate	0.0095 L/s

The resulting plume, after adaptive mesh refinement, is shown in Figure 2-5. The figure has been annotated to illustrate the relevant results that were extracted for comparison with Roberts 97.

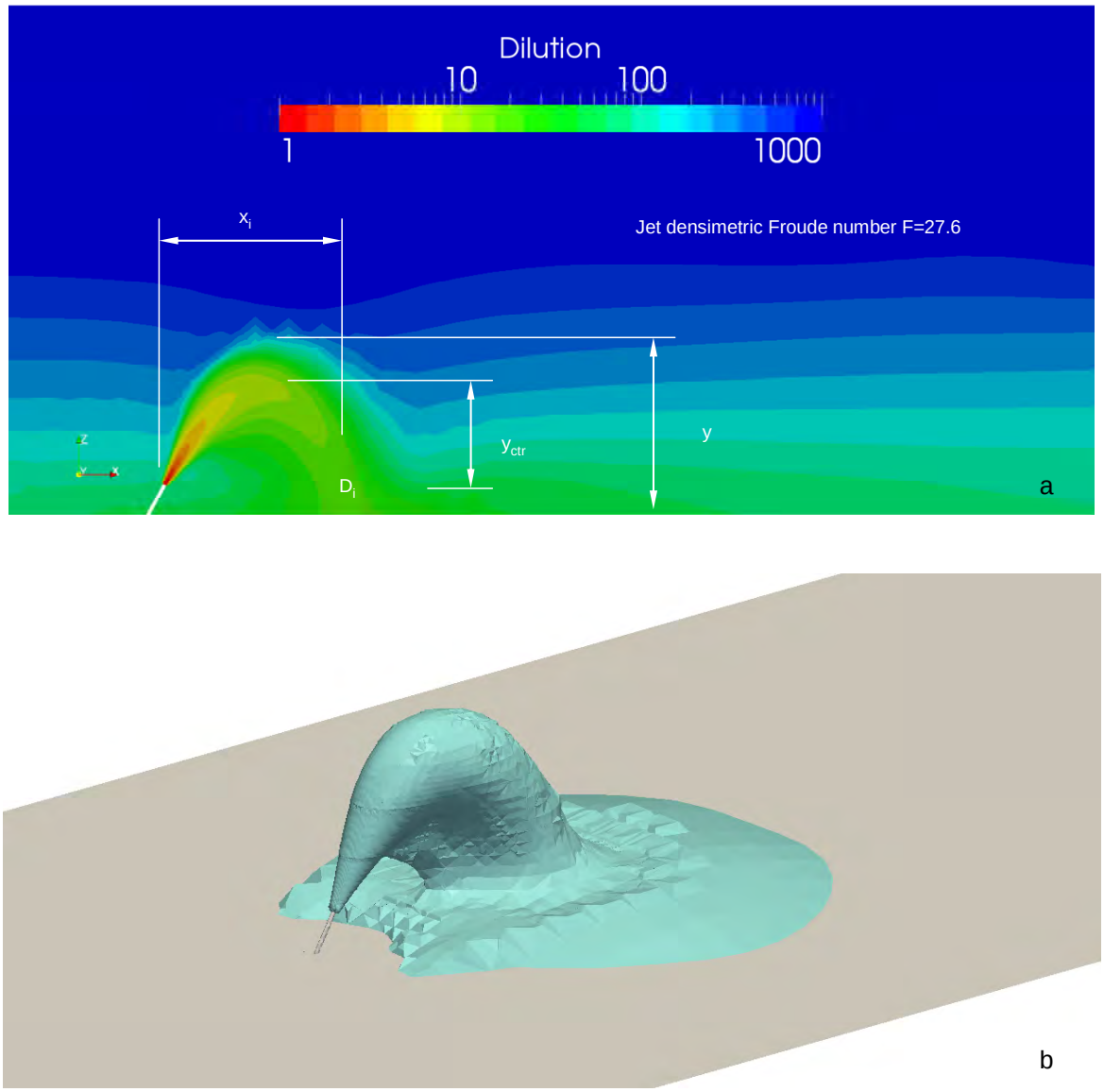

Figure 2-5 CFD Validation case (a) plume cross-section and (b) 50:1 dilution iso-surface

The CFD results (with Roberts 87 and Roberts 97 predictions) are presented in Table 2-3. Impact point dilution D_i is normalised with respect to jet densimetric Froude number F, and plume throw to impact point x_i and height y are normalised with respect to the product of port diameter d with jet densimetric Froude number.

Table 2-3 CFD Validation case results

Parameter	Roberts 97	Roberts 87	CFD
D_i/F	1.6	1.03	0.98
x_i/dF	2.4	-	2.05
y/dF	2.2	2.08	1.85

It is apparent in Table 2-3 that the CFD results match well with those of Roberts 87. Importantly, Roberts 97 predicts both plume heights and throws *greater* than the CFD (and Roberts 87), and this results (non-linearly) in a *greater* dilution prediction by Roberts 97 compared to CFD.

2.4.2 Comparison with CORMIX

Further insight into the above was obtained by introducing a range of small background velocities, U_x, to the CFD simulations and comparing the predictions with those of CORMIX for the same configuration and range of ambient currents. A representative cross-section of the CFD prediction is provided in Figure 2-6, with U_x = 0.02 m/s.

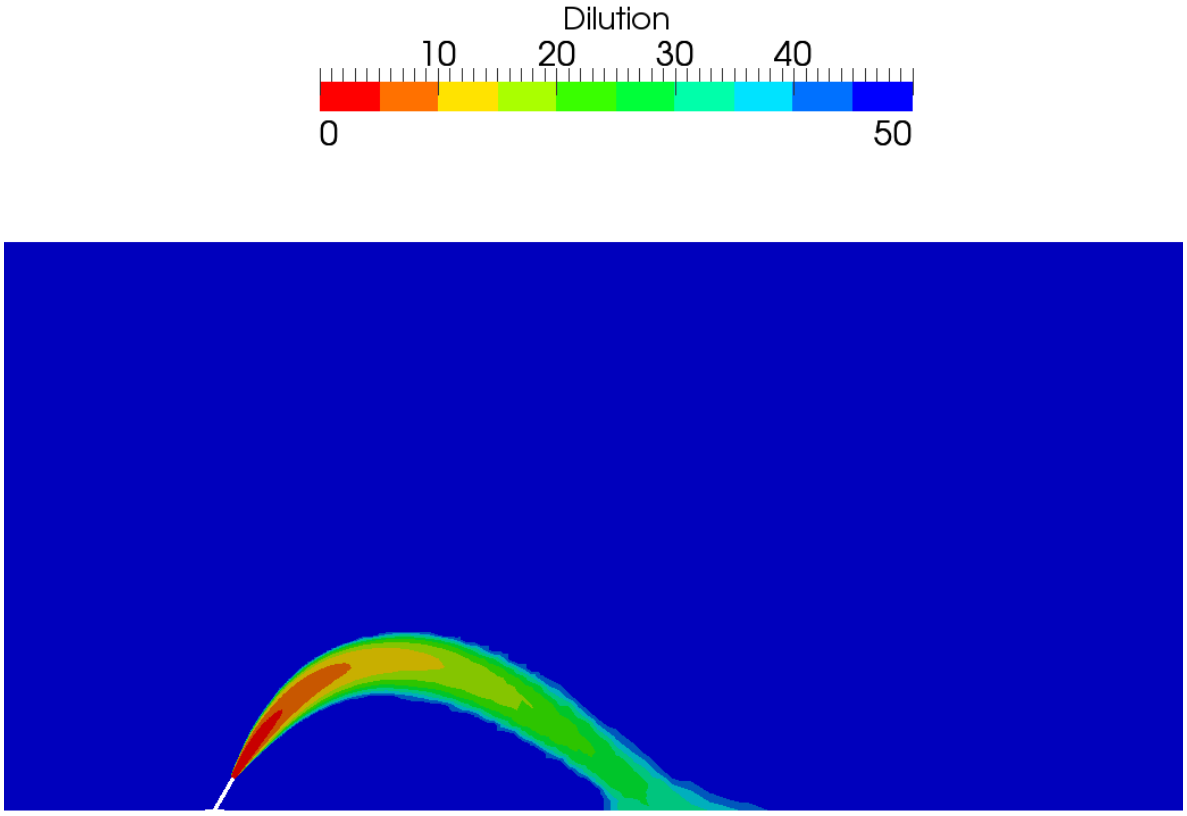

Figure 2-6 CFD simulation of CORMIX configuration. Note the different colour scale to Figure 2-5, with re-entrainment being less obvious in this figure as a result.

Comparative CFD and CORMIX results are provided in Table 2-4 (only U_x = 0.02 m/s) and Figure 2-6 (all background velocities considered). Note that here the height of the plume centreline, y_{ctr} is used instead of it uppermost reach.

Table 2-4 CFD Validation to CORMIX results, U_x = 0.02 m/s

Parameter	CORMIX	CFD
Y_centre (m)	0.12	0.12
D_i[-]	33.4	32
x_i (m)	0.35	0.38

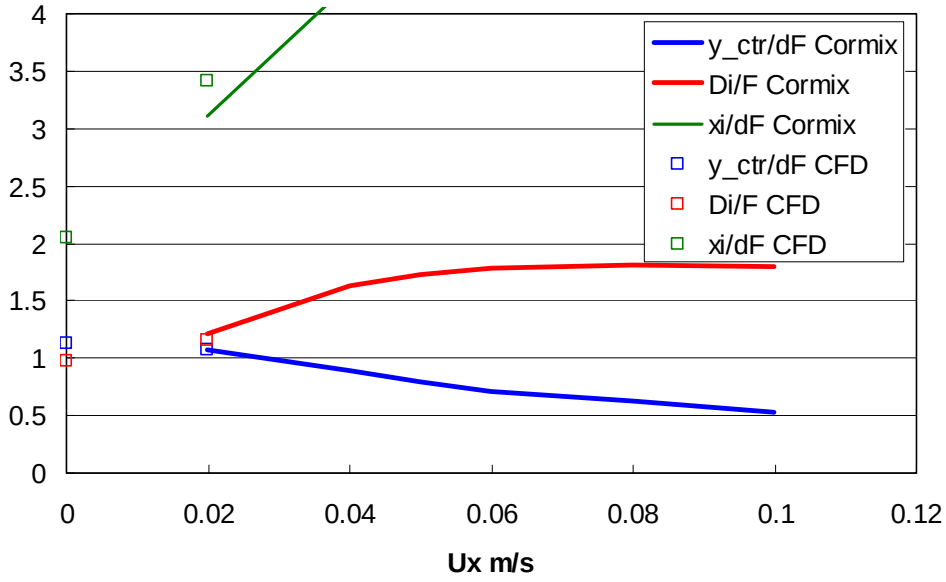

Figure 2-7 CFD Validation against CORMIX

The CFD results for U_x =0.02 m/s agree very well with those of CORMIX, and even though CORMIX cannot easily be used at zero background velocity, the CFD results for U_x =0.0 m/s appear sensibly projected with respect to the non-zero current conditions CORMIX results. It is noted however that CORMIX does warn that for velocities of 0.04 m/s and less that 'upstream spreading' is possible, and this is consistent with the CFD in concept – the plume does not entirely migrate away from the diffuser, but underflows can travel back towards the diffuser port.

2.4.3 Comparison with Field Measurements

A key outcome of the CFD validation study has been the prevalence of re-entrainment of discharged brine for some configurations, especially those associated with diffusers that provide lower plume throws and heights. An example of such is shown in Figure 2-8. Re-entrainment is clearly evident through the stagnant bottom layer of mixed brine that is several metres thick and smothers the diffuser. Commensurate reductions in impact dilution are thus expected, and the extent to which this process has been accounted for in laboratory experiments is unclear.

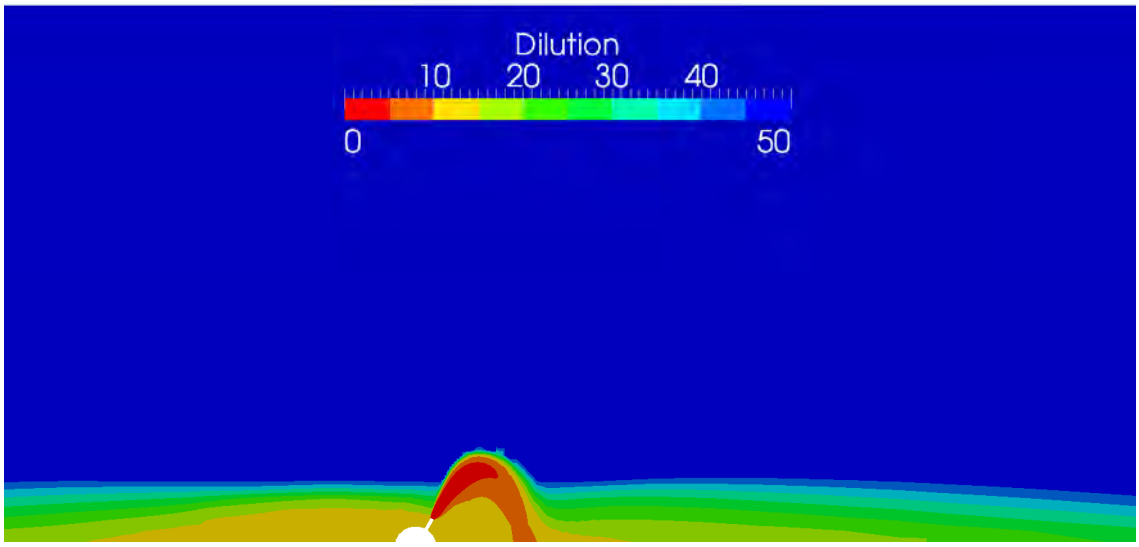

Figure 2-8 Example CFD simulation showing re-entrainment

To illustrate this effect in a 'real world' situation, below is presented field measurements (www.watercorporation.com.au/_files/CockburnSoundFieldStudy.pdf page 26) of the Cockburn Sound diffuser. The figure shows time (not space) evolution of rhodamine, salinity and temperature from vertical profiles taken near the diffuser line (i.e. where the plumes are actively mixing with ambient water and potentially exposed to re-entrainment). The original report caption has been maintained for clarity.

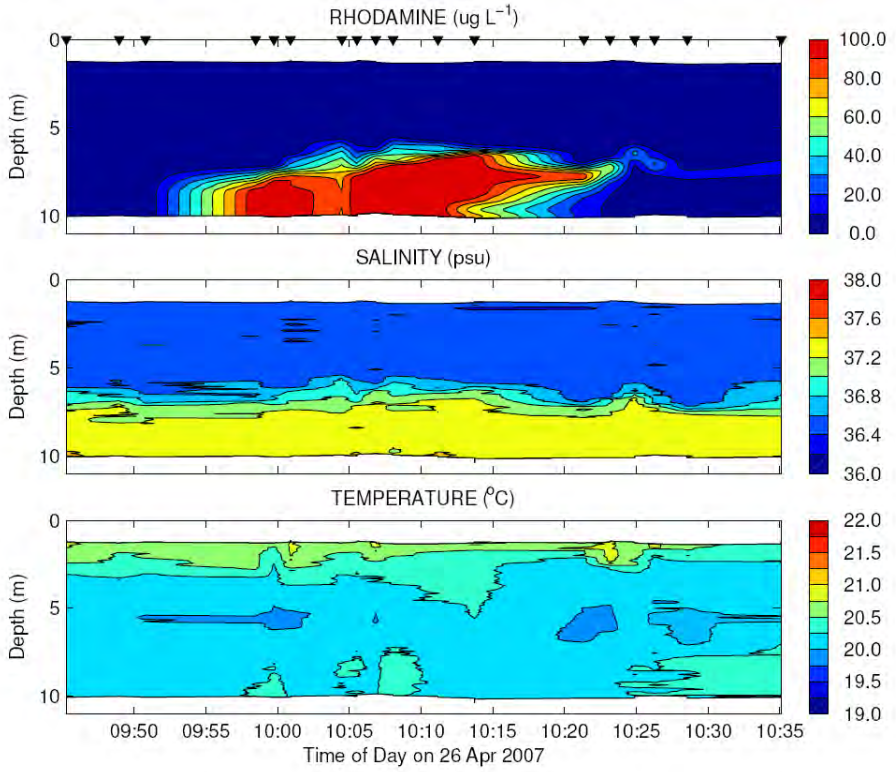

Figure 2-9 Time contour of profile data collected at diffuser during dye release on 26 Apr: rhodamine concentration (top panel), salinity (middle panel) and temperature (bottom panel). Source: www.watercorporation.com.au/_files/CockburnSoundFieldStudy.pdf page 26

The second panel in the figure is remarkably similar to the CFD cross section in Figure 2-8 (albeit on a time abscissa) and demonstrates that the salinity layer due to the accumulated brine is approximately 3 to 4 metres thick. Importantly, the diffuser ports are 1 metre from the sea bed. As a result, there is potential for re-entrainment of previously discharged brine in this situation, and it would be reasonable to expect that application of relationships that did not account for entrainment would overestimate impact dilutions due to this effect. Other sources of mixing would thus be required to increase impact dilutions up to those predicted by such methods.

In this regard, Marti *et al.* (2010) measured end of near field dilutions at the above Cockburn Sound site under three separate discharge regimes. The only regime that had a densimetric Froude number greater than 20 (i.e. where Roberts 97 is thought to be applicable) had an ambient current of approximately 5 cm/s. The predictions of Roberts 97 were compared to the CWR measurements and it was found that the observations matched Roberts 97 well.

This is an interesting result as Roberts 87 claims that under such conditions with non-zero background currents (with ambient Froude numbers of about 0.5) dilutions should be significantly influenced by the ambient current. This means that there is sufficient additional turbulence in the ambient field to increase plume mixing beyond the dilutions predicted by zero current experimental results. The fact that the Marti *et al.* (2010) measurements *match* the Roberts 97 predictions well (for end of near field dilutions), suggests that the plumes required this extra mixing source to do so, and without it, end of near field dilutions might reasonably be expected to fall below those predicted by experimental tools. Clearly, the extent of such a difference is difficult to estimate, however, this result is consistent the differences between the laboratory and modelling tools discussed above.

2.4.4 Summary

In summary, we have shown that Roberts 87, CORMIX (with small background velocities) and CFD predictions (importantly with using commonly accepted model parameters for turbulent mixing) are all very close for the zero current conditions, and that Roberts 97 predicts greater dilutions than this suite of approaches. BMT WBM has no opinion on which methods (if any) are ‘best’ or ‘most correct’, and this analysis has not intended to support or imply such an opinion. On the contrary, BMT WBM believes that the above analysis is sufficient to warrant and support use of advanced numerical tools to examine the steady state and transient nature of multiport diffuser brine discharges plume evolution for the current BHP Billiton application.

These simulations and results are described below.

2.5 Simulations

A total of 37 steady state solutions were computed for a variety of diffuser configurations and background velocities, as listed in Table 2-5 below. The following sub sections provide some insight into the evolution of the investigative path taken in this regard. More detailed tabulated results are listed in Section 3-6. Transient results are described at the end of this section.

Table 2-5 Steady state solutions computed

Name	d [mm]	N ports	Q m^3/s	Ebb 90%	Ebb 70%	Ebb 50%	Ebb 30%	Ebb 10%	Zero Vel	Flood 10%	Flood 30%	Flood 50%	Flood 70%	Flood 90%
DEIS	175	50	4.3	✓	✓	✓	✓	✓	✓	✓	✓	✓	✓	✓
SEIS	175	50	3.1						✓					
ALT1	150	30	3.1						✓					
ALT2/ SEIS	150	20	3.1	✓	✓	✓	✓	✓	✓	✓	✓	✓	✓	✓
ALT3	140	18	3.1						✓					
ALT4	150	14	3.1						✓					
ALT2/ SEIS	142	20	2.79	✓	✓	✓	✓	✓	✓	✓	✓	✓	✓	✓

2.5.1 Zero Background Current DEIS Configuration

Subsequent to the validation process, the first results obtained were those for the Draft EIS (DEIS) configuration at 4.3 m^3/s and zero background velocity, as shown in Figure 2-10 and Figure 2-11. In this configuration the exit velocity from the ports throws the plume less than 6 m into the water column, and this combined with the presence of the other ports produced a 'puddle' around the diffuser. This clearly demonstrates the need to account for plume overlap and interaction in the current study.

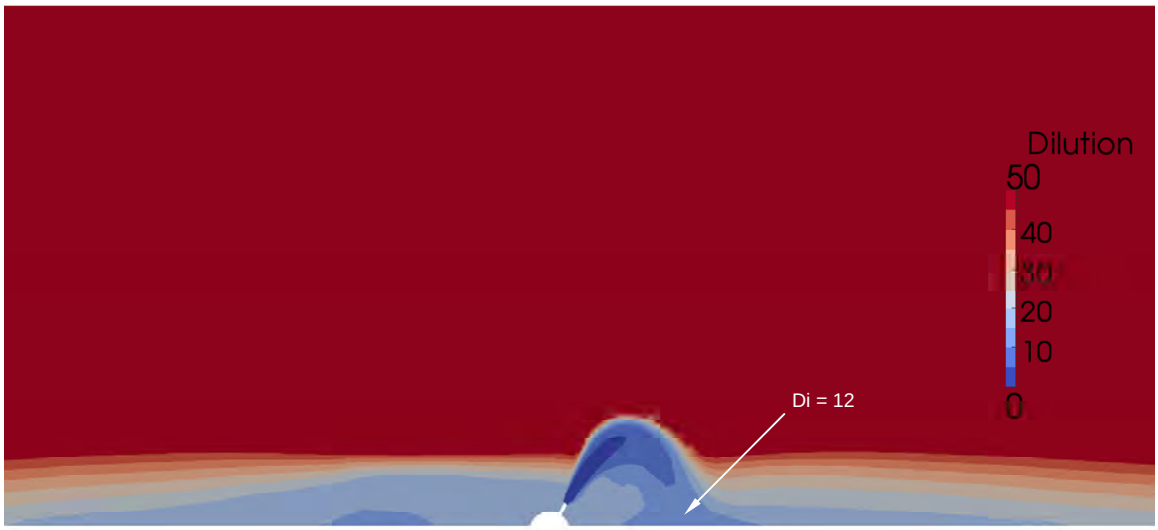

Figure 2-10 DEIS 4.3 m^3/s zero background velocity, plume cross-section

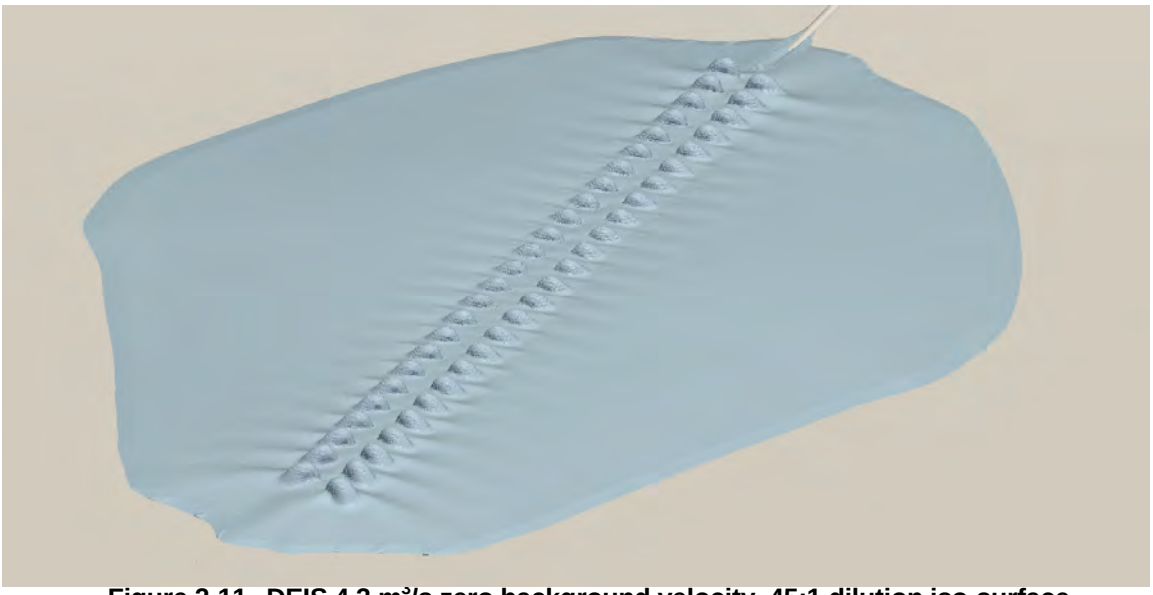

Figure 2-11 DEIS 4.3 m³/s zero background velocity, 45:1 dilution iso-surface

2.5.2 Alternative Configurations

The above result prompted simulation of a range of selected combinations of port diameter and number, as listed in Table 2-4 as ALT1, ALT2, ALT3 and ALT4. Figure 2-11 illustrates the zero background velocity plume that formed for these configurations. As can be seen, using fewer and smaller ports to increase the port exit velocity has the plumes reaching higher into the water column and better dilutions are achieved (as expected). This is particularly evident at bottom impact, but also at 100 m from the diffuser line as summarised in Table 2-5.

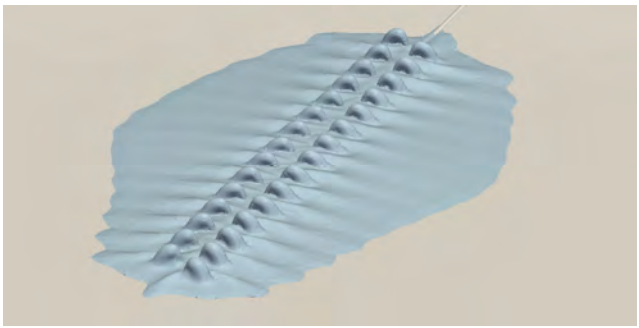

(a) ALT1

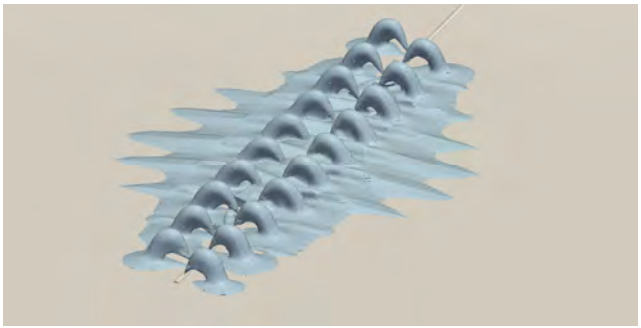

(b) ALT2

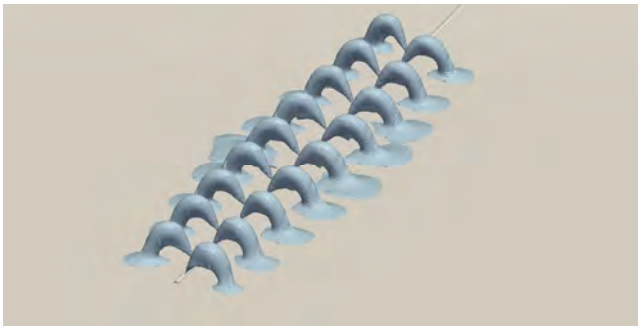

(c) ALT3

(d) ALT4

Figure 2-12 Alternative configurations 3.1 m^3/s zero background velocity, 45:1 dilution iso-surface

Table 2-6 Alternative configurations 3.1 m^3/s zero background velocity, dilution results

Name	d [mm]	N ports	Q m^3/s	Exit Vel m/s	Di	D100
DEIS	175	50	4.3	3.6	12	53
DEIS	175	50	3.1	2.6	10	67
ALT1	150	30	3.1	5.9	21	67
ALT2	150	20	3.1	8.9	27	70
ALT3	140	18	3.1	10.9	31	83
ALT4	150	14	3.1	12.5	39	87

2.5.3 Zero Background Current SEIS Configuration

From the above results, and also considering external engineering factors, BMT WBM was instructed to use the ALT2 configuration for the initial supplementary EIS (SEIS) study at a discharge flow rate of 3.1 m^3/s. Hence ALT2 and SEIS configurations are synonymous hereafter. Figure 2-13 below is Figure 2-12 (b) reproduced.

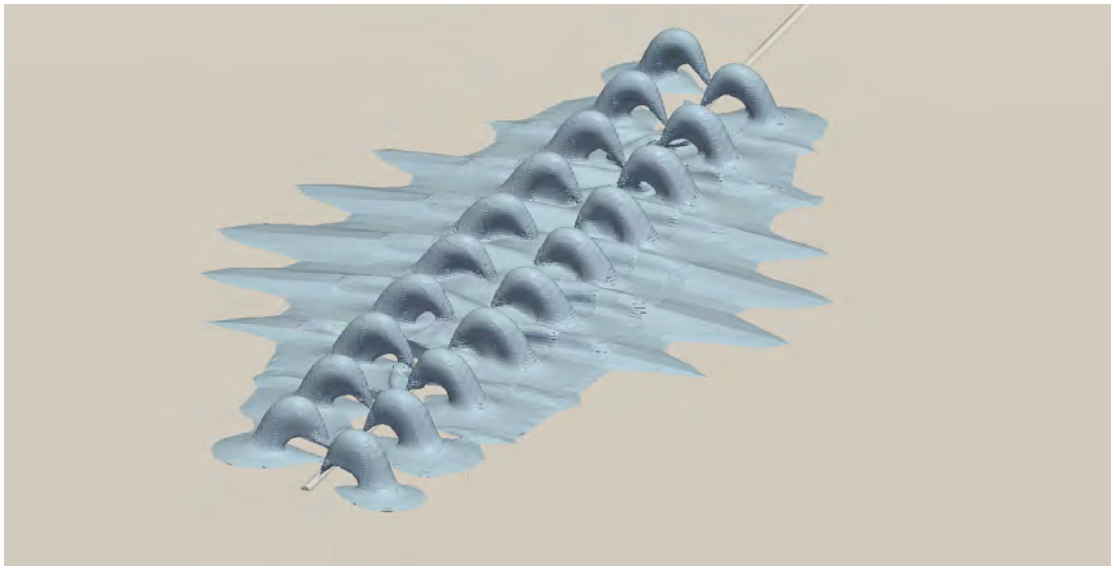

Figure 2-13 ALT2/SEIS 3.1 m^3/s zero background velocity, 45:1 dilution iso-surface

2.5.4 Tidal Flow DEIS Configuration

Following execution of the zero current simulations, a suite of ambient current scenarios were investigated firstly for the original DEIS configuration and flow rate. Figure 2-14 below shows the 45:1 dilution iso-surfaces and 100 m curtains for the DEIS configuration at 4.3 m^3/s with a range go (steady state) tidal flow.

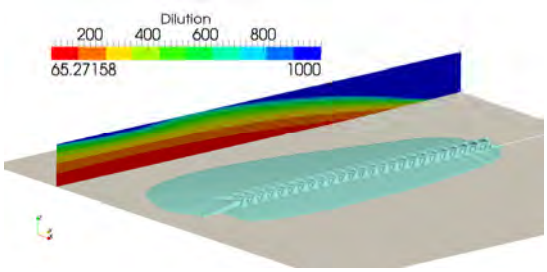

(a) Ebb 10%

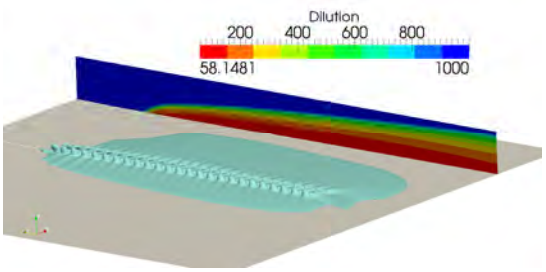

(b) Flood 10%

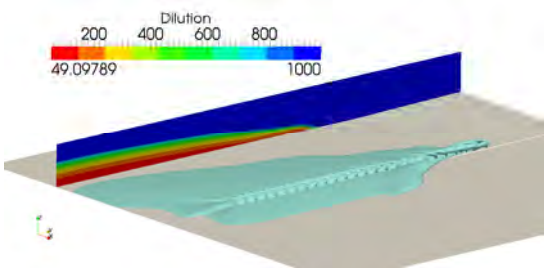

(c) Ebb 30%

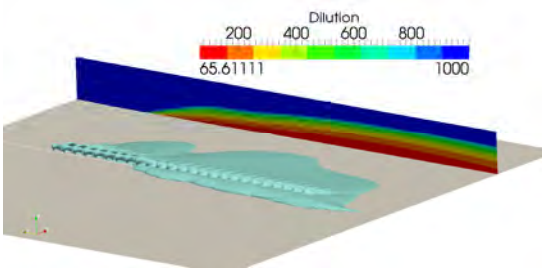

(d) Flood 30%

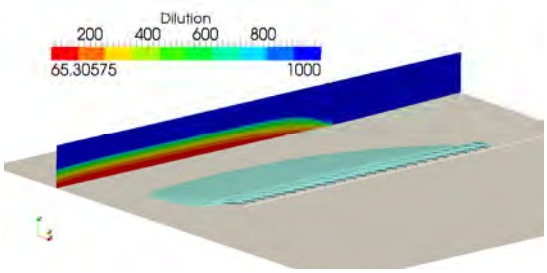

(e) Ebb 50%

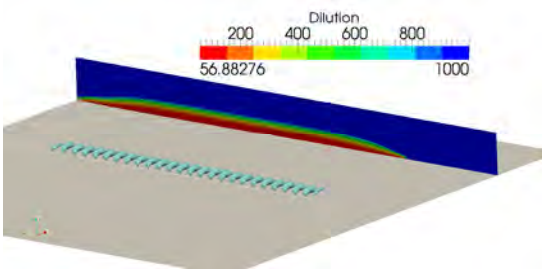

(f) Flood 50%

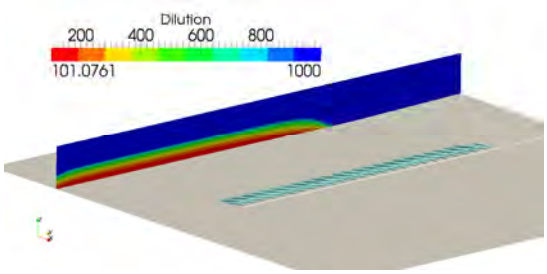

(g) Ebb 70%

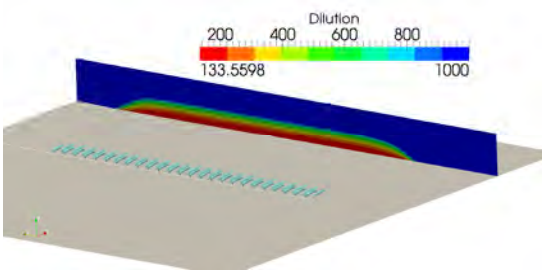

(h) Flood 70%

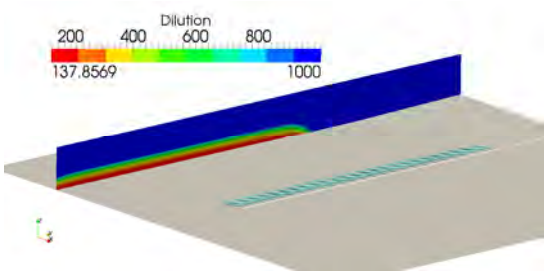

(g) Ebb 90%

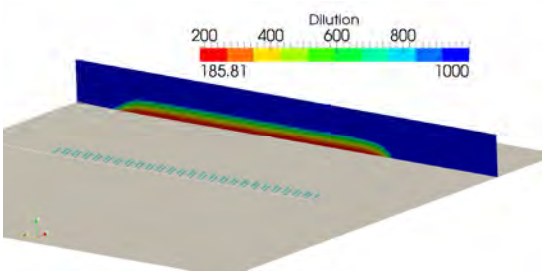

(h) Flood 90%

Figure 2-14 DEIS 4.3 m^3/s 45:1 dilution iso-surfaces and 100 m curtains at ebb and flood tides

2.5.5 Tidal Flow SEIS Configuration

Following review of the above results, a similar suite of simulations were conducted relative to the SEIS configuration. Figure 2-15 below shows the 45:1 dilution iso-surfaces and 100 m curtains for the SEIS configuration at 3.1 m^3/s with tidal flow. A similar set of results were obtained for the 2.79 m^3/s discharge on request. Output dilutions are tabulated in the next section, for which the images have been omitted as they are visually similar to those in Figure 2-15 below.

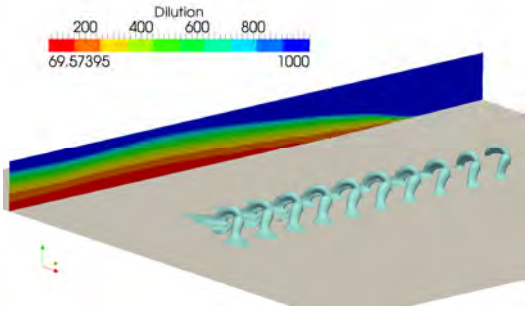

(a) Ebb 10%

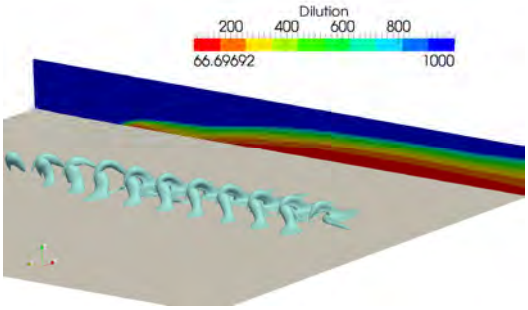

(b) Flood 10%

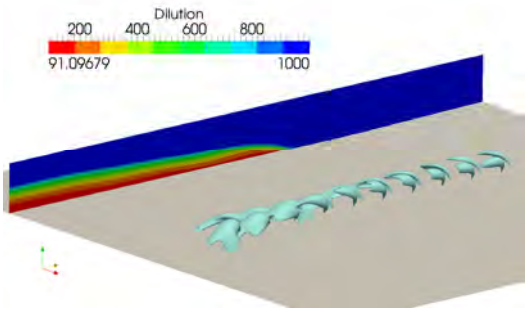

(c) Ebb 30%

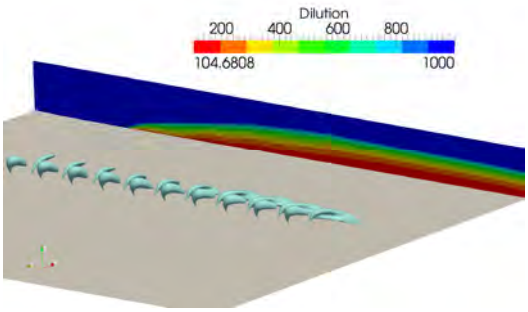

(d) Flood 30%

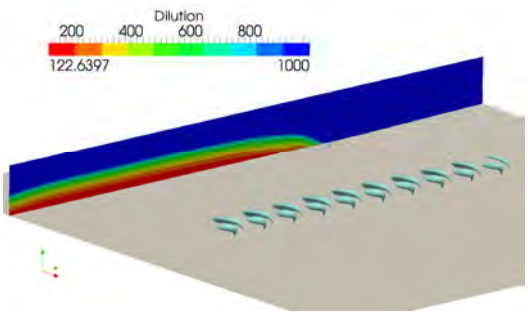

(e) Ebb 50%

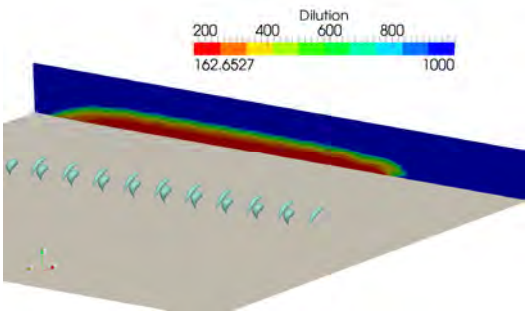

(f) Flood 50%

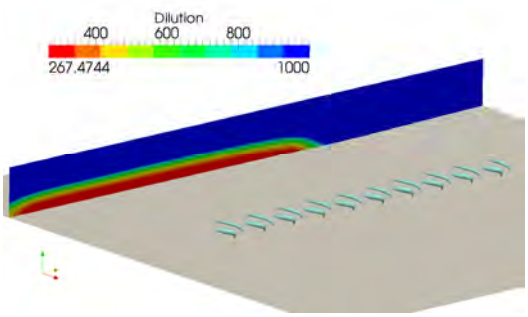

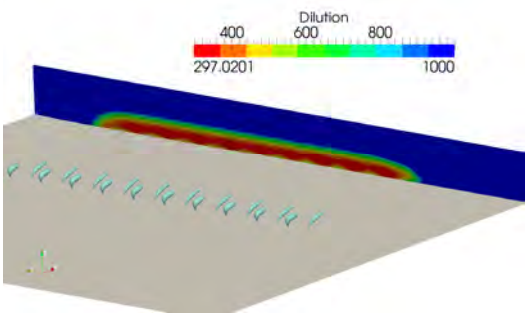

(g) Ebb 70%

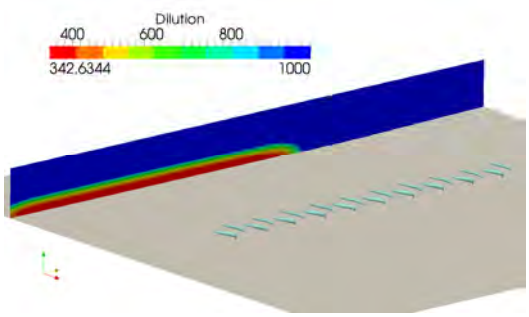

(h) Flood 70%

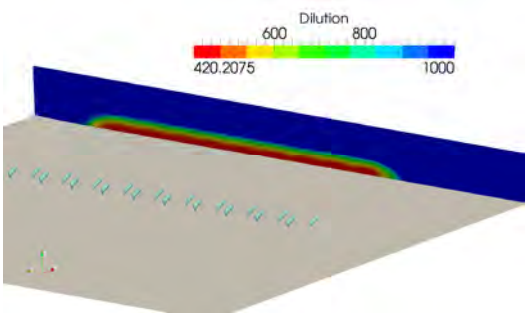

(i) Ebb 90%

(j) Flood 90%

Figure 2-15 SEIS 3.1 m^3/s 45:1 dilution iso-surfaces and 100 m curtains at ebb and flood tides

2.5.6 Transient Dodge Tide SEIS Configuration

A transient simulation of the SEIS configuration at 3.1 m^3/s was run for a period of 12 hrs over a selected dodge tide. This simulation was not intended to reproduce any particular dodge tide or to provide direct comparison with ELCOM results (the two are not comparable), but rather, to demonstrate that the simulation is possible, and to provide some indication of the likely transient dynamics of the selected diffuser. A more detailed transient investigation is possible to supplement these preliminary results. The transient results were not used for seeding ELCOM simulations.

Velocity profile data (from ELCOM) as a function of depth and time was applied on the model boundaries. Model boundary faces with influx used outfall concentrations as output by ELCOM. The depth averaged velocity as a function of time is shown in Figure 2-16.

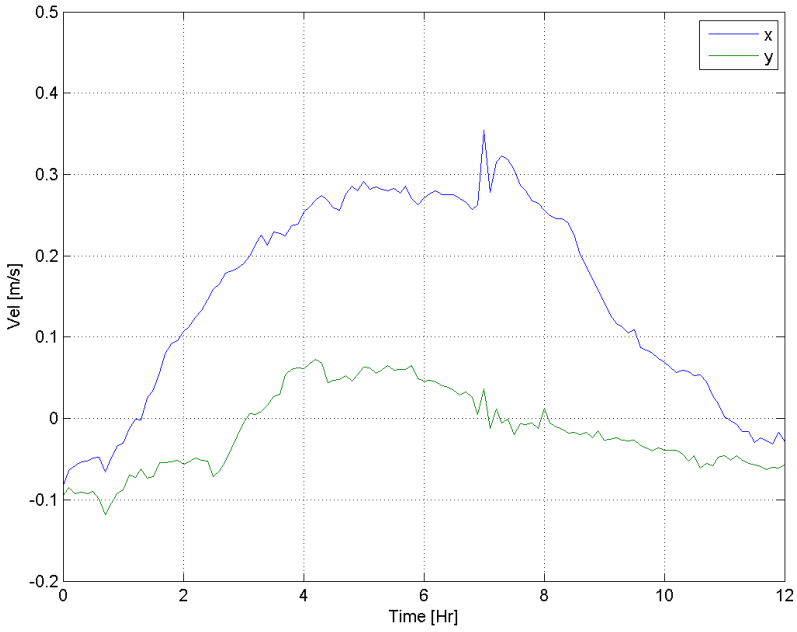

Figure 2-16 Transient dodge tide velocity profile

Figure 2-17 below shows the first hour of the results (10 min intervals) using the 45:1 dilution iso-surfaces and transverse curtains of dilution.

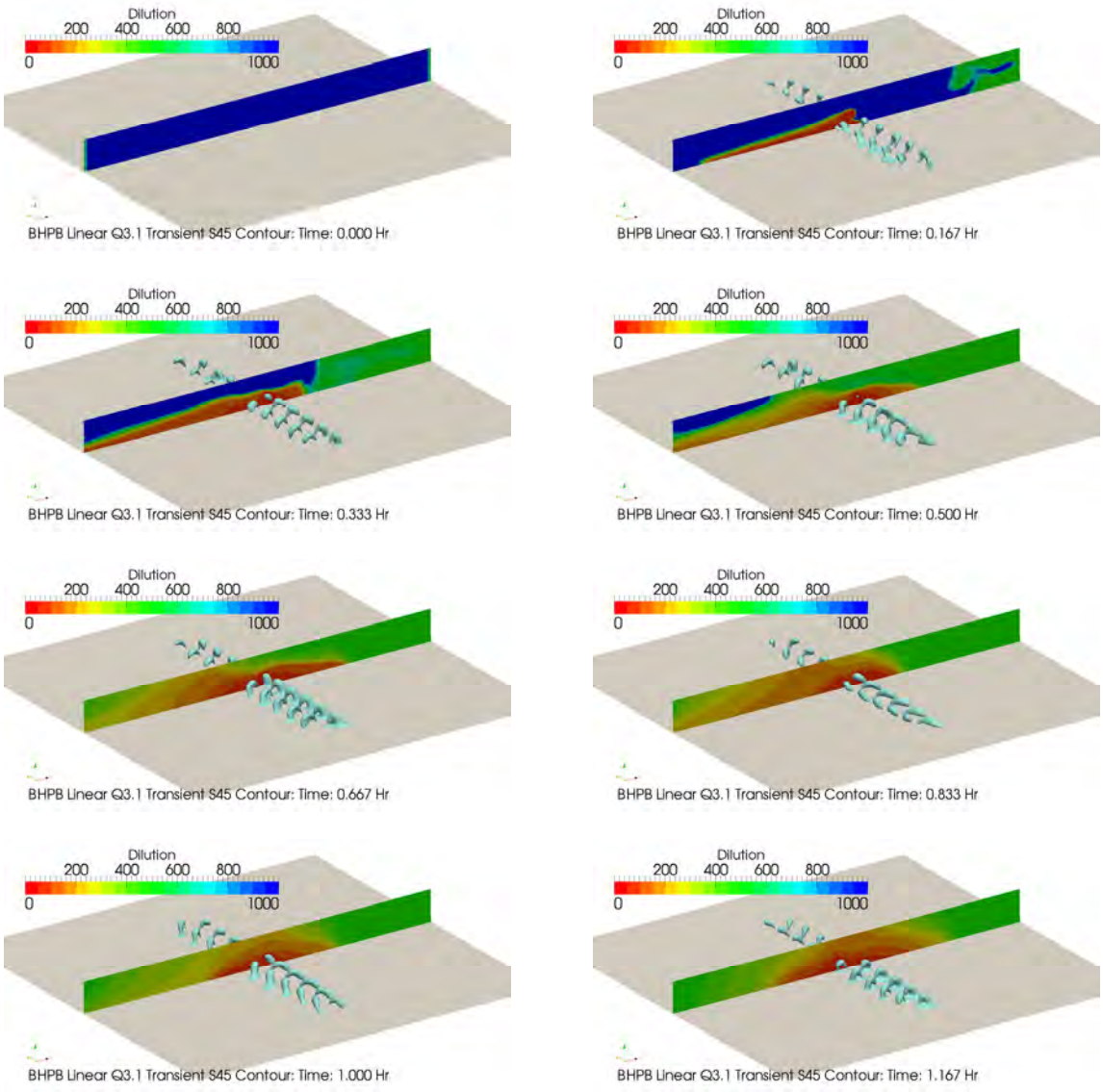

Figure 2-17 Transient dodge tide – first hour

2.6 Key Results

Table 2-7 to Table 2-9 list the key dilutions obtained from the CFD for the:

- DEIS configuration at 4.3 m^3/s;
- SEIS configuration at 3.1 m^3/s, and
- SEIS at 2.79 m^3/s.

It is noted that the dilutions at 100m presented below are not directly comparable to ELCOM predictions at 100m, as the CFD runs are steady state in nature, and thus do not account, for example, for the subsequent advection of brine potentially accumulated around the diffuser during a preceding zero current condition. The ELCOM simulations better capture this dynamic (i.e. non-steady state) process by using the CFD steady state results to seed the diffuser input (locally), then simulate any further afield advection and dispersion of potentially accumulated brine away from the diffuser under dynamic tidal conditions. It is thus stressed that these steady state results are not to be directly compared with dynamic ELCOM predictions: the two modelling frameworks are not comparable in this regard.

Table 2-7 DEIS 4.3 m^3/s key dilutions

Case	Minimum bottom dilution > 20 m	Min dilution at 100 m downstream
Zero background	~18	
Ebb 10%	18.8	65.3
Ebb 30%	18.6	49.1
Ebb 50%	30.8	65.3
Ebb 70%	75.5	101
Ebb 90%	106	138
Flood 10%	18.6	58.1
Flood 30%	21.2	65.6
Flood 50%	43.0	56.9
Flood 70%	129	134
Flood 90%	152	186

Table 2-8 SEIS 3.1 m^3/s key dilutions

Case	Minimum bottom dilution > 20 m	Min dilution at 100 m downstream
Zero background	28.7	78.3
Ebb 10%	32.9	69.6
Ebb 30%	42.5	91.1
Ebb 50%	88.6	123
Ebb 70%	268	267
Ebb 90%	356	343
Flood 10%	32.3	66.7
Flood 30%	43.1	105
Flood 50%	152	163
Flood 70%	321	297
Flood 90%	436	420

Table 2-9 SEIS 2.79 m^3/s key dilutions

Case	Minimum bottom dilution > 20 m	Min dilution at 100 m downstream
Zero background	25.9	84.9
Ebb 10%	35.0	70.9
Ebb 30%	43.5	93.0
Ebb 50%	76.3	128
Ebb 70%	313	292
Ebb 90%	377	355
Flood 10%	34.0	65.5
Flood 30%	46.6	110
Flood 50%	164	171
Flood 70%	340	307
Flood 90%	478	445

2.7 ELCOM Seeding

Having undertaken these steady state CFD simulations, the results presented above were used to seed the injection of brine to the ELCOM models. To do so, the outfall dilutions at the bottom surface of the model were considered, (as shown as an example in Figure 2-18(a) below for the DEIS configuration at 10% ebb tide). A methodology was then developed to determine an appropriate dilution factor to use for injection into the ELCOM cells, which are 40 m by 40 m at the location of the diffuser. This is described in detail elsewhere in this report, however at this time it is noted that the *minimum* concentration observed more than 20 m from the diffuser (i.e. half a cell width) in both of the lateral directions was used to seed the ELCOM simulations. Figure 2-9 (b) shows the dilutions at the bottom surface with the inner rectangle 40 m by 240 m blanked off as an example. In this example, the dilution used to seed the ELCOM runs was 18.8.

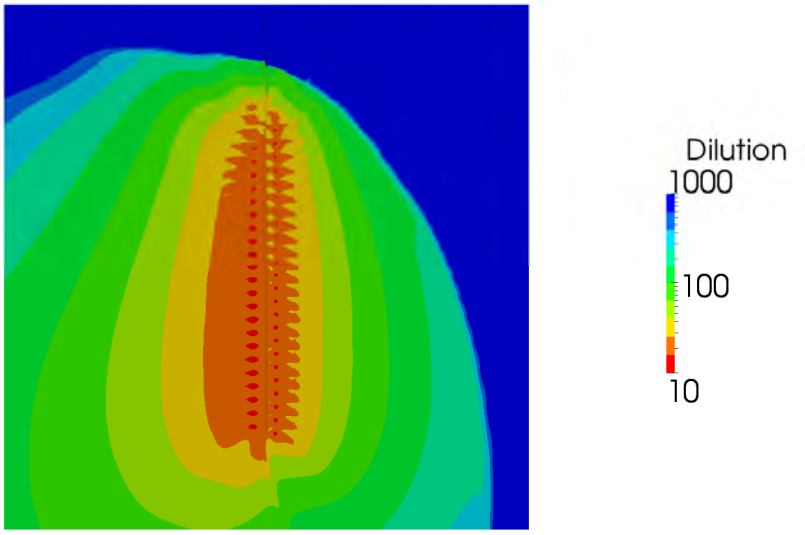

(a) Whole domain

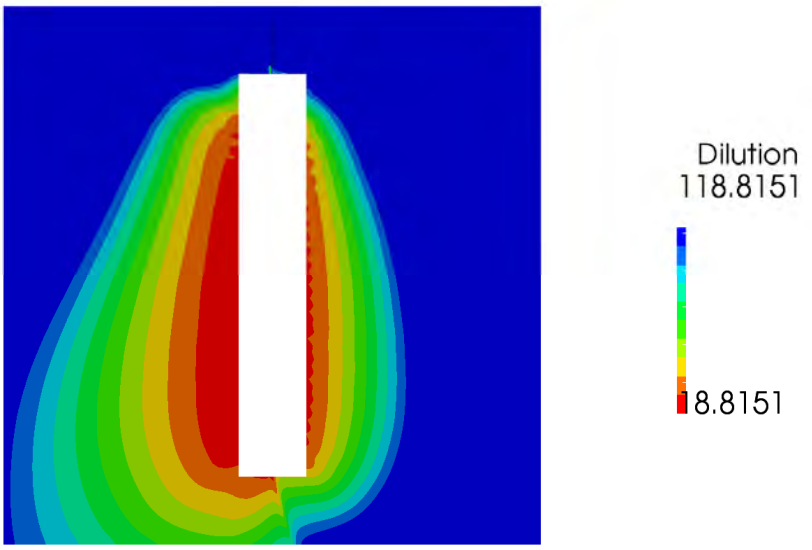

(b) Domain considered for seeding ELCOM injection

Figure 2-18 DEIS 4.3 m^3/s zero background velocity, bottom surface dilutions

2.8 Summary

- CFD has been applied to calculate the evolution of negatively buoyant plumes from a multiport diffuser over a range of steady state (and one transient) tidal flow conditions.
- The CFD framework and predictions has been benchmarked against other tools, with good agreement reached with the majority of historical techniques;
- The performance of the Draft EIS configuration diffuser was assessed in detail and an improved design for the initial Supplementary EIS was determined in conjunction with BHP Billiton.
- The CFD results for the various steady state simulations for the SEIS diffuser configuration were processed to create lookup tables (as a function of tidal flow) of injection dilutions to use within the ELCOM models.

- The effects of plume overlap and outfall re-entrainment were found to be significant. Carrying this effect into the ELCOM model has been achieved by developing a defensible seeding mechanism.
- As empirical correlations based on experimental data are only available for single port diffusers, we believe this establishes the use of CFD as best-practice for calculation of near field dilutions around multiport diffusers of this nature.

3 HIGH RESOLUTION SCENARIO ASSESSMENTS

Results presented in the previous section identified the detailed characteristics of the outfall discharge plume in the near field zone. The assessment presented in this section aims to characterise the transport and dispersion of brine at larger scales, taking into consideration the temporal and spatial variability of the flow field as a combination of the tidal and atmospheric forcing experienced in Spencer Gulf. The validated model of Spencer Gulf presented in Appendix 17.5.2 of the SEIS (hereafter BMT WBM model or high resolution model) was used as the basis for the simulations presented in this section, as it provided high resolution in the surroundings of the outfall whilst producing manageable run times.

3.1 Model Grid and Bathymetry

The high resolution model used in the simulations has the same set-up as the validated model previously reported (SEIS Appendix 17.5.2). The model domain was discretised using a non-uniform grid in both vertical and horizontal directions with the model bathymetry extracted from the Digital Elevation Model presented in SEIS Appendix 17.5.2. This grid was designed to provide accurate information in the Northern Spencer Gulf, particularly at the location of the proposed diffuser, at which the horizontal grid resolution was 40 m. Horizontal grid resolution was progressively decreased to 300 m at Port Augusta and to 5km at the southern end of the domain. The detail of the domain at the location of the proposed outfall is presented in Figure 3-1. A non-uniform grid size was used in the vertical direction with a resolution of 1.00 m at the seabed level at the proposed diffuser location. The resulting mesh consisted of 228 by 293 by 31 cells with a total of 244,755 maximum wet cells. A 24 s time step was chosen to produce model stability and manageable run times.

3.2 Simulation Period and Initial Conditions

For the assessments presented herein results of two simulations are presented. One simulation represented a scenario without the proposed desalination plant discharge that was used to provide a background for comparisons and generation of appropriate boundary conditions for the proposed diffuser (see Section 3.3). The other simulation represented a scenario with the proposed desalination plant discharge. Simulations were performed for a period of one 1 year between 1st of November 2007 and 1st of November 2008.

Initial conditions for the model required the initialisation of background scalar fields with the long term influence of the proposed desalination plant discharge. To this end, simulations were produced for a three year time period on the low resolution ELCOM model (see Section 4) with and without the inclusion of the proposed desalination plant discharge. In these low resolution simulations the same injection method described below was used (see Section 3.3.1). The resultant scalar fields were then interpolated from the low resolution model to form the initial scalar fields in the high resolution model. This methodology ensured manageable run times and inclusion of long term influences within the high resolution simulations. The different scalar fields for simulations including the proposed desalination plant discharge are presented in Figure 3-2 to Figure 3-5. For consistency the same field preparation technique was used for simulations without the proposed desalination plant discharge.

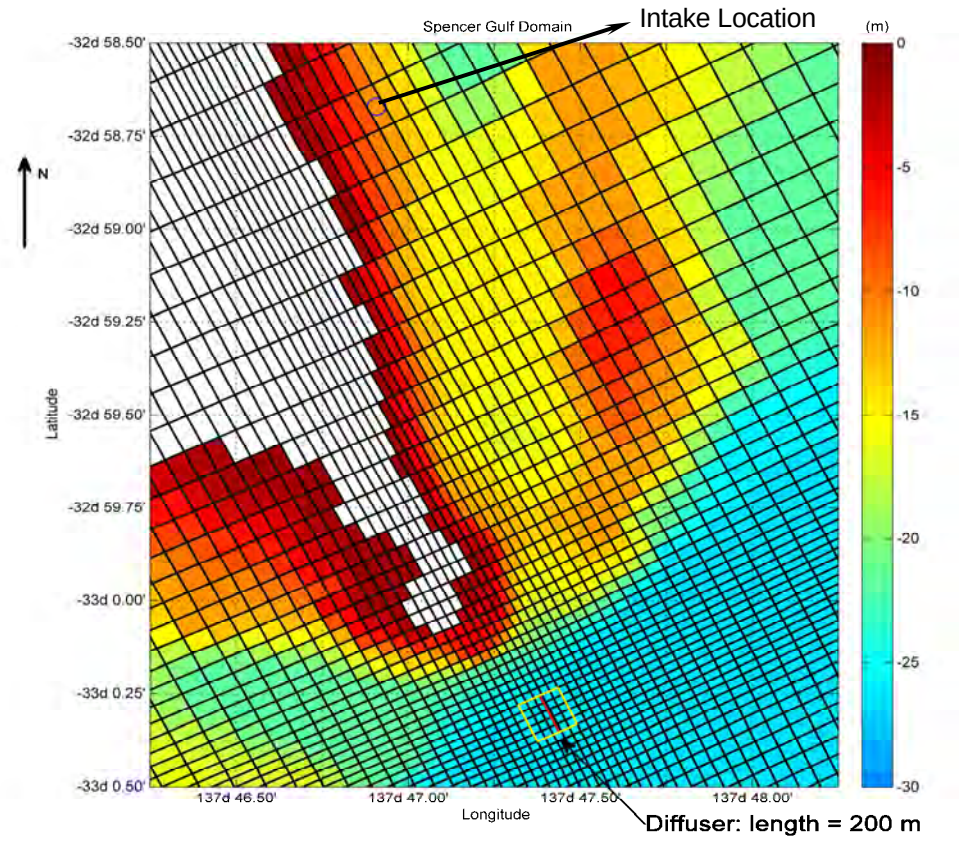

Figure 3-1 High resolution model grid and bathymetry at the location of the proposed intake and outfall. The area within the yellow rectangle defines the location of the boundary condition cells representing the outfall.

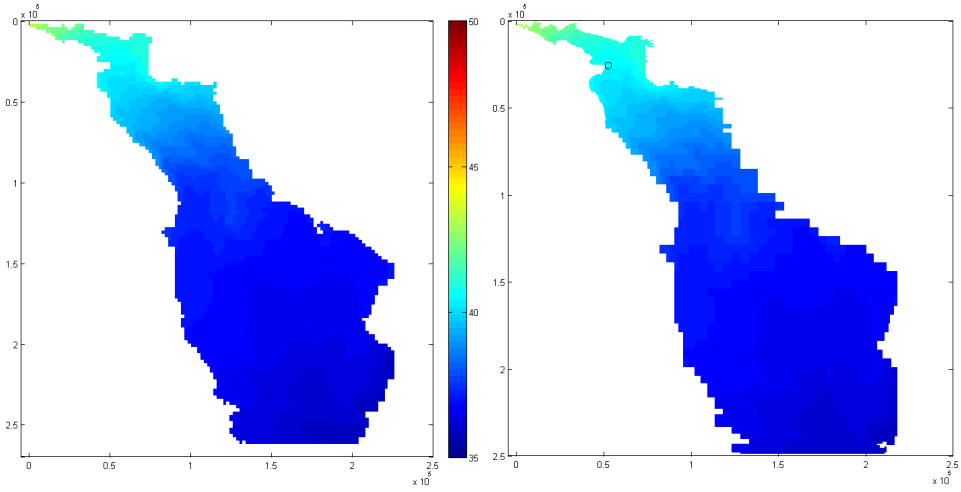

Figure 3-2 Results of the initial salinity field interpolation from low (left) to high (right) resolution model - 1st of November 2007. Horizontal scale is given in metres and the grid is rotated 64 degrees anti clockwise from the North direction.

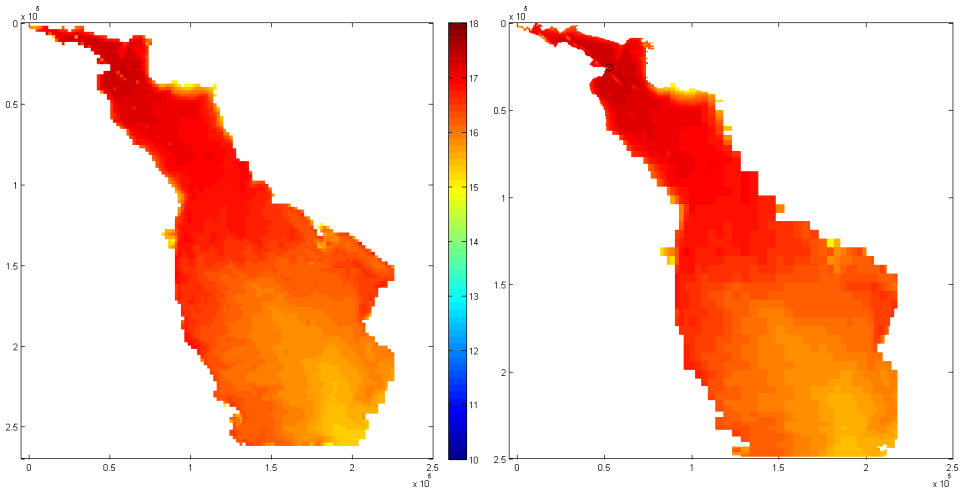

Figure 3-3 Results of the initial temperature field interpolation from low (left) to high (right) resolution model - 1st of November 2007. Horizontal scale is given in metres and the grid is rotated 64 degrees anti clockwise from the North direction.

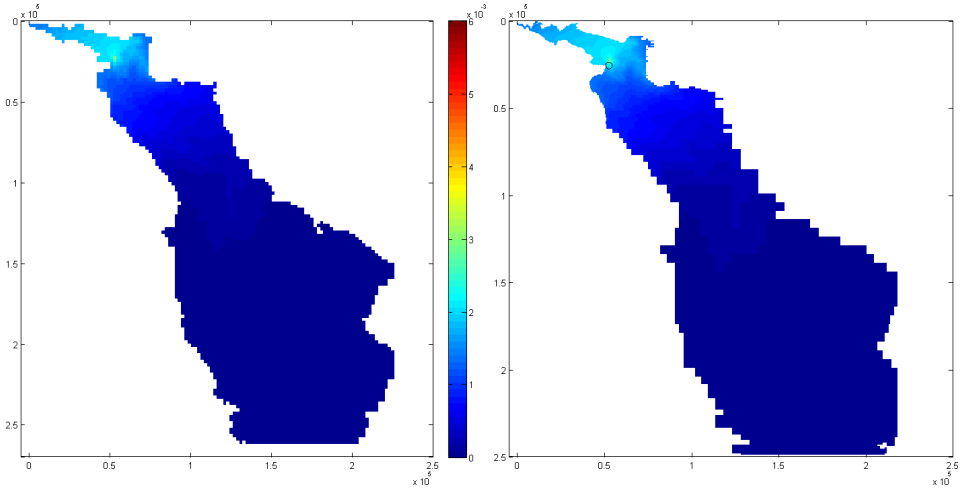

Figure 3-4 Results of the initial tracer (equivalent to inverse of dilution) field interpolation from low (left) to high (right) resolution model - 1st of November 2007. Horizontal scale is given in metres and the grid is rotated 64 degrees anti clockwise from the North direction. Circle on right pane show the location of the proposed outfall.

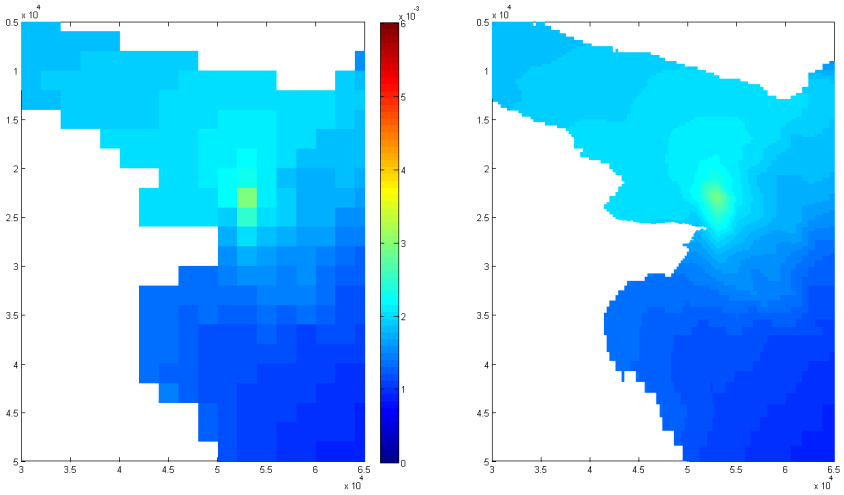

Figure 3-5 Zoom of the initial tracer (inverse of dilution) interpolation result presented in Figure 3-4 with detail in the proximities of the proposed outfall. Horizontal scale is given in metres and the grid is rotated 64 degrees anti clockwise from the North direction.

3.3 Boundary Conditions

The common boundary conditions for the two simulations were presented in SEIS Appendix 17.5.2 and the reader is referred to this document for further details. These boundary conditions are summarised as follows:

- Meteorological:
  - Hourly meteorological forcing from the Weather Research Forecast model. The forcing includes air temperature, relative humidity, solar radiation, incoming long wave radiation, wind speed and wind direction;
  - Daily rainfall from the Bureau of Meteorology SILO database;
- Open Boundary:
  - Hourly water surface elevations at the open boundaries from the combination of BMT ARGOSS global tidal model with the mean water levels from HYCOM data assimilation model;
  - Daily and vertically varying water salinity and temperature from the HYCOM data assimilation model;
- Other:
  - Same salinities and temperatures assumed in the DEIS for salt lake inflow north of Port Augusta and for the Thomas Playford power station in Port Augusta.

For the simulation including the proposed desalination plant discharge, the boundary flow was assumed to originate from the seabed. The flow was distributed over five to 25 cells according to the diluted discharge flow rate (see below). The locations of these cells are illustrated in Figure 3-1. Details of the desalination plant discharge are summarised as follows:

- outfall flow rate: Q_o = 3.07 m^3/s;

- outfall salinity: S_o = 75;
- outfall temperature: $T_o = T_i$,+1 where T_i is the temperature at the intake (see below);
- intake flow rate: Q_i = 5.38 m^3/s.

The above parameters were used to produce the required model boundary conditions as described below.

3.3.1 Nearfield and High Resolution Model Linkage

The BMT WBM model has a horizontal grid resolution of 40mx40m in the location of the proposed outfall. While this represents a relatively high resolution for a hydrodynamic model covering the entire Spencer Gulf, this resolution is unable to properly account for the nearfield mixing of the proposed brine discharge. This resolution is also comparable to the distance at the point of impact of the nearfield plume with the seabed. If one adopted the proposed discharge salinity directly into the hydrodynamic model, unrealistic salinities (also plume dilutions, temperatures and any other scalars involved) would result in the location and immediate vicinity of the diffuser, as these would not take into consideration the extent of the nearfield dilution, which occurs at spatial scales very similar to the grid resolution (see Section 2). As such, BMT WBM developed an injection method that preserves the salt mass being discharged whilst adopting the realistic salinities, temperatures, and dilutions based on the results of the nearfield CFD simulations. This is a critical element of this study that ensures consistency between near and far field predictions. A schematic of this method is given in Figure 3-6. A step-by-step description of this injection method is given below.

Step 1. Depth-averaged velocities for ebb and flood tides were obtained from the velocity profiles measured in the March-June 2009 field campaign at the proposed diffuser location (SEIS Appendix 17.5.2).

Step 2. Cumulative distribution for each of the tidal phases were obtained (Figure 3-7).

Step 3. Real profiles representative of the 10th, 30th, 50th, 70th, and 90th percentiles were extracted from the time series to be used as background ambient conditions for nearfield CFD simulations (some representative are presented in Section 2).

Step 4. CFD simulations were performed for each of these representative profiles (Section 2);

Step 5. The nearfield CFD results were tabulated to express the function between depth-averaged ambient velocities and plume dilution. An example for the tabulated dilutions for the scenario assuming the maximum proposed outfall flow rate of 3.07 m^3/s is given in Figure 3-8.

Step 6. Baseline Spencer Gulf hydrodynamic simulations (i.e., without the inclusion of the proposed discharge) were processed for the provision of background depth-averaged velocities. An example of these velocities is given in Figure 3-9.

Step 7. Dilutions as a function of the modelled background velocities were obtained from the table produced in step 5 (i.e. Figure 3-8)

Step 8. Salinities and other scalar fields at the boundary cells representing the proposed diffuser were computed as a function of the dilutions obtained in step 7 (Figure 3-10). The fluid entrained in the plume was assumed to have scalar characteristics of the depth averaged

scalars in the background baseline simulations. This assumption is consistent with the plume travel path reaching higher parts of the water column (Section 2)

Step 9. Outfall discharges were re-computed to balance the brine mass flux in the discharge (Figure 3-10). The final scalars and discharges used as boundary conditions were calculated as follows.

Given the following problem data:

S_a - Ambient salinity (depth averaged salinity in the background simulation)

T_a - Ambient temperature (depth averaged salinity in the background simulation)

S_o - Salinity at diffuser nozzle (equals 75 g/L)

T_o - Temperature at desalination intake (from background simulation)

C_o – Tracer concentration at diffuser nozzle (equals 1)

Q_o – Discharge at nozzle (equals 3.07 m^3/s in this example)

D – inverse of dilution at point of impact (given by the "look-up" table)

The following quantities are used as boundary conditions in the model:

C – Tracer concentration at point of impact (equals D for $C_o = 1$)

S – Salinity at point of impact

T – Temperature at point of impact

Q - Discharge at point of impact

In order to conserve the brine mass flux:

$$QC = QD = Q_o C_o = const.$$

Such that

$$Q = \frac{Q_o C_o}{D}$$

Salinities (S) were computed as follows:

$$S = \frac{\frac{1}{D} S_a + S_o}{\frac{1}{D} + 1} = \frac{S_a + D S_o}{(1 + D)}$$

Temperatures (T) were assumed to increase by 1°C due to the desalination process, such that:

$$T = \frac{\frac{1}{D}T_a + (T_i + 1)}{\frac{1}{D} + 1} = \frac{T_a + D(T_i + 1)}{(1 + D)} = \frac{T_a + D(T_o)}{(1 + D)}$$

The assumed boundary conditions for tracer, temperature, and salinity in the model were given by *D*, *T,* and *S*, respectively. Of particular importance were tracer concentrations and salinities, which defined the spatial and temporal character of the diluted discharge, and the relevant environmental salinities for ecological assessments.

Step 10. A salt sink was introduced to remove excess entrained salt and the required sink was distributed at specified bottom cells in the domain. The excess entrained salt originates from a background salinity that is different from zero (as opposed to the tracer field used for the mass balance that has a zero baseline background). This salt sink was required such that no artificial salt would accumulate in the computational domain as a result of the injection method. The excess entrained salt ($\Delta(QS)$) is obtained by the following relationship:

$$\Delta(QS) = QS - Q_o S_o$$

with the variables as defined above. Outflow boundary condition cells were set up such that $\Delta(QS)$ could be removed from the computational domain. These cells were specified in such a way that

1) they occupied a relatively large area, such that the sink discharge would have minimal disruption in the local hydrodynamics;

2) they were relatively close to the proposed outfall such that "artificial" excess salt did not accumulate in the Northern Spencer Gulf; and

3) the salinities at the outflow cells were similar in the simulation with and without the desalination plant discharge, such that the sink discharge could be accurately computed. Computation of the sink discharge (Q_d) was given by

$$Q_d = \frac{\Delta(QS)}{S_d}$$

- where S_d was given by the average salinity at the outflow cells. The average used to compute S_d was weight by the size of the outflow area corresponding to each particular outflow cell.

The outflow cell locations for low and high resolution models are shown in Figure 3-11.

It is noted that at any time the magnitude of the salt sink discharge was proportional to the dilution, such that the maximum outflow rates occurred during spring tides, when the nearfield processes provided superior dilution.

3.3.2 Outfall Flow Distribution

During neap tides and turns of the tides, when current velocities are low, the boundary condition flow was distributed over five cells corresponding exactly to location of the proposed outfall diffuser (200

m). With increased flow velocity, particularly during spring tides, dilutions were increased thus, producing increased discharge rates at the outfall boundary. In order to keep the computation stable (i.e. vertical Courânt-Friedérich-Lévy – CFL < 1), flow was spread over more computational cells, maintaining the same scalar fields obtained from the injection method described above. The cells used to increase the boundary condition area were located parallel to the diffuser line and were accommodated two grid-cell lines northwest and southeast of the diffuser line (Figure 3-1). For convenience the cells encompassing the diffuser line are called the central diffuser line and adjacent boundary condition cells are called (north and south) side diffuser lines. The following flow distribution as a function of the boundary condition discharge rate was assumed:

- Q < 250 m3/s: flow rate was distributed over the central diffuser line alone;
- 250 ≤ Q < 500 m3/s: flow rate was distributed over the central line and another side line in the side of tide flow direction;
- 500 ≤ Q < 750 m3/s: flow rate was distributed over the central line and two side lines in the side of tide flow direction;
- 750 ≤ Q < 1000 m3/s flow rate was distributed over the central line, the two side lines depending on tide flow direction, and the side line adjacent to the diffuser in the opposite side of the tide flow direction
- Q > 1000 m3/s all boundary cells were used.

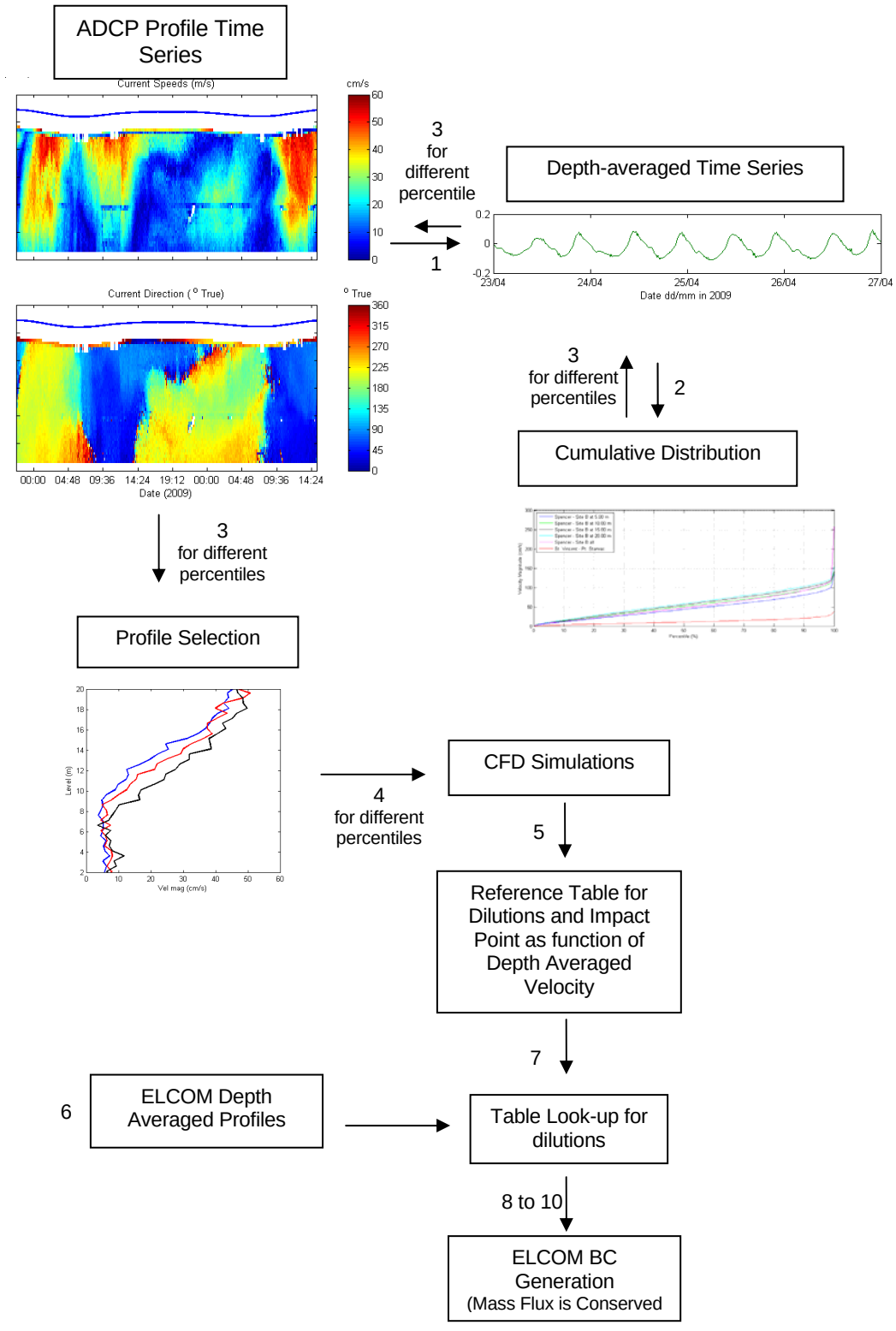

Figure 3-6 Schematic of the injection method

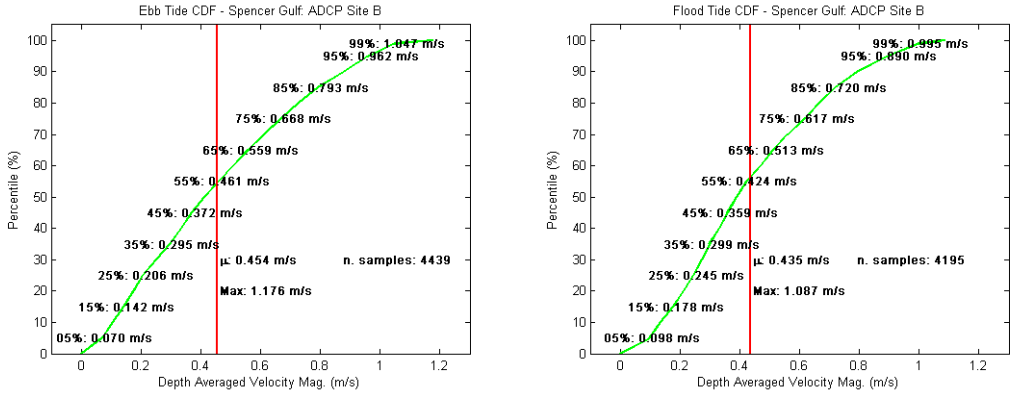

Figure 3-7 Cumulative distribution of the depth-averaged measured ambient background velocity for ebb and flood tides (SEIS Appendix 17.5.2)

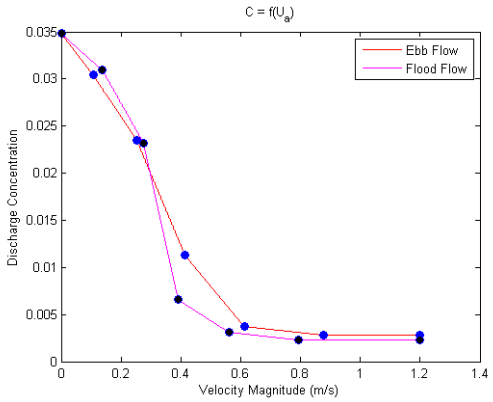

Figure 3-8 Tabulated dilutions as a function of depth-averaged ambient background velocity

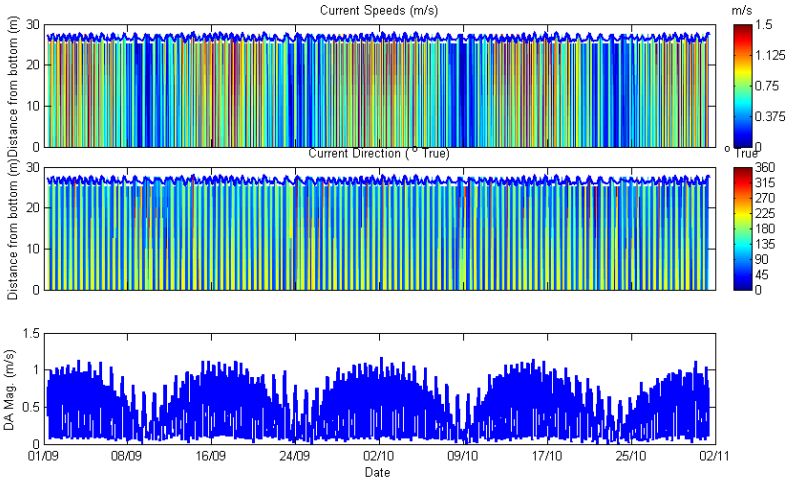

Figure 3-9 Modelled background velocity profiles and resulting depth-averaged time series used to obtain nearfield dilutions

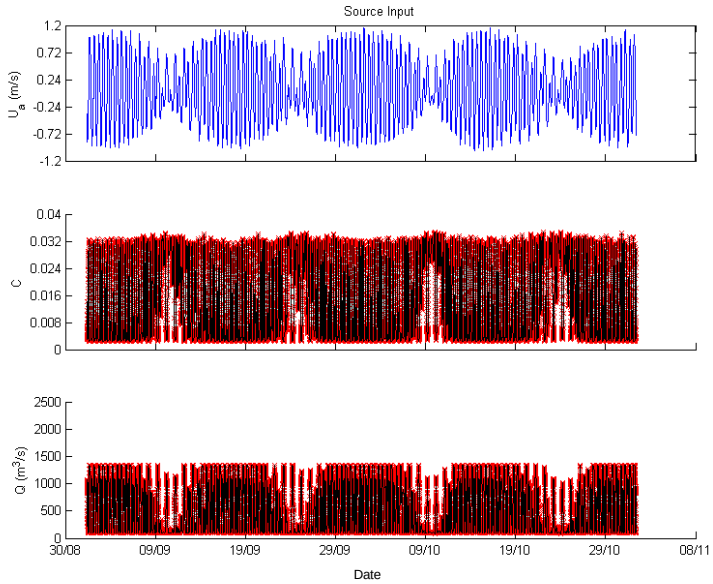

Figure 3-10 Input boundary conditions for the proposed diffuser in the high resolution model. Top panel: depth averaged velocities (ebb is negative); middle panel: trace concentration used to compute dilutions (in relation to a concentration 1 at the diffuser nozzle); bottom panel: corrected discharge rates.

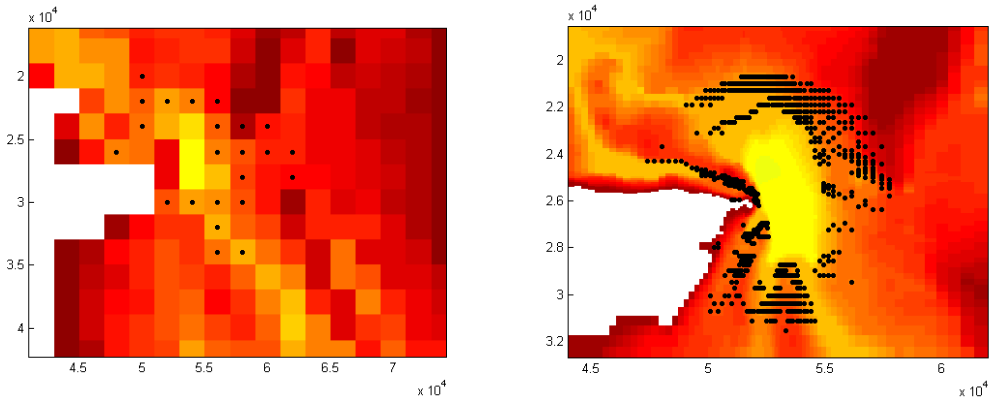

Figure 3-11 Salt sink locations (dots) for the high (left) and low resolution models (right). Colour scale indicates the bathymetry. Horizontal scale is given in metres and the grid is rotated 64 degrees anti clockwise from the North direction.

3.4 Simulation Results

3.4.1 Control Points

Time series at different control points chosen by the EIS team are presented below. These points are consistent with the time series presented in the DEIS and also include complimentary point sets. The locations of the different points are presented in Figure 3-12 to Figure 3-15. The time series were output at a frequency of 4 minutes and dilutions compared to targets of 45:1, 55:1, and 85:1.

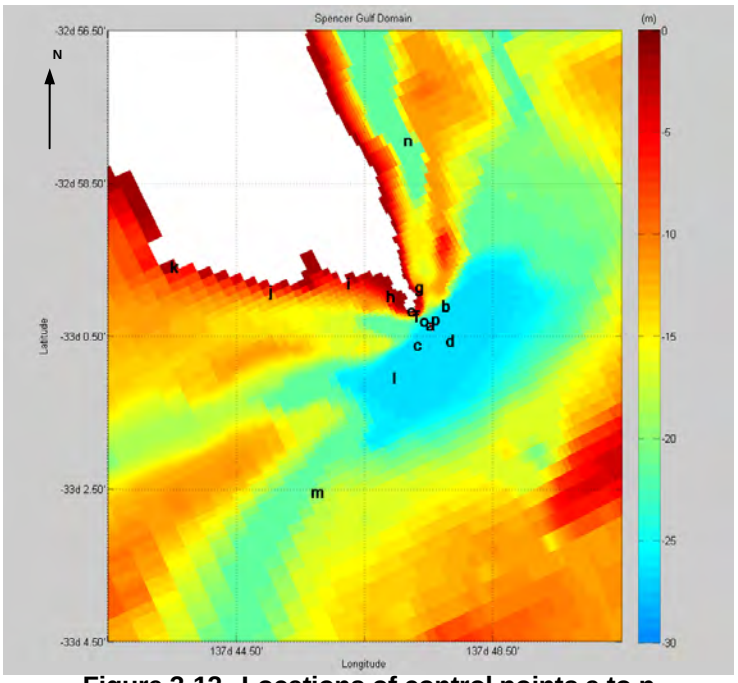

Figure 3-12 Locations of control points a to p

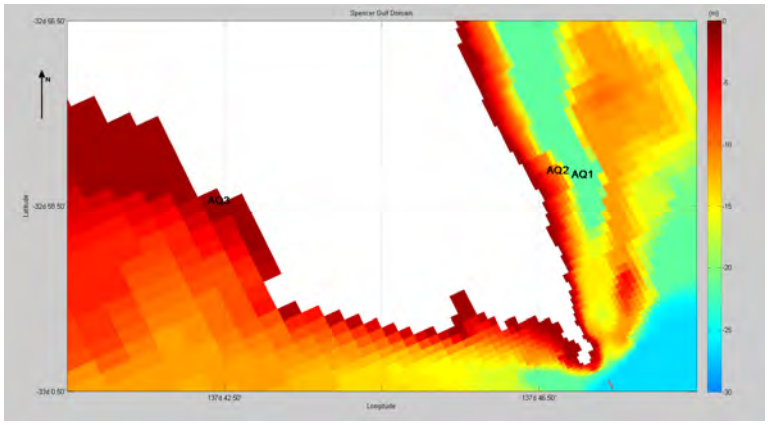

Figure 3-13 Locations of control points AQ1, AQ2, and AQ3 (aquaculture)

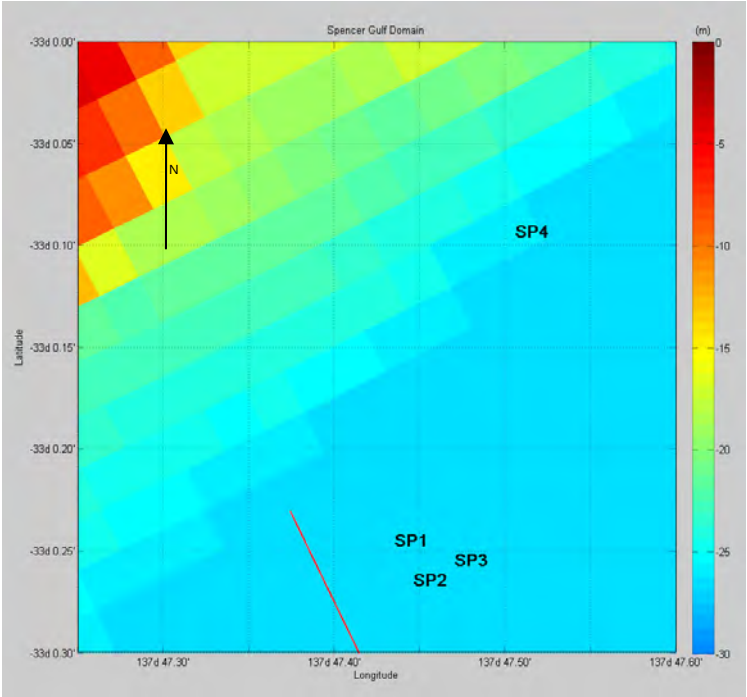

Figure 3-14 Locations of control points SP1, SP2, SP3 and SP4 (sponge beds)

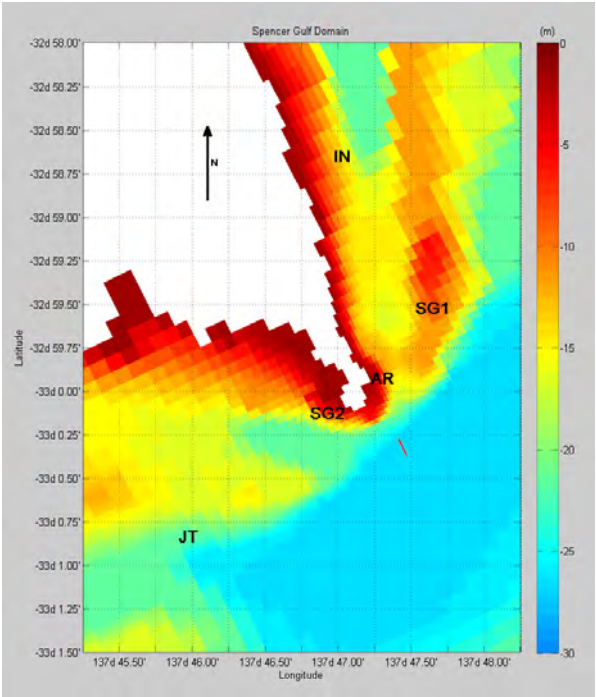

Figure 3-15 Locations of control points SG1, SG2 (seagrass), JY (Santos Jetty), AR (artificial reef) and IN (intake)

Bottom salinities at Sites a to p for both simulations are presented in Figure 3-16 to Figure 3-17. The corresponding dilution statistics at the model bottom cells are presented in Table 3-1. The first two weeks were removed from the time series for analysis as these were deemed to avoid model warmup issues.

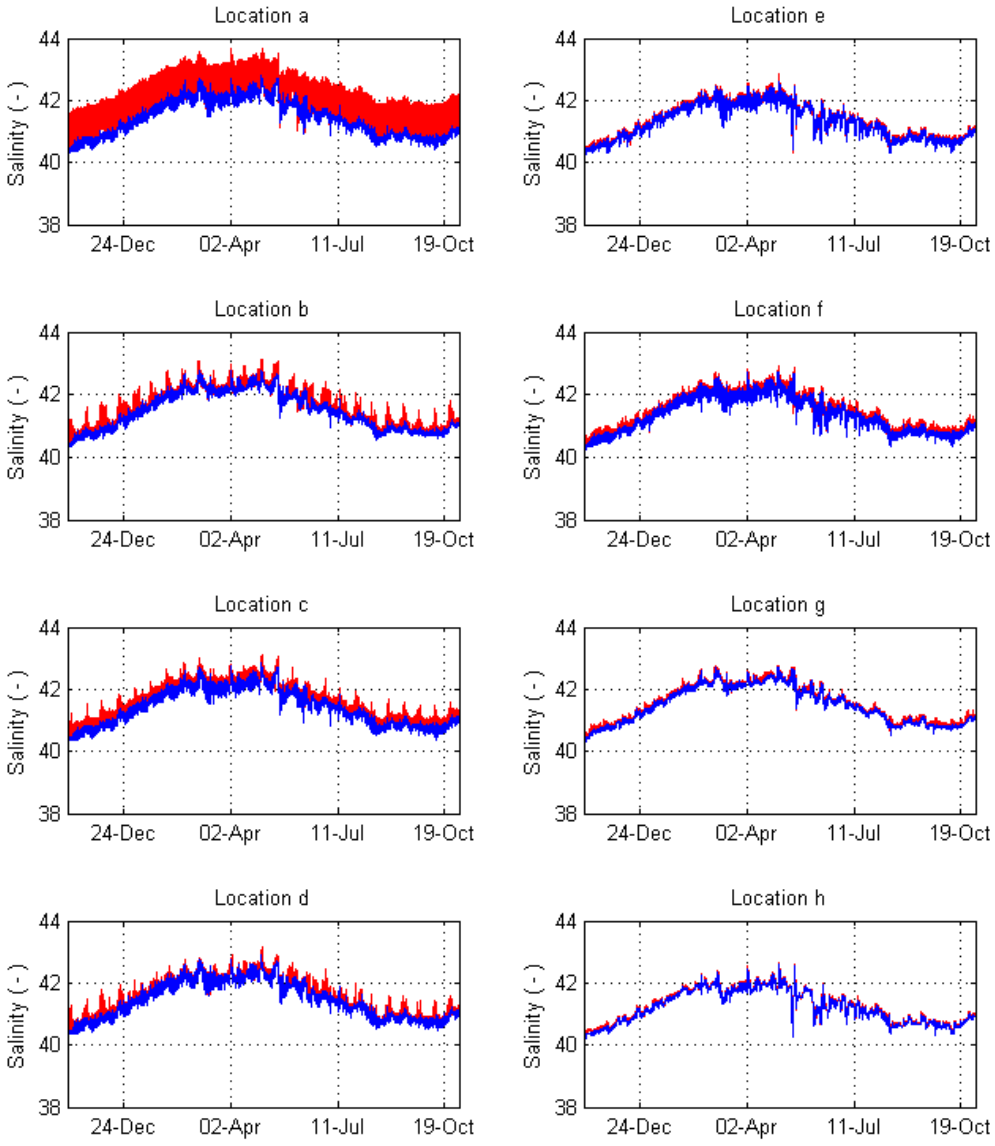

Figure 3-16 Salinities at the bottom for point a to h. Red: with proposed desalination outfall. Blue: Baseline

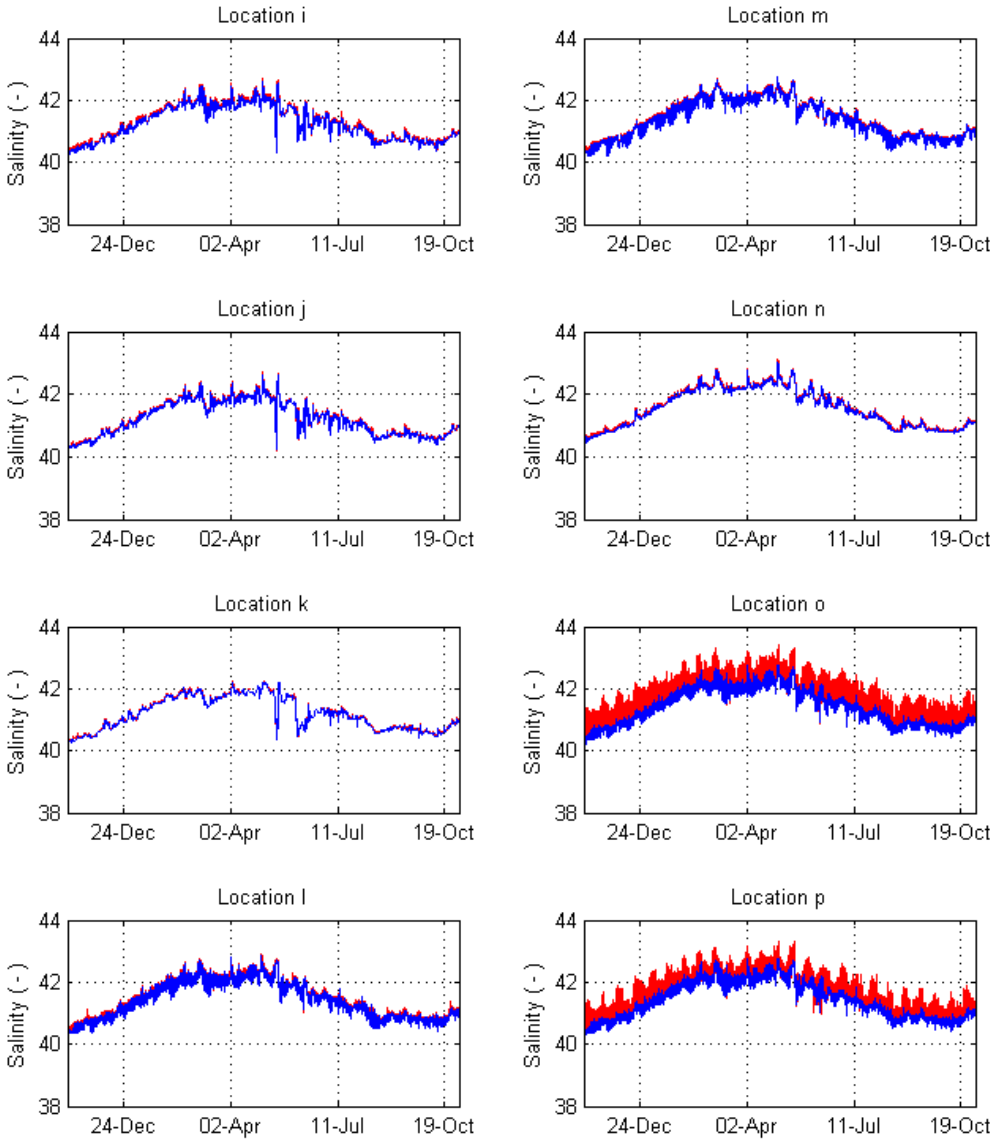

Figure 3-17 Salinities at the bottom for points i to p. Red: with proposed desalination outfall. Blue: Baseline

Table 3-1 Dilution statistics obtained for time series at the control points. Dilutions less than 85:1 are bolded.

Site	Percentiles									Occurrence of dilutions less than target dilutions					
	Min	1	5	10	25	50	75	90	95	<45 cnt	<45 pct	<55 cnt	<55 pct	<85 cnt	<85 pct
A	**29**	**30**	**31**	**33**	**45**	164	335	428	436	**32045**	**25.3**	**40234**	**31.8**	**51932**	**41**
B	**38**	**49**	110	213	350	410	446	477	491	**572**	**0.5**	**2288**	**1.8**	**4841**	**3.8**
C	**39**	**55**	101	127	246	408	459	488	505	**261**	**0.2**	**1254**	**1**	**4196**	**3.3**
D	**36**	**57**	147	253	382	436	473	496	509	**352**	**0.3**	**1062**	**0.8**	**3536**	**2.8**
E	145	246	318	356	410	461	517	579	624	0	0	0	0	0	0
F	**83**	131	184	227	316	400	465	526	571	0	0	0	0	**4**	0
G	**80**	152	244	293	357	406	455	478	489	0	0	0	0	**10**	0
H	151	297	394	425	468	515	578	635	684	0	0	0	0	0	0
I	99	275	365	412	457	504	560	610	656	0	0	0	0	0	0
J	134	324	420	457	496	545	597	647	699	0	0	0	0	0	0
K	373	441	477	488	535	586	637	709	786	0	0	0	0	0	0
L	**70**	153	268	351	409	450	481	507	527	0	0	0	0	**43**	0
M	229	353	389	408	438	473	506	546	576	0	0	0	0	**0**	0
N	343	371	396	404	427	460	477	491	501	0	0	0	0	0	0
O	**31**	**34**	**42**	**58**	253	404	457	491	514	**8063**	**6.4**	**11841**	**9.3**	**17018**	**13.4**
P	**33**	**38**	**53**	87	256	396	437	472	488	**4127**	**3.3**	**6704**	**5.3**	**12306**	**9.7**
SG1	130	219	304	344	390	425	459	480	492	0	0	0	0	0	0
SG2	120	266	341	380	435	491	555	613	660	0	0	0	0	0	0
SG3	**76**	164	295	356	411	452	485	533	570	0	0	0	0	24	0
SG4	123	214	296	331	374	412	453	478	496	0	0	0	0	0	0
SG5	164	318	368	385	410	449	472	486	498	0	0	0	0	0	0
AQ1	343	369	394	403	425	458	477	490	501	0	0	0	0	0	0
AQ2	285	366	392	402	423	459	477	491	503	0	0	0	0	0	0
AQ3	445	464	484	495	538	590	648	724	825	0	0	0	0	0	0
SP1	**31**	**35**	**41**	**47**	169	382	435	464	482	**10834**	**8.5**	**17826**	**14.1**	**24166**	**19.1**
SP2	**31**	**35**	**41**	**48**	168	382	435	464	482	**10232**	**8.1**	**17312**	**13.7**	**24323**	**19.2**
SP3	**31**	**38**	**51**	**68**	193	389	436	470	486	**4031**	**3.2**	**7781**	**6.1**	**17521**	**13.8**
SP4	**35**	**42**	**73**	156	339	406	441	475	489	**2033**	**1.6**	**4185**	**3.3**	**7514**	**5.9**

Salinities for the three lower-most cells at points a, c, and p are presented in Figure 3-18, indicating that consistent vertical mixing takes place between cells a (diffuser location) and the other sites, consistent with CFD predictions.

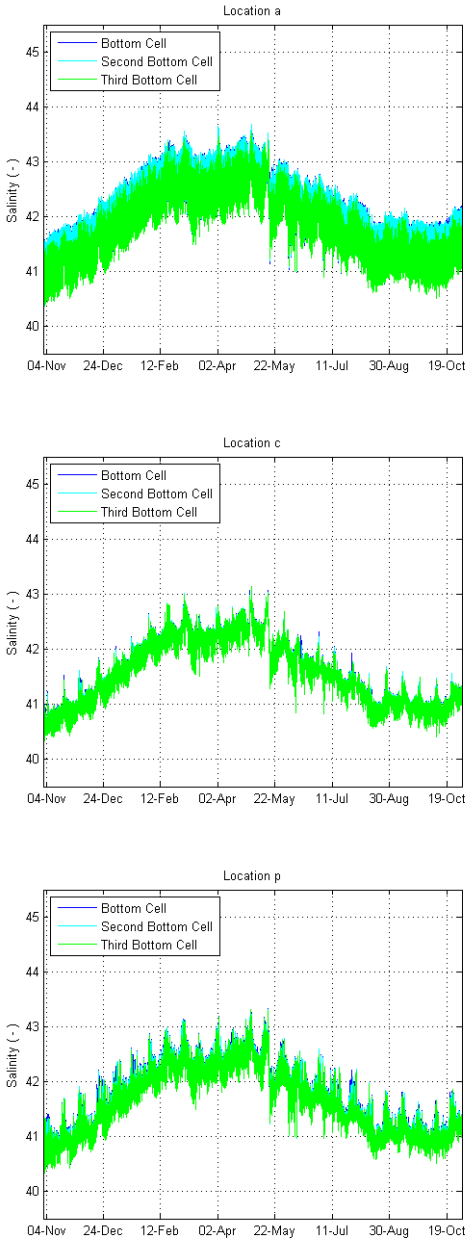

Figure 3-18 Salinities at the bottom for points a, c and p

3.4.2 Curtain along the Diffuser Line

Analysis of minimum dilution over the simulation period on a vertical curtain running from inshore to offshore the diffuser line from corresponding to points d to e (Figure 3-12) is presented in Table 3-2. The longest duration that modelled dilutions were continuously lower than the target dilutions is presented in Table 3-3 to Table 3-5.

Table 3-2 Minimum dilutions in a curtain from points d to e over the entire one year simulation. Dilutions smaller than 85:1 given in bold. Hatched cells represent land cells. k is the vertical cell index, and z is the cell elevation given in mAHD. Cell grid sizes varied between 40 and 65 m.

		Dilution						
		e	f	o	a	q	r	d
Distance Along the Path		0	178.2	405.2	584.9	764	950.7	1188.7
K = 31	z = 0.98	196	211	229	260	266	269	204
K = 30	z = -1.02	193	167	209	219	210	196	204
K = 29	z = -3.02	146	163	189	214	212	203	205
K = 28	z = -4.92	145	147	178	215	215	218	206
K = 27	z = -6.65		116	161	187	211	206	203
K = 26	z = -8.22		96	144	164	197	205	200
K = 25	z = -9.67		93	139	146	197	185	200
K = 24	z = -11.02		87	131	136	185	179	188
K = 23	z = -12.27		**84**	113	132	176	175	176
K = 22	z = -13.42		**83**	92	124	127	163	169
K = 21	z = -14.47			**75**	117	122	159	157
K = 20	z = -15.47			**58**	112	112	151	143
K = 19	z = -16.47			**53**	96	105	127	128
K = 18	z = -17.47			**47**	85	101	105	123
K = 17	z = -18.47			**40**	**72**	**59**	**81**	106
K = 16	z = -19.47			**37**	**47**	**58**	**48**	102
K = 15	z = -20.47			**34**	**41**	**54**	**54**	**70**
K = 14	z = -21.47			**32**	**36**	**51**	**56**	**52**
K = 13	z = -22.47			**31**	**33**	**48**	**49**	**52**
K = 12	z = -23.52			**31**	**29**	**37**	**41**	**49**
K = 11	z = -24.67			**31**	**29**	**33**	**34**	**42**
K = 10	z = -25.92				**29**	**32**	**34**	**36**

Table 3-3 Longest duration that modelled dilutions (in seconds) in a curtain from points d to e were lower than 85:1 over the entire one year simulation. Hatched cells represent land cells. k is the vertical cell index, and z is the cell elevation given in mAHD. Cell grid sizes varied between 40 and 65 m.

		Longest Duration of Dilutions Lower than 85:1 in seconds						
		e	f	o	a	q	r	d
Distance Along the Path		0	178.2	405.2	584.9	764	950.7	1188.7
K = 31	z = 0.98	0	0	0	0	0	0	0
K = 30	z = -1.02	0	0	0	0	0	0	0
K = 29	z = -3.02	0	0	0	0	0	0	0
K = 28	z = -4.92	0	0	0	0	0	0	0
K = 27	z = -6.65		0	0	0	0	0	0
K = 26	z = -8.22		0	0	0	0	0	0
K = 25	z = -9.67		0	0	0	0	0	0
K = 24	z = -11.02		0	0	0	0	0	0
K = 23	z = -12.27		960	0	0	0	0	0
K = 22	z = -13.42		1200	0	0	0	0	0
K = 21	z = -14.47			1440	0	0	0	0
K = 20	z = -15.47			3360	0	0	0	0
K = 19	z = -16.47			4320	0	0	0	0
K = 18	z = -17.47			5520	0	0	0	0
K = 17	z = -18.47			12240	2400	2400	2400	0
K = 16	z = -19.47			15840	4080	3600	2400	0
K = 15	z = -20.47			20880	8400	8400	4800	1440
K = 14	z = -21.47			37440	18480	10800	9600	4080
K = 13	z = -22.47			44160	34800	15600	14400	5040
K = 12	z = -23.52			70560	93120	28800	26400	12480
K = 11	z = -24.67			79920	181200	69600	55200	29280
K = 10	z = -25.92				231360	91200	72000	60960

Table 3-4 Longest duration that modelled dilutions (in seconds) in a curtain from points d to e were lower than 55:1 over the entire one year simulation. Hatched cells represent land cells. k is the vertical cell index, and z is the cell elevation given in mAHD. Cell grid sizes varied between 40 and 65 m.

		Longest Duration of Dilutions Lower than 55:1 in seconds						
		e	f	o	a	q	r	d
Distance Along the Path		0	178.2	405.2	584.9	764	950.7	1188.7
K = 31	z = 0.98	0	0	0	0	0	0	0
K = 30	z = -1.02	0	0	0	0	0	0	0
K = 29	z = -3.02	0	0	0	0	0	0	0
K = 28	z = -4.92	0	0	0	0	0	0	0
K = 27	z = -6.65		0	0	0	0	0	0
K = 26	z = -8.22		0	0	0	0	0	0
K = 25	z = -9.67		0	0	0	0	0	0
K = 24	z = -11.02		0	0	0	0	0	0
K = 23	z = -12.27		0	0	0	0	0	0
K = 22	z = -13.42		0	0	0	0	0	0
K = 21	z = -14.47			0	0	0	0	0
K = 20	z = -15.47			0	0	0	0	0
K = 19	z = -16.47			1440	0	0	0	0
K = 18	z = -17.47			2160	0	0	0	0
K = 17	z = -18.47			3600	0	0	0	0
K = 16	z = -19.47			6480	1200	0	2400	0
K = 15	z = -20.47			16080	5040	2400	2400	0
K = 14	z = -21.47			22080	9360	2400	0	1680
K = 13	z = -22.47			37440	25920	4800	4800	1920
K = 12	z = -23.52			50400	55680	20400	10800	2400
K = 11	z = -24.67			70320	120720	63600	24000	12960
K = 10	z = -25.92				161520	66000	40800	28560

Table 3-5 Longest duration that modelled dilutions (in seconds) in a curtain from points d to e were lower than 45:1 over the entire one year simulation. Hatched cells represent land cells. k is the vertical cell index, and z is the cell elevation given in mAHD. Cell grid sizes varied between 40 and 65 m.

		Longest Duration of Dilutions Lower than 45:1 in seconds						
		e	f	o	a	q	r	d
Distance Along the Path		0	174.8	392.9	572.6	751.6	608.5	1175.8
K = 31	z = 0.98	0	0	0	0	0	0	0
K = 30	z = -1.02	0	0	0	0	0	0	0
K = 29	z = -3.02	0	0	0	0	0	0	0
K = 28	z = -4.92	0	0	0	0	0	0	0
K = 27	z = -6.65		0	0	0	0	0	0
K = 26	z = -8.22		0	0	0	0	0	0
K = 25	z = -9.67		0	0	0	0	0	0
K = 24	z = -11.02		0	0	0	0	0	0
K = 23	z = -12.27		0	0	0	0	0	0
K = 22	z = -13.42		0	0	0	0	0	0
K = 21	z = -14.47			0	0	0	0	0
K = 20	z = -15.47			0	0	0	0	0
K = 19	z = -16.47			0	0	0	0	0
K = 18	z = -17.47			0	0	0	0	0
K = 17	z = -18.47			1680	0	0	0	0
K = 16	z = -19.47			4560	0	0	0	0
K = 15	z = -20.47			8400	1200	0	0	0
K = 14	z = -21.47			16320	2640	0	0	0
K = 13	z = -22.47			35040	12480	0	0	0
K = 12	z = -23.52			35520	44160	7200	2400	0
K = 11	z = -24.67			50400	83760	34800	13200	5280
K = 10	z = -25.92				102480	64800	28800	21600

3.4.3 Dilution Contour Maps and Time Series

Dilution contour maps are presented for the 85:1 and 45:1 dilution targets. These dilutions were expressed in terms of 0^{th}, 1^{st}, 10^{th}, and 50^{th} percentiles. They do not represent snapshots in time, but rather are cumulative maps of brine extents. These percentiles were calculated for each bottom cell of the model and represent the relative period in which dilutions remain below the given target. For example, the 0^{th} percentile represents the minimum dilution observed in each model computational cell over the simulation period. The dilution maps are presented in Figure 3-19 to Figure 3-21. The model results indicated that the area corresponding to dilutions less than 85:1 is zero for the 50^{th} percentile and above. The relative areas for each dilution target and percentile are presented in Table 3-6.

It is noted that the subsequent figures represent dilution maps that differ from those presented in the DEIS for the following reasons:

a) The SEIS maps are produced over a one year period, whereas the DEIS maps were generated over a 40 day period.

b) The SEIS mps include a spatially variant long term (background) tracer initial condition whereas the DEIS maps were produced with no long term (spin-up) influences included within the simulation framework.

c) The SEIS model (from which the maps and data were generated) was of a much high temporal and spatial resolution (24 seconds and 40 metres, respectively) compared to the DEIS 'mid field' model (8 minutes and 200m, respectively). This results in much less numerical diffusion in the SEIS model than the DEIS model, and hence the more accurate and controlled transport of low dilution brine parcels.

d) The SEIS model was calibrated to a much higher standard (with extensive supporting targeted field data collection programs) than the DEIS model, to the extent that the SEIS model was able to better reproduce high (advective) currents, again leading to better representation of brine movement compared to the DEIS.

e) The SEIS model used a sophisticated linkage to a supporting near field model and superior to those used in the DEIS, this providing a more realistic and defensible suite of predictions than previously presented.

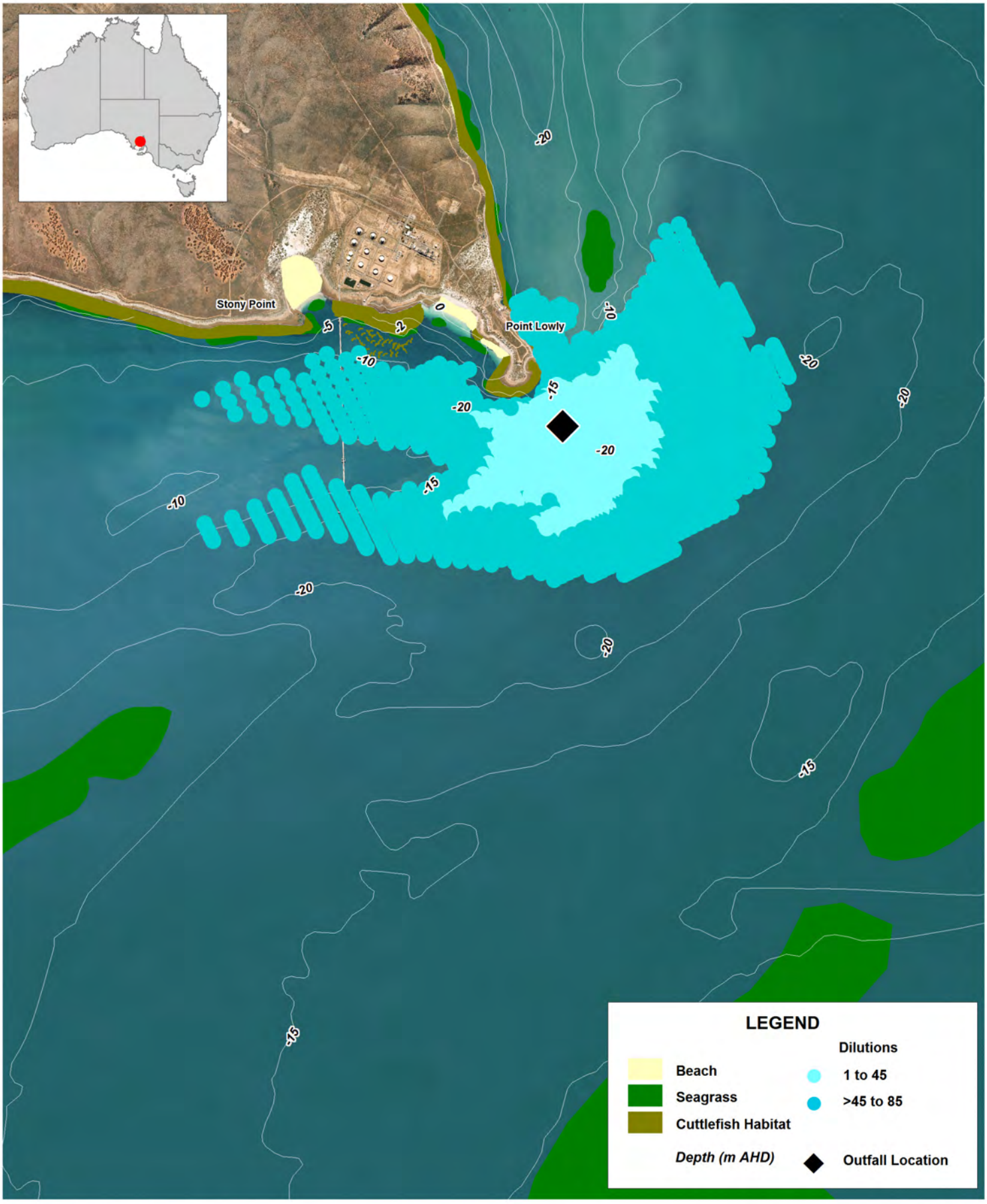

Title:

0th Percentile (Minimum) Dilution November 2007 to November 2008

Figure: 3-19

Rev: A

Air photo from Google Earth.

N

0 1 2km

Approx. Scale

BMT WBM

www.wbmpl.com.au

Filepath :

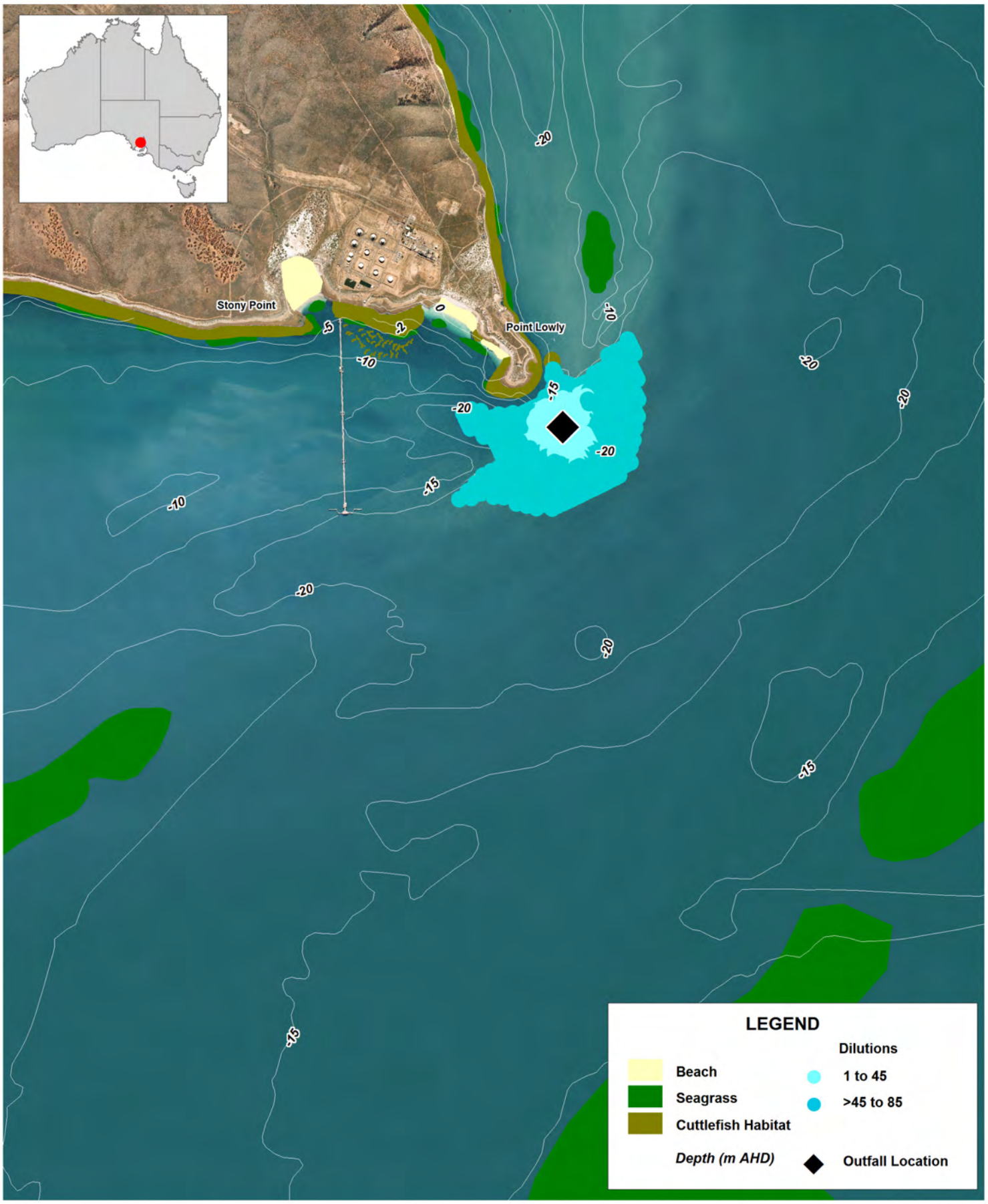

Title:

1st Percentile Dilution
November 2007 to November 2008

Figure: **3-20**

Rev: **A**

BMT WBM endeavours to ensure that the information provided in this map is correct at the time of publication. It does not warrant, guarantee or make representations regarding the currency and accuracy of information contained in this map.

Air photo from Google Earth.

N

0 1 2km

Approx. Scale

BMT WBM

www.wbmpl.com.au

Filepath :

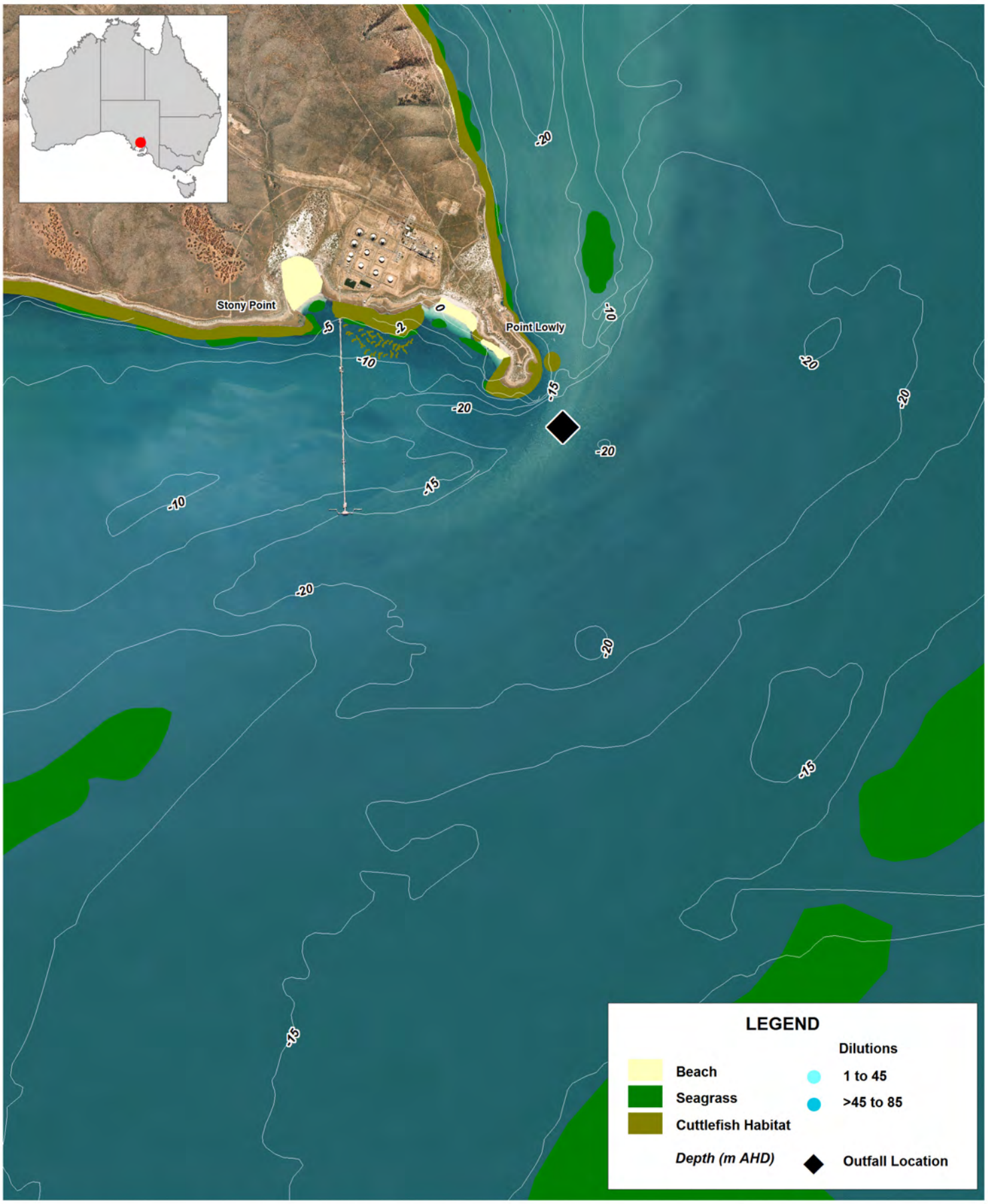

Title:

50th Percentile Dilution
November 2007 to November 2008

Figure: 3-21

Rev: A

BMT WBM endeavours to ensure that the information provided in this map is correct at the time of publication. It does not warrant, guarantee or make representations regarding the currency and accuracy of information contained in this map.

Air photo from Google Earth.

N

0 1 2km

Approx. Scale

BMT WBM

www.wbmpl.com.au

Filepath :

Table 3-6 Areas for the dilution target percentiles

Percentile	Area < 45:1 Dilution (m2)	Area < 55:1 Dilution (m2)	Area < 85:1 Dilution (m2)
0th	2,451,200	4,982,400	12,174,400
1st	379,200	849,600	2,027,200
10th	49,600	91,200	196,200
50th	0	0	0

The areas for the dilution target percentiles (footprints) can be put into perspective when compared to time series of areas under the dilution target (Figure 3-22). These were calculated by summing all cell areas at a given time step that presented a (dilution) less than each of the dilution targets. Figure 4-23 shows that in the worst cases, the instantaneous areas (as opposed to the areas presented in Figure 3-19 to Figure 3-21), were always less than half of the 0th percentile dilutions in Table 3-6, and the 98th percentile of the time series were less than one tenth of the 0th percentile dilution footprints (Figure 3-22). In other words, for the one year simulation, 98 percent of the time, the area of the brine discharge below a given dilution target was smaller than one tenth of the area given by the corresponding 0th percentile footprint.

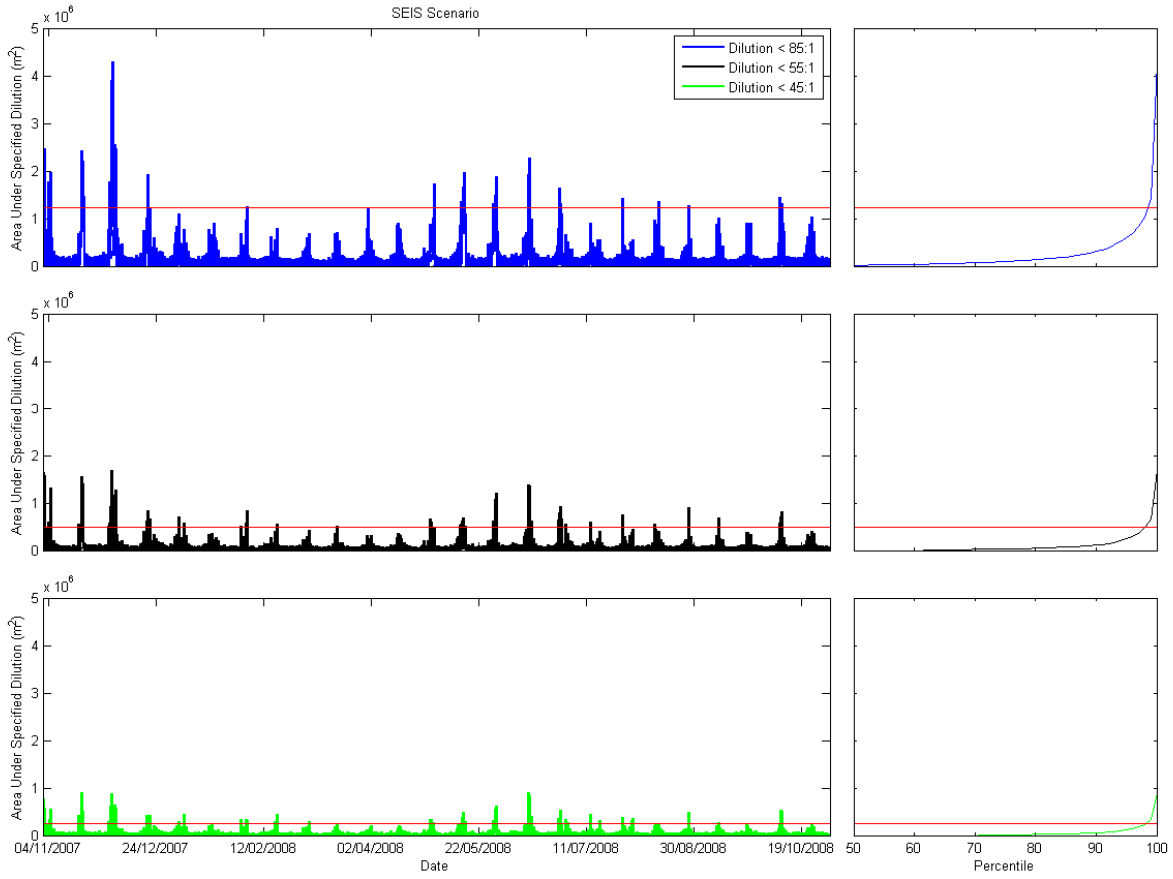

Figure 3-22 Time series for areas encompassing the dilution targets. Red line indicates an area equivalent to one tenth of the 0th percentile dilution presented in Table 3-6.

4 LONG TERM SIMULATIONS

In order to address considerations regarding the long term behaviour of the proposed return water discharge and investigate associated gulf wide influences, a lower resolution model was derived from the previously described high resolution model. Contrasting to the high resolution model for which the intent was focused in capturing detailed fine scale hydrodynamic processes at the region in the proximities of the proposed diffuser, the intent of this model was to provide indications of gross large scale (Northern Spencer Gulf and whole Spencer Gulf) and long term trends (inter-annual and climate change variability) aimed at assessment of broad scale processes and possible process changes. In addition, as described earlier, these simulations adopted a low resolution grid (hereafter low resolution model or low resolution simulation) and were used to provide background initial conditions for scalars (salinity, temperature, and tracers) for the high resolution model. The low resolution model is briefly described below.

4.1 Model Schematisation

4.1.1 Model Grid and Bathymetry

The model domain was designed to cover a similar area used in the high resolution model previously validated (SEIS Appendix 17.5.2). The model domain was discretised using a uniform 2 km grid size in both horizontal directions and the model bathymetry was extracted from the Digital Elevation Model presented in (SEIS Appendix 17.5.2). The horizontal grid superimposed on the model bathymetry is presented in Figure 4-1. A non-uniform grid size was used in the vertical direction (Figure 4-2). The resulting mesh consisted of 132 by 114 x 31 cells with a total of 106,060 maximum wet cells. An 1800 second time step was chosen to produce model stability and model output compatible with the high resolution model.

4.1.2 Simulation Period and Initial Conditions

Forcing data was available for all days in the years between 2004 and 2008 allowing simulations to be performed with concomitant data for a period of 4 years from November 2004 to November 2008. November was chosen for initial conditions as it generally coincides with the lowest salinities observed in the gulf, such that the cycle of salt build-up during summer and salt ejection in winter could be captured from the starting time of the simulation. Similarly to the high resolution model presented in BMT WBM (2010) salinity and temperature data collected on 1-2 November 1983 by Dr. Rick Nunes-Vaz (Nunes 1985) and HYCOM data at the open boundary were used to provide model initial conditions.

In order to assess any long term effects of the proposed desalination plant and to contrast the results with the effects of climate change (see Section 5), the data between 2004 and 2008 was appended successively 16 times such that a time series between 2004 and 2072 could be constructed. This allowed assessment of the effects of the desalination plant in the long term commensurate with the expected project life.

4.1.3 Model Forcing

The low resolution model adopted the same original forcing data used in the high resolution model previously validated (SEIS Appendix 17.5.2). This forcing included:

- The salt lake inflows in the northern boundary of the domain,
- The inflows and outflows associated with Port Augusta Power Station,
- Hourly water surface elevations at the open boundary conditions as derived from the combination of global tide model with mean surface elevations obtained from a global data assimilation model ,
- Daily temperature, and salinity at the open boundary conditions as derived from a global data assimilation model,
- Hourly and 16-20 km spatial resolution meteorological forcing (air temperature, solar radiation, net long wave radiation, relative humidity, wind speed and wind direction) as derived from the Weather Research Forecast model, and
- Daily rainfall derived from the Bureau of Meteorology SILO database.

The open boundary conditions were imposed in the South and South Eastern ends of the rotated domain (Figure 4-1) and adopted the data illustrated in Figure 4-3 (not all data shown for clarity). It can be seen that there is no appreciable change between east and west boundary conditions, however, there is strong seasonal variation in the temperature and salinity, consistent with the "density" plug for the salt ejection mechanism imposed by upwelling at the shelf (see Nunes-Vaz et al. 1990).

The forcing distribution at the free surface for the low resolution model is shown in Figure 4-4 and the forcing at selected boundary condition sets are shown in Figure 4-5. The data is plotted at daily resolution (11:30 AM each day) for clarity and reveals the strong latitudinal variability, particularly in the relative humidity air temperature that are the drivers for increased summer evaporation rates in the Northern Gulf.

For the long term simulations the meteorological data forcing and the salinity and temperatures at the open boundaries were successively appended to the end of the time series until forcing between 2004 and 2072 were obtained. For the water surface elevations at the open boundaries, data for the period was reconstructed from harmonic analysis of the 2004-2008 period. The residuals between the raw tidal data and the harmonic components of the 2004-2008 period was the added to the harmonic components on a similar fashion of the meteorological and scalar data at the open boundaries. Discussion of the 2004-2008 data is presented with the climate change forcing parameterisation in Section 5.1.1.

Additionally, the model adopted inflows from the desalination plant outfall and outflows from the desalination plant intake. The flow rates, salinity, and temperature associated with the desalination plant are described below.

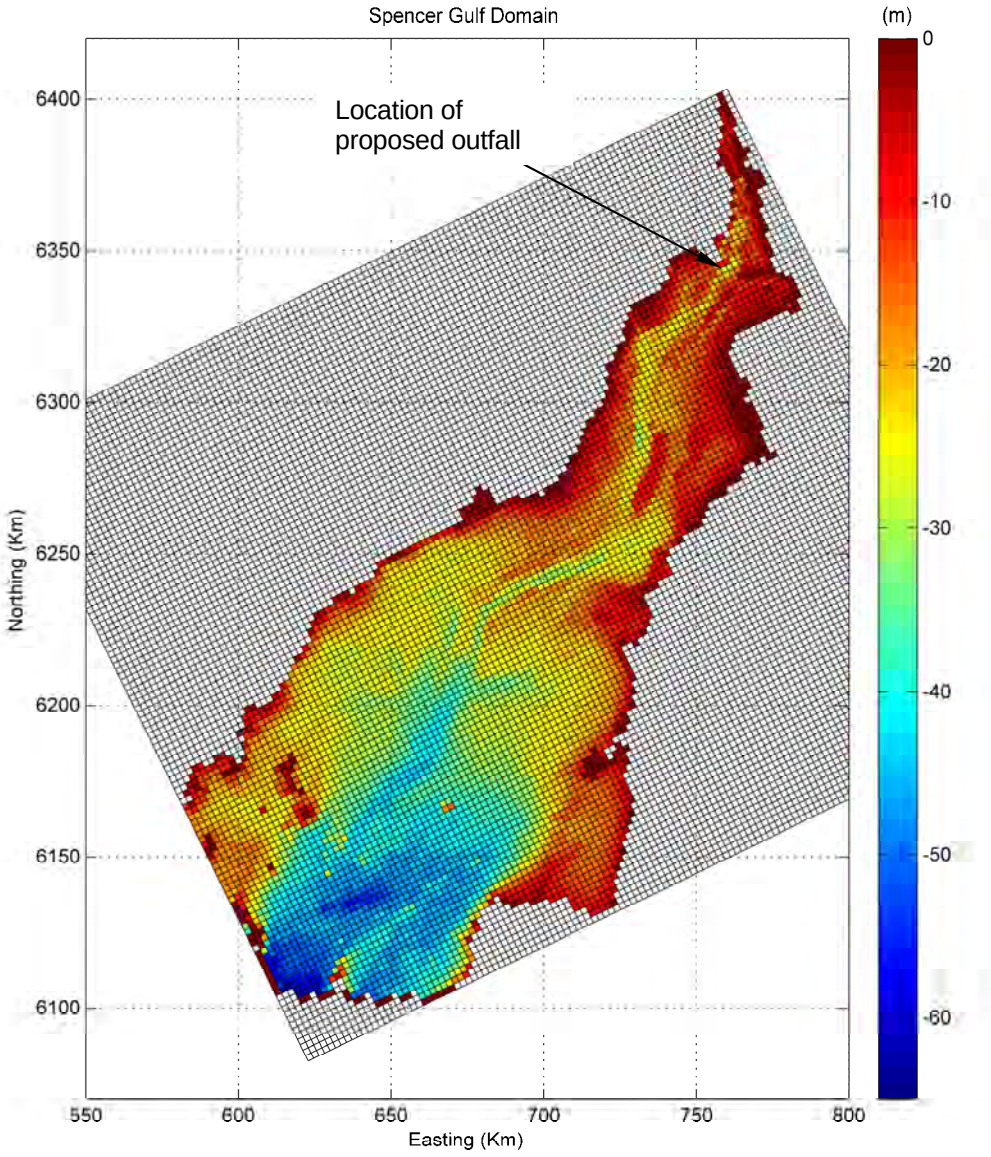

Figure 4-1 Model horizontal grid superimposed on bathymetry. Level referenced to Australian Height Datum (mAHD).

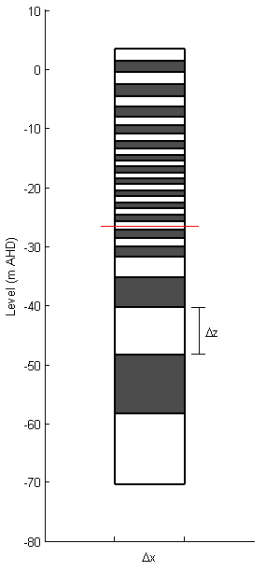

Figure 4-2 Vertical grid distribution. Red line indicates seabed level at the proposed diffuser location.

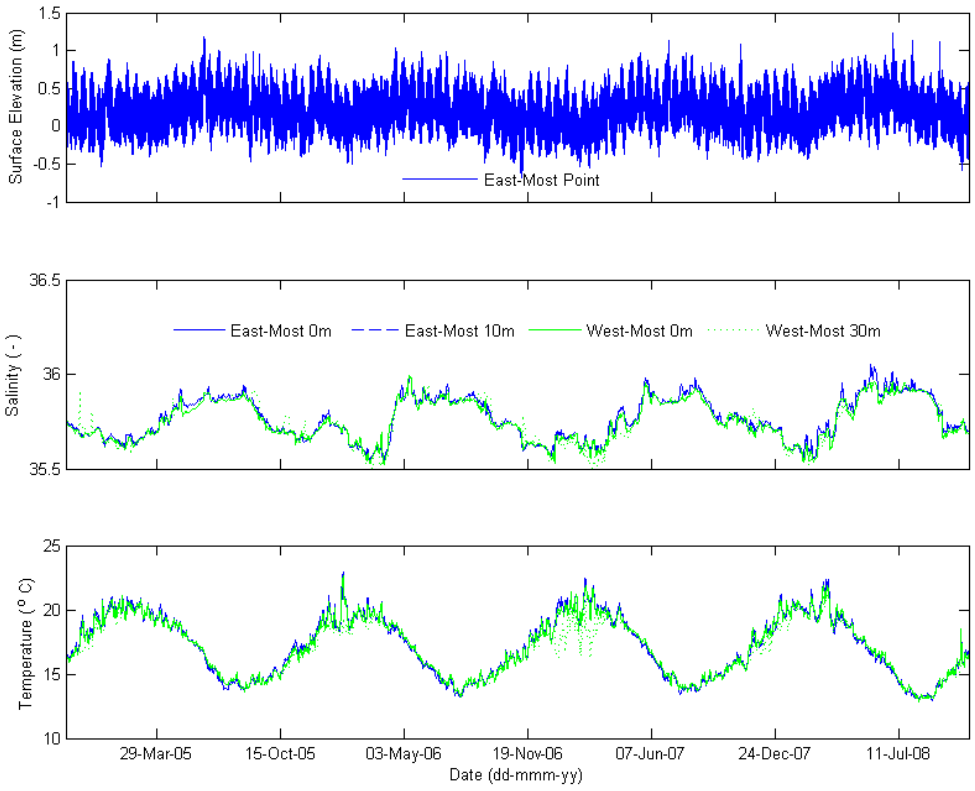

Figure 4-3 Data forcing at open boundary conditions

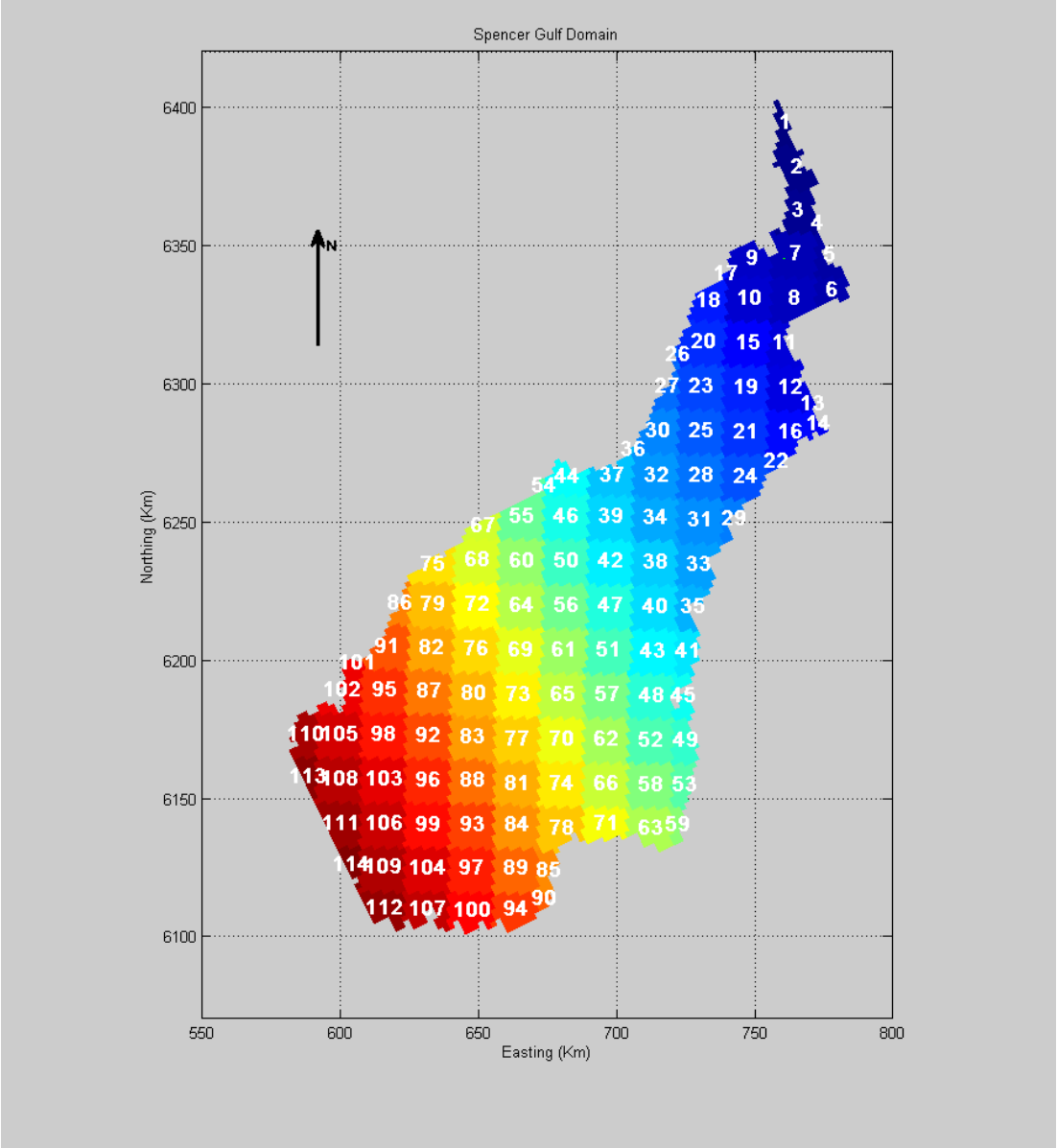

Figure 4-4 Distribution of the forcing at the free surface. The colours and numbers indicate sets where a same surface boundary condition is adopted.

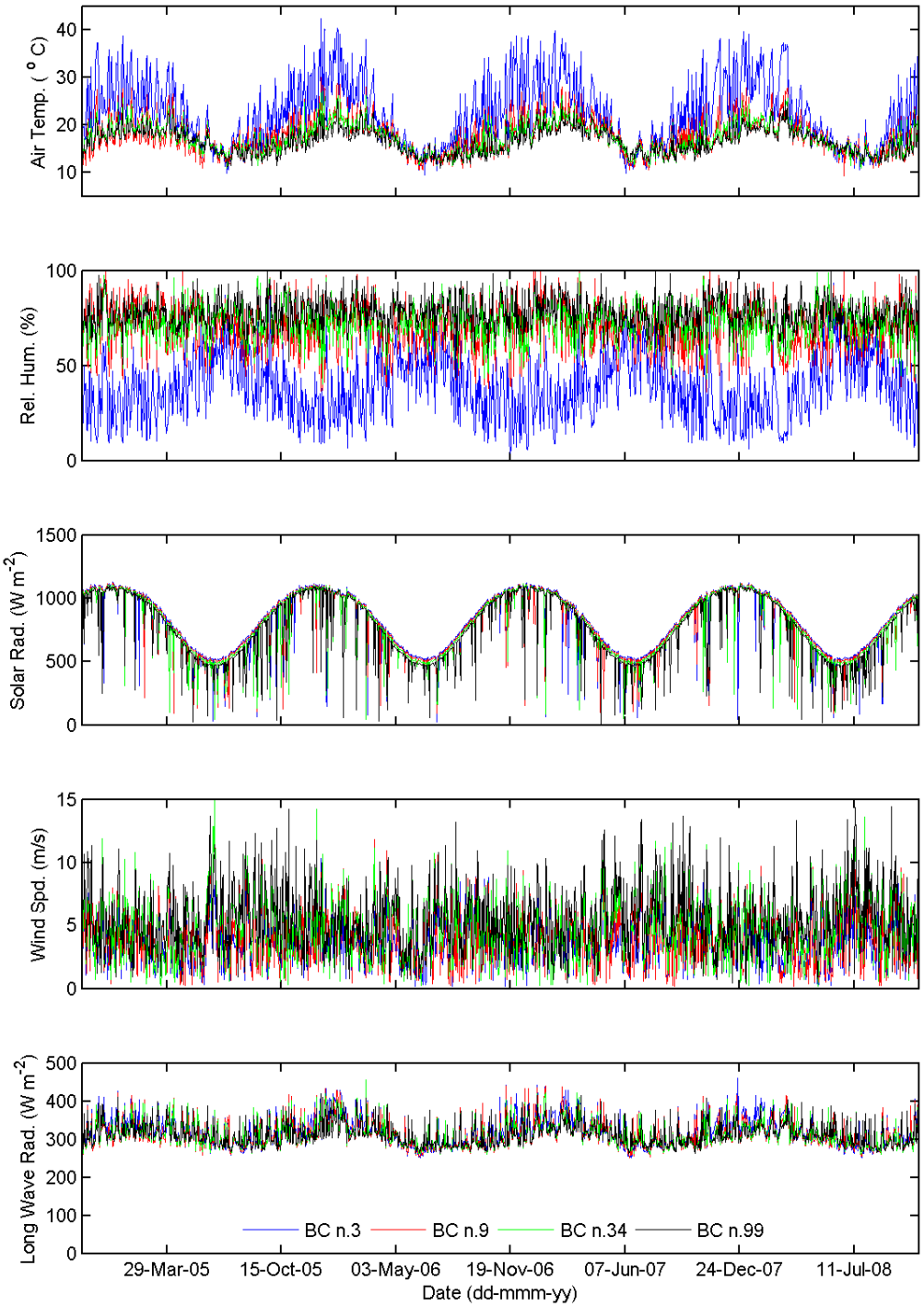

Figure 4-5 Forcing at selected surface boundary condition sets. Boundary condition numbers can be associated with the values shown in Figure 4-4. Strong north-south variation in key atmospheric data sets is clear.

4.2 Desalination Input

The long term and broad scale effects of the proposed desalination plant intake and outfall were accounted for in one of the simulation sets (for the period between 2004 and 2072) and assumed yearly average discharge rates throughout the simulation. The characteristics of the proposed desalination plant discharge are summarised in Table 4-1.

Table 4-1 Assumed proposed desalination plant discharges in the simulations

Simulation Code	Period (Nov to Nov)	Intake Rate m^3/s	Outfall Rate m^3/s
B	2004-2072	0.00	0.00
B+D	2004-2072	4.95	2.79

Outfall discharge salinity and temperature assumed the initial dilution as described for the high resolution simulations. As a result of the grid resolution, velocities from the low resolution model at the location of the proposed discharge were consistently lower than velocities computed with the high resolution model. This occurs because a 2 km grid is of a too coarse a resolution to describe the fine scale and non-uniform flow features in the flow convergence through "The Rip". In order to apply the same methodology in the low resolution method context (i.e. locate a correct dilution from CFD analyses), a linear scaling between depth averaged velocity magnitudes in the low and high resolution models was obtained for both ebb and flood tides (Figure 4-6), and the scaling was then applied to the low resolution model velocities before looking up expected dilutions from the CFD results. The scaling associated with the minimum root mean square error (RMSE) between the high resolution data and the scaled low resolution data was applied in the computation of dilutions at the outfall discharge.

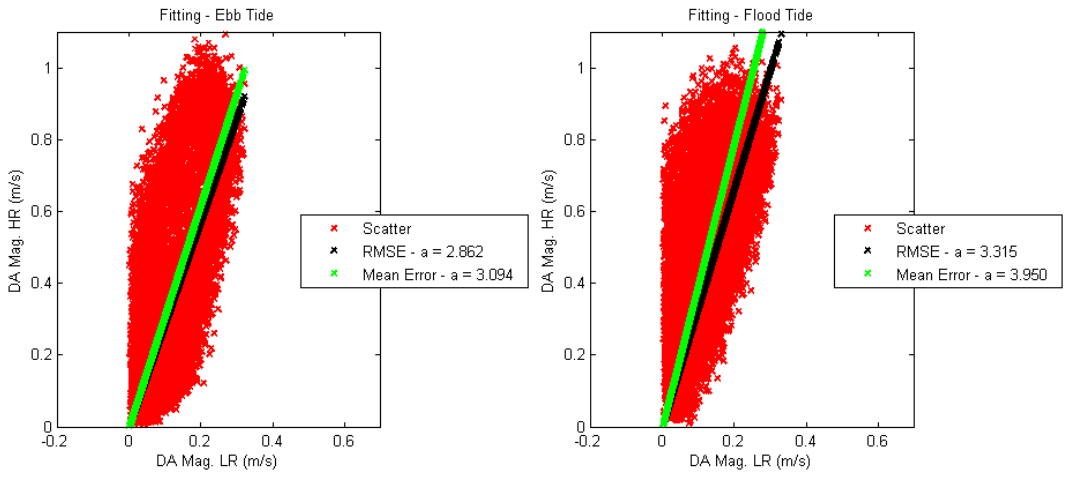

Figure 4-6 Velocity scaling between low and high resolution models at the proposed outfall location

4.3 Model Validation

Model validation was performed to show the model's ability in reproducing large scale features in Spencer Gulf, particularly the salt ejection mechanism, tide amplification, and latitudinal and seasonal gradients of temperature and salinity. This level of validation is commensurate with the description of the features of broad scale processes in Spencer Gulf and has been set to match the intended model use as described above.

4.3.1 Salt Ejection

The mechanisms responsible for salt dynamics in Spencer Gulf have been extensively described in the high resolution model validation report and Appendices of the DEIS and the reader is directed to these references for further details. The ability of the low resolution model to reproduce this dynamics is illustrated in Figure 4-7 and Table 4-2. Figure 4-7 shows very clearly the consistency between the salt fluxes given by the low and high resolution models, which were based in the same high temporal and spatial resolution forcing, indicating that both models are equivalent when used to assess the broad scale features in Spencer Gulf, reproducing the tendency of salt accumulation in summer and salt ejection in winter.

Annual salt budgets indicated a difference of less than 3.1% between high and low resolution models, with very similar incoming and outgoing tidal fluxes (Table 4-2). For the 2004-2005 year, the low resolution model indicated a small tendency of salt accumulation in the Gulf, which was reversed for the average of the 2004-2008 period as shown in the high resolution model results (Table 4-2). These results indicate that both modelling approaches produce a near-zero net salt flux in the gulf with equivalent seasonal dynamics.

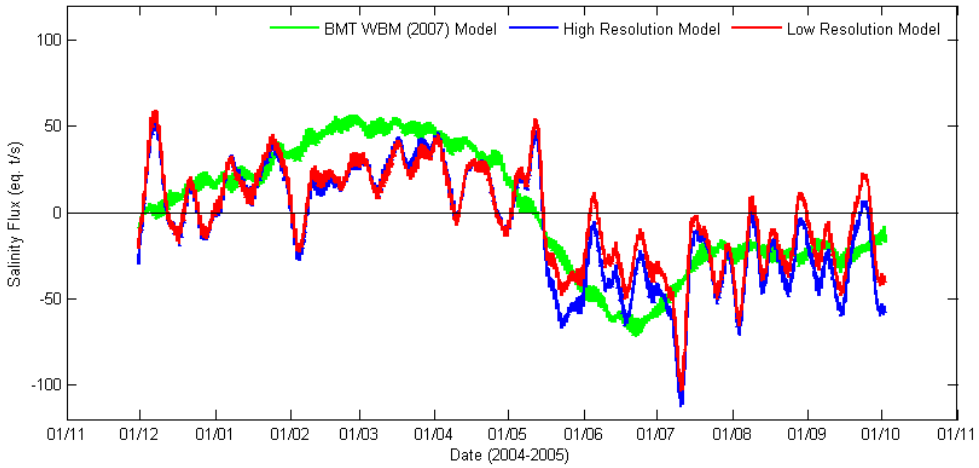

Figure 4-7 Salt fluxes obtained from the low and high resolution models

Table 4-2 Salt fluxes comparisons between high and low resolution model. Salinity values were assumed to be g/L.

Salt Flux Item	High Resolution 2004-2005	Low Resolution 2004-2005	Low Resolution 2004-2008 (Average)
	Gt/an	Gt/an	Gt/an
Tidal Influx	+253	+261	+262
Tidal Eflux	-254	-261	-262
Other inflows	+0	+0	+0

4.3.2 Salinity and Temperature Variation

Figure 4-8 and Figure 4-9 shows salinity and temperature contrasted with field data collected in the 1980s (Nunes 1985) at different locations (Port Augusta, Yatala Harbour, Point Lowly, and Wallaroo) across Spencer Gulf. These data indicate that the model was able to reproduce the increased data range variation with latitude in Spencer Gulf and also the seasonal variation revealed in the measured data set. Salinities at Port Augusta were under predicted by the model. As the high resolution model successfully reproduced the full data range variation at Port Augusta, it is believed that the low resolution model smears out the strong salinity gradients observed in that part of the Gulf (Nunes 1985) as a result of decreased grid resolution and associated increased numerical dispersion.

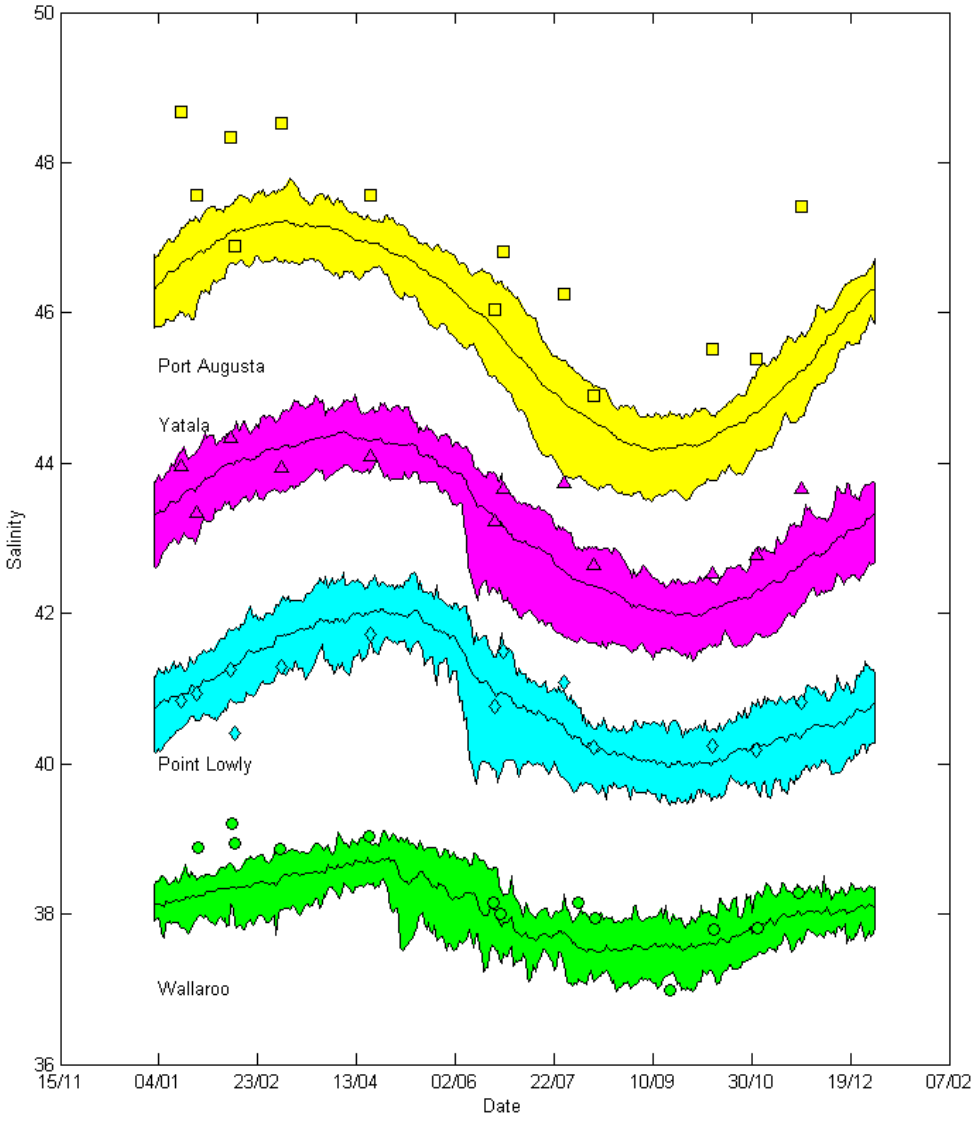

Figure 4-8 Modelled salinity evolution at different locations in the Gulf for the 2004-2008 period contrasted with field data from the 1980s (Nunes 1985). Coloured areas shows the data range evolution for each day of the year in the 2004-2008 period, the centre line shows the average for each day of the year in the 2004-2008 period, and the top and bottom lines show respectively the maximum and minimum for each day of the year in the 2004-2008 period. Field data is shown by the solid markers: circles for Wallaroo, diamonds for Point Lowly, triangles for Yatala Harbor, and squares for Port Augusta. Both modelled and field data at Port Augusta are uniformly and positively offset by 1.5 units (relative to actual values) and at Yatala Harbor by 1.0 unit. This has been done for clarity.

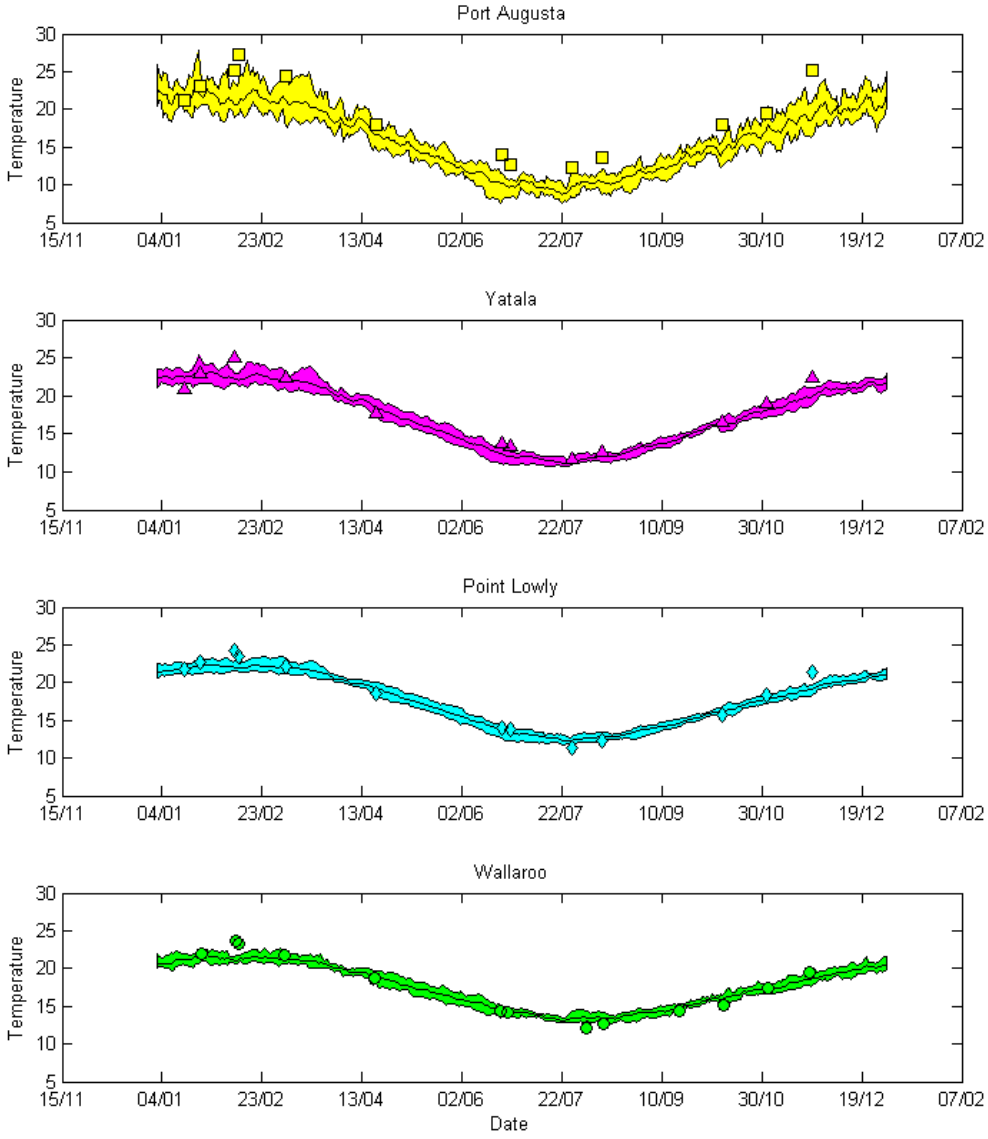

Figure 4-9 Modelled temperature evolution at different locations in the Gulf for the 2004-2008 period contrasted with field data from the 1980s (Nunes 1985). Same symbols as Figure 4-8.

4.3.3 Tidal Amplification and Modulation

The characteristics of the tides in Spencer Gulf were examined in detail during validation of the high resolution model, showing the adopted modelling framework was able to reproduce three major tidal features in Spencer Gulf.

- Tidal amplification of both diurnal and semi diurnal harmonics between Port Lincoln and Whyalla;
- Phase variation of these harmonics between Port Lincoln and Whyalla; and

- The relatively small semi-diurnal component associated with the (semi-diurnal) nodal point near Wallaroo.

Results of the low resolution model surface elevations were contrasted with the high resolution model to illustrate the low resolution model's ability in reproducing the tidal features of Spencer Gulf (Figure 4-10 and Figure 4-11). The results show both models reproduced very similar results at the different locations (Yatala Harbour, Point Lowly, and Wallaroo), particularly with respect to the tidal amplification between Wallaroo and Yatala Harbour, and the minimal semi-diurnal tidal influence at Wallaroo. In general, tidal range was underpredicted in the low resolution model, as expected from increased numerical dissipation associated with the lower grid resolution.

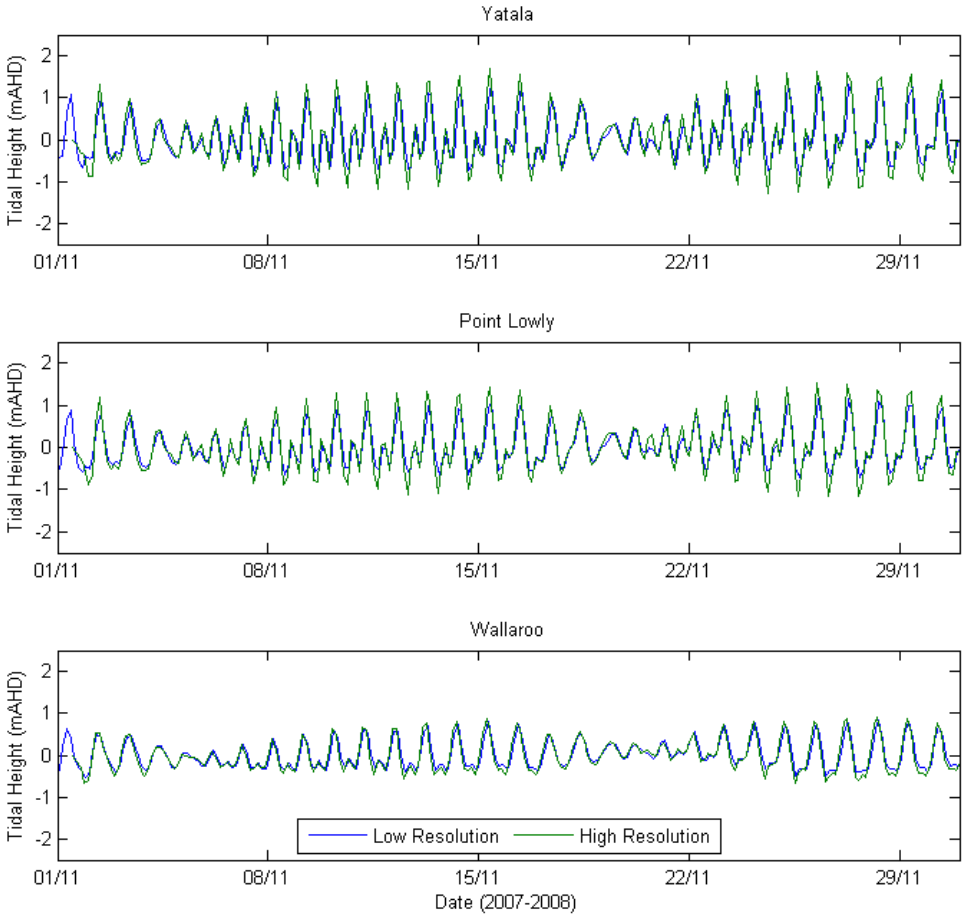

Figure 4-10 Comparison of tidal elevations obtained from the low and high resolution models November 2007

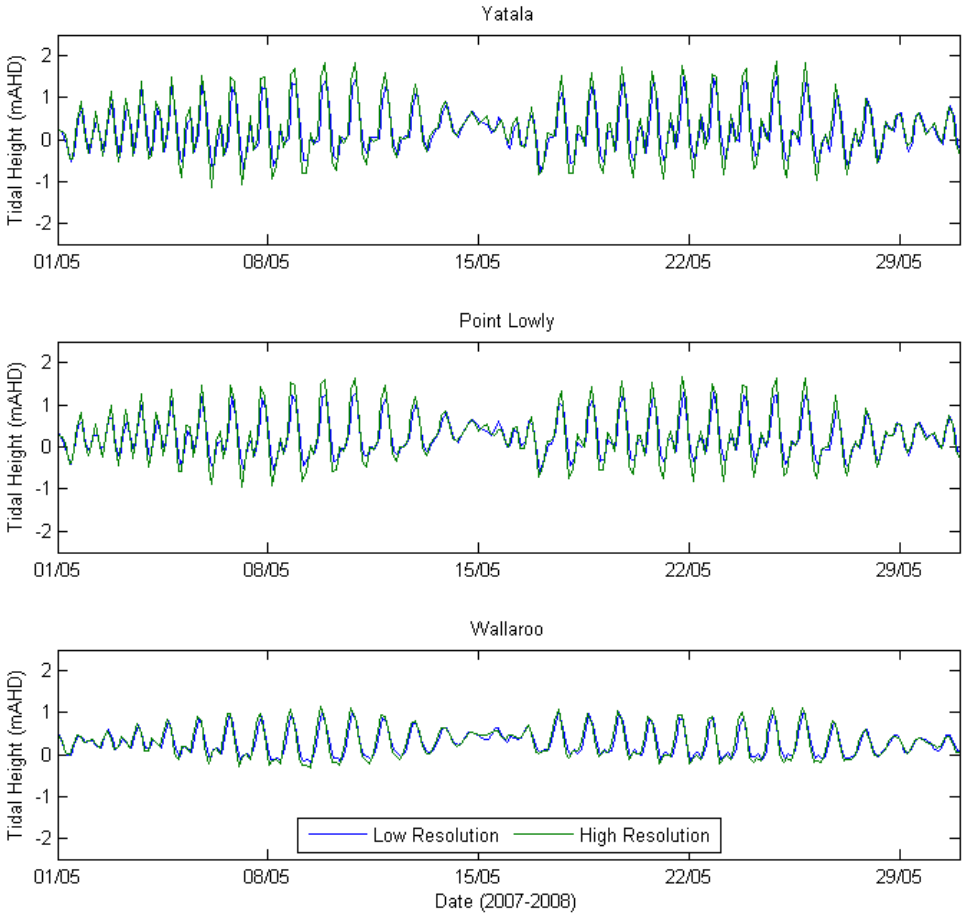

Figure 4-11 Comparison of tidal elevations obtained from the low and high resolution models in May 2008

4.4 Long-Term and Broad Scale Desalination Effects

The long term and broad scale effects of the proposed desalination plant in Spencer Gulf were assessed for two different areas. The first represents the whole Spencer Gulf and refers to model results extracted throughout the entire computational domain. The second area represents the Northern Spencer Gulf and refers to model results extracted from all computational cells located north of latitude 33.0^{o} S.

Figure 4-12 to Figure 4-15 show the time evolution of the Northern Spencer Gulf average salinities from simulation with and without the desalination plant. Two features can be identified in these plots. First, the seasonal aspects of the salinity in the Northern Gulf were not disrupted by the proposed discharge, such that salt accumulation in summer months and salt ejection in winter were not affected. Second, the brine discharge, although it induced increased average salinities in the Northern Spencer Gulf, did not produce continuing increases in salinities with time.

The average Northern Gulf salinity increase in the long term can be illustrated from the cumulative distributions presented in Figure 4-16 for the entire time series (2004 to 2072) and percentiles for

past (2004 to 2008) and future time horizons (2028 to 2032 and 2068 to 2072). No significant change in the difference between salinity percentiles (with and without the proposed discharge) can be distinguished for different periods. These were maintained always between 0.06 and 0.10 for the means and any of the presented percentiles, irrespective of period under consideration. The modelling results therefore indicated that the effects of the desalination discharge in the Northern Spencer Gulf salinities are within the range 0.06 to 0.10.

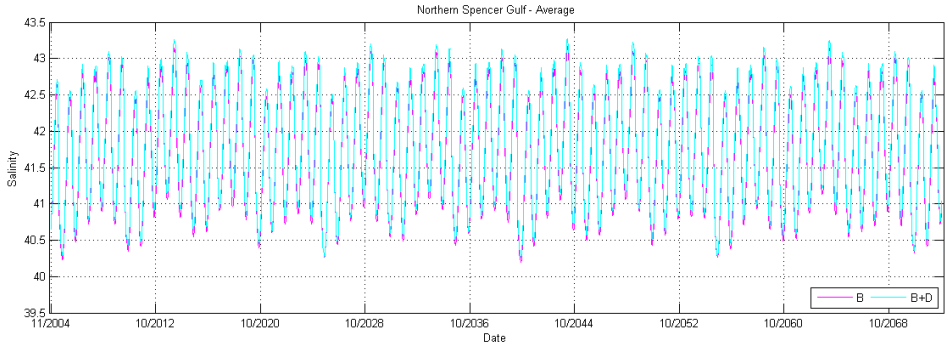

Figure 4-12 Modelled Northern Spencer Gulf averaged salinities with and without the proposed desalination plant outfall discharge for the 2004 to 2072 period.

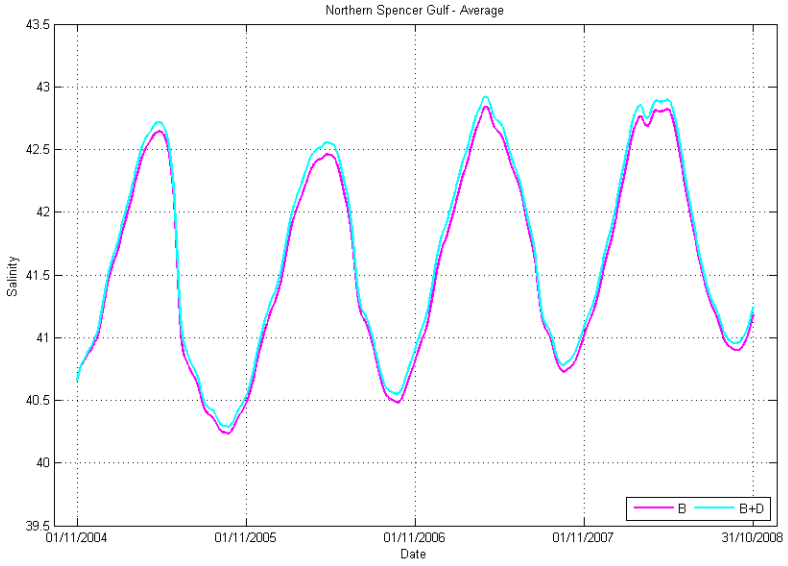

Figure 4-13 Modelled Northern Spencer Gulf averaged salinities with and without the proposed desalination plant outfall discharge for the 2004 to 2008 period.

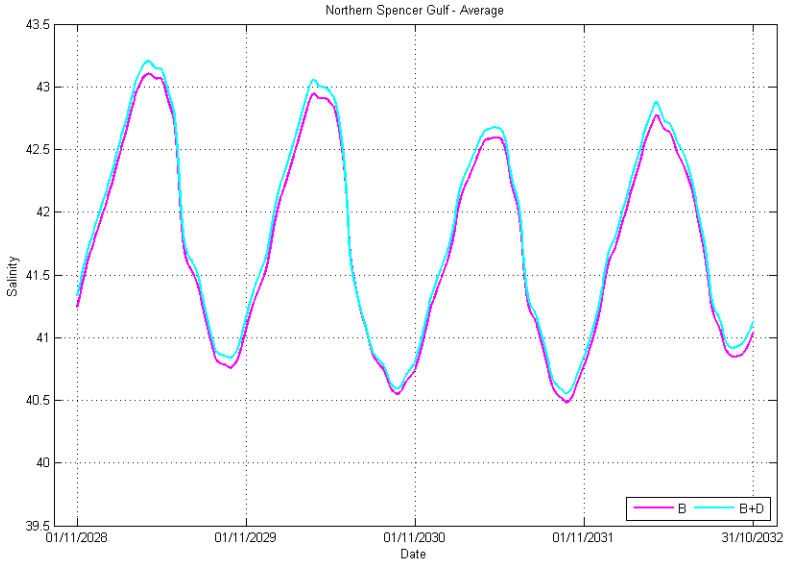

Figure 4-14 Modelled Northern Spencer Gulf averaged salinities with and without the proposed desalination plant outfall discharge for the 2028 to 2032 period.

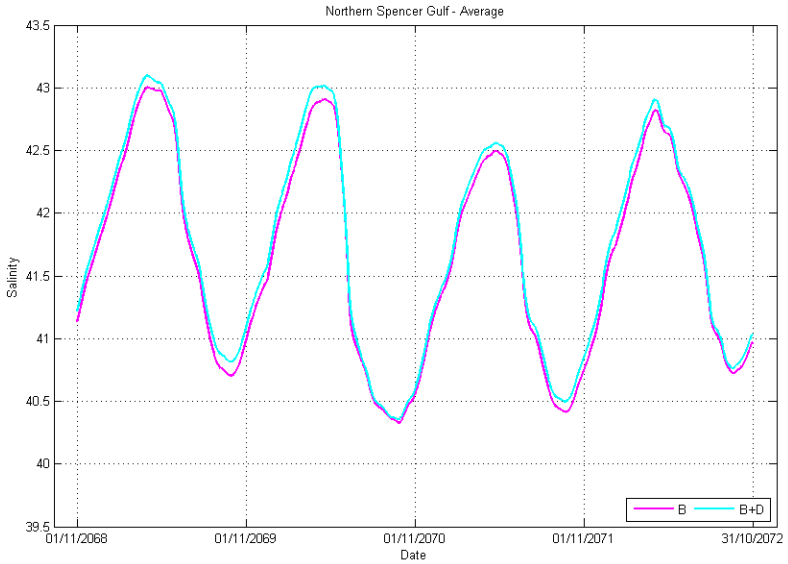

Figure 4-15 Modelled Northern Spencer Gulf averaged salinities with and without the proposed desalination plant outfall discharge for the 2068 to 2072 period.

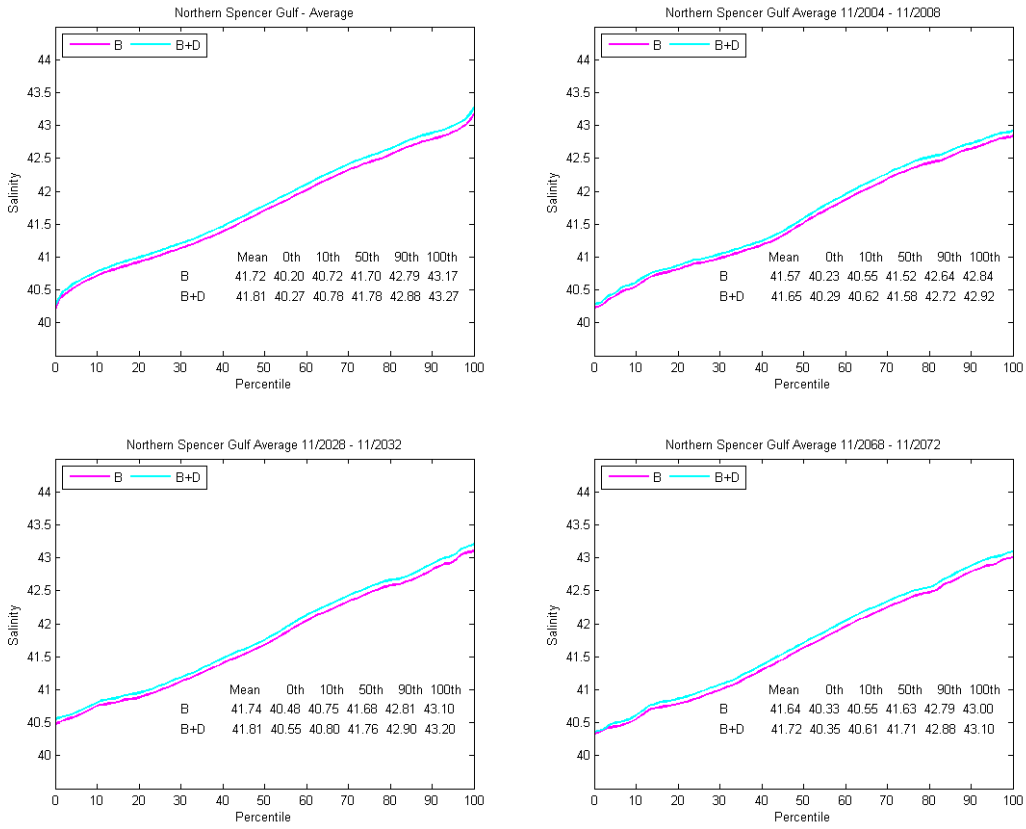

Figure 4-16 Modelled cumulative distributions of the Northern Spencer Gulf averaged salinities with and without the proposed desalination plant outfall discharge. Top left panel: 2004 to 2072 period; top right panel: 2004-2008 period; bottom left panel: 2028-2032 period; Bottom right panel: 2068-2072 period.

The modelled effects of the proposed desalination discharge over the entire Spencer Gulf were less pronounced than the effects in the Northern Spencer Gulf alone. Figure 4-17 to Figure 4-20 illustrate the average Spencer Gulf salinities for past and future time horizons. Similar conclusions to the Northern Gulf averaged salinities can be made for the entire Spencer Gulf, with the comment that the influences are of a much lesser magnitude. For example, the difference in percentiles irrespective of period were always smaller than 0.02 (Figure 4-21), and therefore below the accuracy of state of the art instruments used to measure salinity in the field.

Table 4-3 shows the magnitude of the annual salt fluxes from the different sources within Spencer Gulf. Firstly, it shows that the desalination plant intake and outfall balance each other, or in other words, although the proposed desalination plant contributed to larger salinities (particularly) in the Northern Spencer Gulf, it returns the same amount of salt extracted from the Gulf via its intake. Secondly it shows that the salt fluxes imposed by the desalination plant are about 0.0024% of tidal salt fluxes.

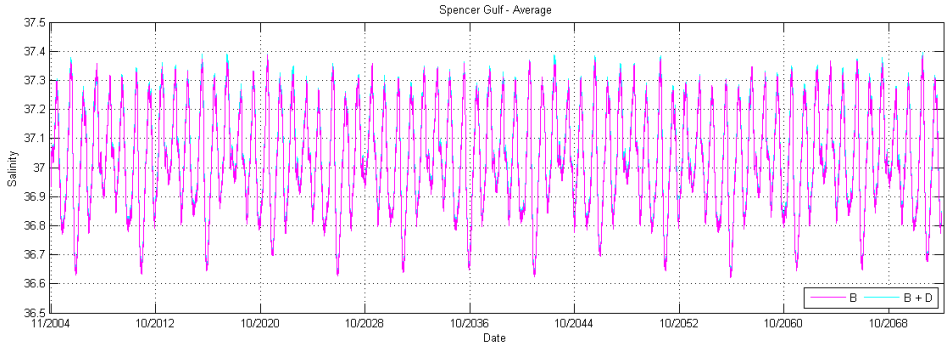

Figure 4-17 Modelled entire Spencer Gulf averaged salinities with and without the proposed desalination plant outfall discharge for the 2004 to 2072 period

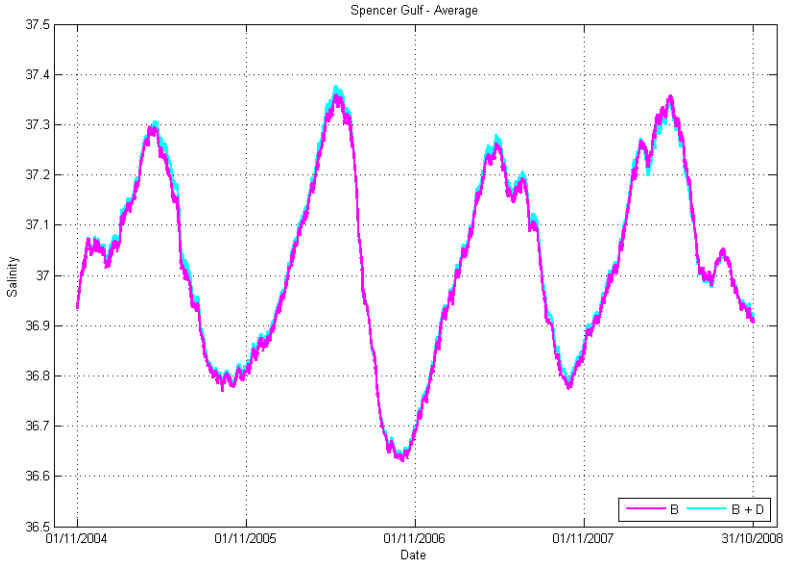

Figure 4-18 Modelled entire Spencer Gulf averaged salinities with and without the proposed desalination plant outfall discharge for the 2004 to 2008 period

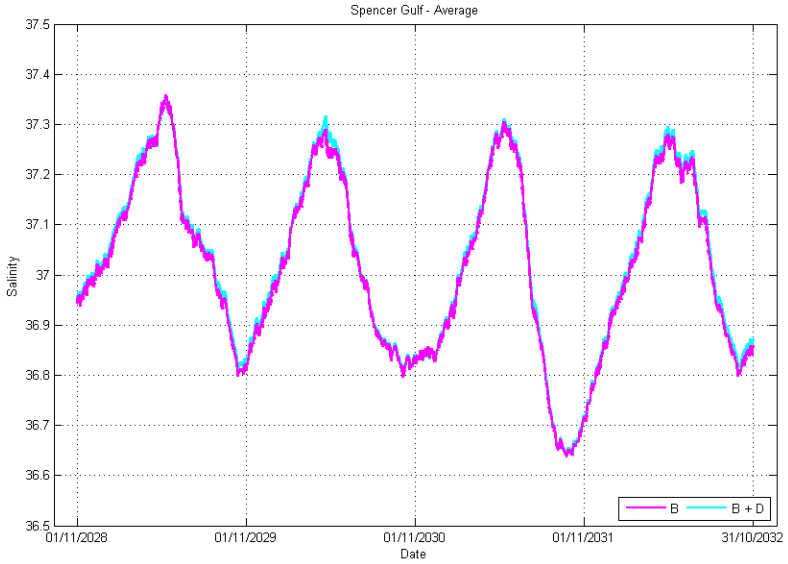

Figure 4-19 Modelled entire Spencer Gulf averaged salinities with and without the proposed desalination plant outfall discharge for the 2028 to 2032 period

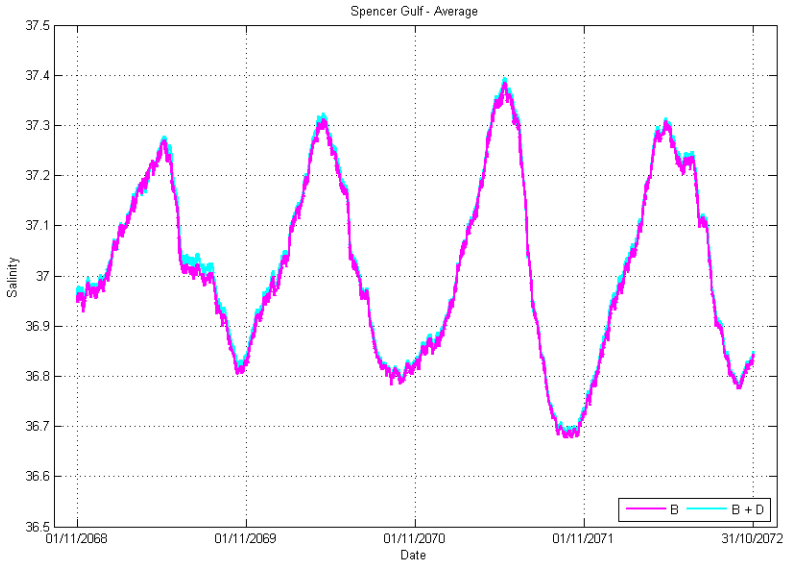

Figure 4-20 Modelled entire Spencer Gulf averaged salinities with and without the proposed desalination plant outfall discharge for the 2068 to 2072 period

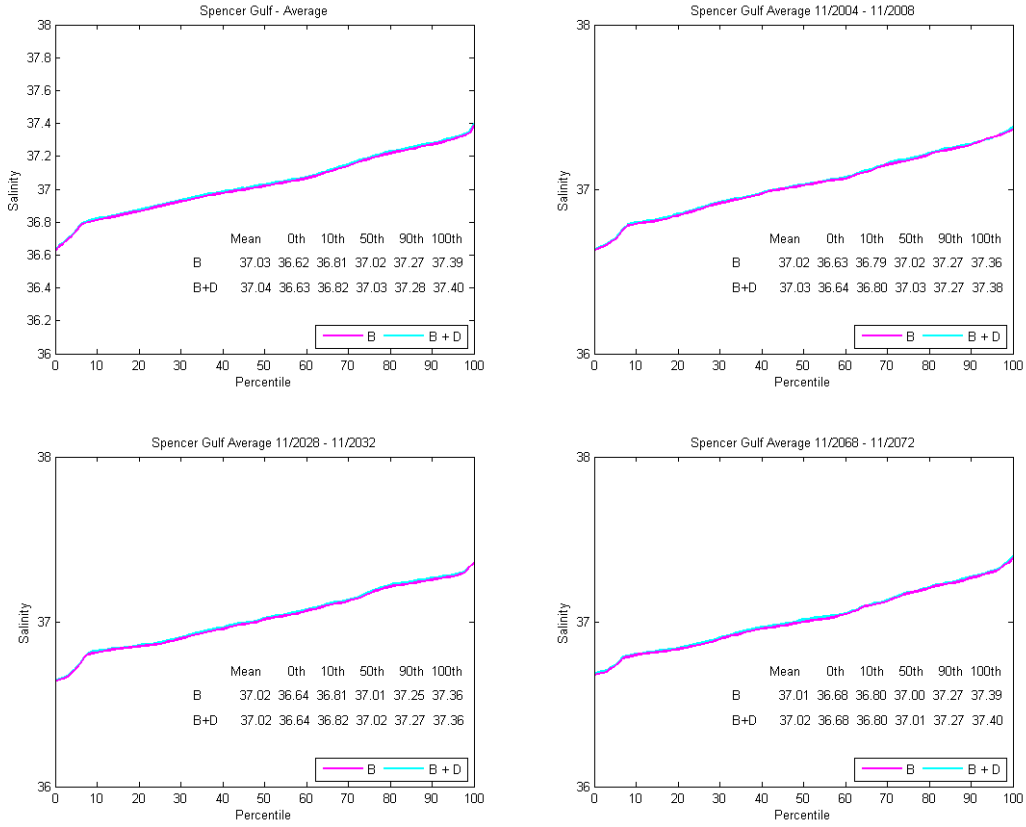

Figure 4-21 Modelled cumulative distributions of the entire Spencer Gulf averaged salinities with and without the proposed desalination plant outfall discharge. Top left panel: 2004 to 2072 period; top right panel: 2004-2008 period; bottom left panel: 2028-2032 period; Bottom right panel: 2068-2072 period.

Table 4-3 Simulated salt fluxes with and without the effect of the proposed desalination plant. Salinity values were assumed to be g/L.

Salt Flux Item	B: 2004-2008 (Average)	B: 2004-2072 (Average)	B+D: 2004-2008 (Average)	B+D: 2004-2072 (Average)
	Gt/an	Gt/an	Gt/an	Gt/an
Tidal Influx	+262	+261	+261	+261
Tidal Eflux	-262	-261	-261	-261
Desal. Return	0.00	0.00	+0.01	+0.01
Desal. Intake	0.00	0.00	-0.01	-0.01
Other inflows	+0.00	+0.00	+0.00	+0.00
Desalination intake and return salinities do not balance due to the constant 75 salinity assumed in the return water compared to the ambient salinities used in the intake calculations				

5 CLIMATE CHANGE SIMULATIONS

In order to address considerations regarding the long term behaviour of the proposed return water discharge within the context of climate change, further low resolution model simulations were undertaken where climate forcing was altered. Again, the influence of these changes were examined in terms of gulf wide and long term trends, matching the level of effort expended on model validation.

5.1 Model Schematisation

With the exception of boundary condition data, the same model configuration described in Section 4 was used for the assessment presented in this section. The climate change methodology to define the parameterisation used to alter the model forcing was externally peer-reviewed before and after its implementation. This methodology is described below.

5.1.1 Climate Change Parameterisation

The assessment presented herein assumes conditions consistent with the Special Report on Emissions Scenarios (SRES) A1FI storyline (IPCC 2007). This A1F1 storyline reflects the following scenario:

"A future world of very rapid economic growth, a global population that peaks in mid-century and declines thereafter, and the rapid introduction of new and more efficient technologies, but with a reliance on fossil intensive energy".

This scenario is the most conservative, does not assume CO_2 stabilization scenarios and imposes the larger increased atmospheric CO_2 concentrations, global temperature increase, and sea level rise (IPCC 2007). This is consistent with concerns raised in the DEIS Public Environmental Review (PER) process and recent Australian-context projections (Steffen 2009).

5.1.1.1 Meteorological Forcing

Suppiah et al. (2006) made projections within the South Australia context for future air temperature and rainfall changes based on 13 Global Climate Models (GCM) that were deemed to perform satisfactorily. These projections were then summarized for different seasons and climatic regions in South Australia for different future time horizons (2030 and 2070), in relation to a baseline defined as the thirty years period between 1974 and 1990. In short, "local changes were calculated as a local warming per ^{o}C of global warming by linearly regressing the local seasonal mean temperatures against global average temperatures smoothed by an 11-year running mean", such that "…the degree of change for a particular future date can then be calculated by multiplying the selected values on the map by the global warming value at that date" (Suppiah et al. 2006). This process was performed for all 13 models to arrive at a range of variation expected for future time horizons.

The projections of climate change made by Suppiah et al. (2006) were used to define the construction of air temperature and rainfall data used to force the low resolution hydrodynamic model. Construction of the forcing time series adopted the following general procedure:

- Monthly and seasonal means for the 2004-2008 Spencer Gulf-averaged (i.e. from the WRF model) data set were calculated;
- Monthly and seasonal means for the 1975-2004 (30-year centered in 1990) period were obtained from the IPCC DDC (Data Distribution Centre) HADCRUT3v data series;
- Monthly and seasonal means for the period 1988-1992 were computed (5 years centered on 1990);
- The anomaly of the Spencer Gulf monthly means with respect to the 1975-2004 and 1988-1992 data were computed for verification of data "quality" relative to the 3-decadal period;
- The estimates of air temperature and rainfall variation per degree of global warming from Suppiah et al. (2006) for Eyre Peninsula and Northern & Yorke NRM regions were used to calculate the increase to Spencer-Gulf average data set to achieve the same degree of temperature rise and rainfall reduction (detailed further below).

The IPCC DDC data was used to estimate how much increase would be applied to the 2004-2008 Spencer Gulf data, given the Suppiah et al. (2006) results were relative to the 1975-2004 period.

It should be noted that IPCC DDC data air temperatures were calculated as averages of all land and water (i.e. ship mounted) based stations at a $5^{o}x5^{o}$ resolution (Jones et al. 1999) by first calculating the average between minimum and maximum temperatures from each station in a given day and then computing the spatial average. The monthly-averages available from the IPCC DDC were then computed from this daily spatially-averaged data set. Hourly Spencer Gulf data was available over an area covering approximately $6^{o}x6^{o}$. Averaging of air temperatures were computed from a similar process to Jones et al. (1999), in which all Spencer Gulf (including both land and water based locations) maximum and minimum temperature for each day were used to provide a location daily mean, followed by a spatial averaging process for the latitude and longitude covered by the IPCC DDC data over Spencer Gulf.

Figure 5-1 shows the comparison between the IPCC DDC data and 2004-2008 Spencer Gulf data sets. Despite the differences in temporal and spatial nature of the data sets it can be seen that both data presented an equivalent evolution for the period 2004-2008 (i.e. both reflect the same features of the same climatic area). Additionally, the 5-year data between 2004 to 2008 provides a representation of observed annual ranges within the 1975-2004 data set. For example, 2005 is representative of a year that presented relatively small annual variations and 2006 is representative of a year that presented relatively large annual variations, with other years within a more normal annual variation range.

The seasonal averages of the different data sets are presented in Figure 5-2. While a small discrepancy can be seen between the different data sets, for the purposes of the current broadscale long term assessment, the meteorological forcing data, presented in Appendix 17.5.2, provides a robust starting point for applying climatic variations. Finer details of the methodology used to impose the climatic variations in the Spencer Gulf data set are presented below.

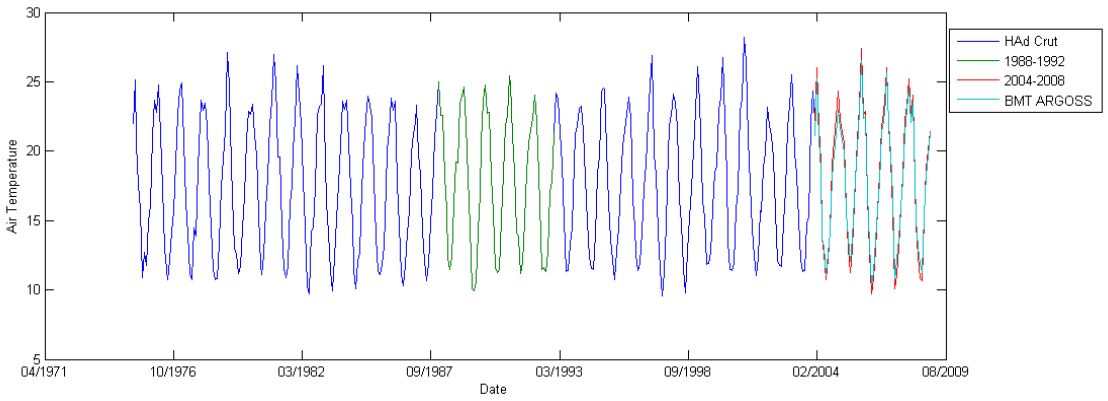

Figure 5-1 Comparison of monthly-averaged air temperatures between IPCC DDC HadCRUTv3 data with the Spencer Gulf WRF model data sets

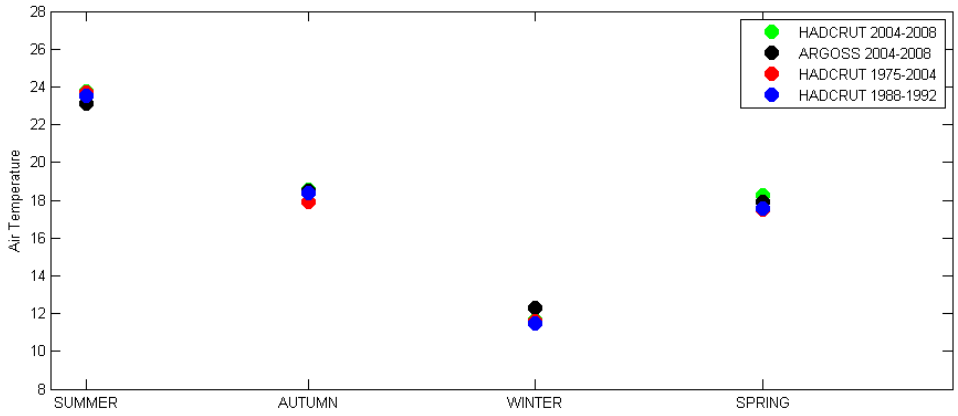

Figure 5-2 Comparison of seasonal averages between IPCC DDC HadCRUTv3 data with the Spencer Gulf WRF model data sets

With specification of climatic change for the 2030 and 2070 time horizons (from Suppiah et al., 2006) and the definition of a starting point climate record (2004 to 2008) presented above, the following procedure was used to define the climate data forcing the low resolution hydrodynamic model.

1 The seasonal variation for the future time horizons (2030 and 2070) given by Suppiah et al. (2006) was added to the seasonal average given by the IPCC DDC data (30-year centred in 1990) to form the seasonal averages at the future time horizon;

2 The difference between the seasonal averages at the future time horizons and the Spencer Gulf 2004-2008 seasonal averages was calculated, forming the baseline centred in 2006;

3 A linear increase between 2004-2008 (centred 2006) and the 2028-2032 (centred 2030) time horizon and the between the 2028-2032 and 2068-2072 (centred 2070) time horizons seasonal averages was assumed stipulating the required increase in 5-year seasonal averages;

4 The first year of the baseline (starting from 2004-2008) was appended to the end of the time series to form a new 5-year baseline (i.e., 2005-2009 centred 2007 for the first move);

5 A initial multiplication factor (initial guess) for each season was applied to the appended time series;

6 A new 5-year average of the IPCC DDC equivalent data was computed iteratively until the 5-year seasonal average matched the desired stipulated variation;

7 Steps 4 to 6 were repeated until a time series for the complete 2004-2072 data forcing was produced.

While the above procedure was described for air temperature, similar procedures were applied for all other meteorological variables with the exception to incoming long wave radiation. Changes for rainfall data, as previously described, were imposed on the daily records of the BoM SILO database.

The difference for these other data sets was that the changes imposed were based on projections of the Climate Change in Australia report (CSIRO 2007). However, data for these other variables were not available for the horizon centered around 1990, such that linear changes between 1990 and 2030 and between 2030 and 2070 were assumed. In these cases, the daily averages were based on the hourly data sets (instead of minimum and maximum considered for air temperatures in each day). Changes imposed at each of the future horizons, seasons and variables are presented in Table 5-1 and Table 5-2.

The resulting data sets can be compared to the baseline for the meteorological forcing in Figure 5-3 to Figure 5-8.

Projected changes for long wave radiation were not available. Changes for longwave radiation were imposed by assuming the effects of changes in air temperature alone (i.e. assuming greenhouse gases effects in the resulting radiation were already taken into account in the temperature change). The approach used assumed a relationship between cloud cover (C), air temperature (T_a), and long wave radiation (R_l).

$$R_l = \left(1 + 0.17C^2\right) C_\varepsilon T_a^6 \qquad (1)$$

Where C_ε is a constant (Swinbank 1963). Re-arranging (1) gives

$$C^2 = \frac{1}{0.17}\left(\frac{R_l}{C_\varepsilon T_a^6} - 1\right) \qquad (2)$$

A cloud cover time series for each surface boundary condition set was estimated from the 2004-2008 WRF incoming long wave radiation and air temperature and successively appended to form a cloud cover time series between 2004 and 2072. The prognostic air temperatures were then substituted into equation to compute the change in incoming longwave radiation due to air temperature change alone.

5.1.1.2 Open Boundary Forcing

The effects of climate change in the model open boundaries were accounted for in the mean sea level, and sea surface temperatures. No changes were imposed on oceanic salinities and water temperatures below the surface.

The applied sea level rise follows the projection in the Climate Change in Australia report (CSIRO 2007) that defines a 0.59 m mean sea level by 2100 from the 1990 baseline. In order to apply these changes the following approach was used:

- Harmonic analysis was performed on the surface elevation data between 2004 and 2008;
- Tidal elevations were reconstructed from the harmonic analysis for the period 2004 to 2008 and 2004 to 2072;
- Residuals between the surface elevation data and the reconstructed tides were calculated for the period between 2004 and 2008, and successively appended to the 2004-2008 time series to form a residual time series between 2004 and 2072;
- The final water surface elevation time series for the baseline simulation was constructed from adding the residuals time series to the reconstructed tidal elevations;
- The final water surface elevation time series for the climate change simulation was constructed by adding the assumed sea level rise to the baseline time series.

Figure 5-9 shows an illustration of obtained water levels for the climate change simulations.

Sea surface temperatures assumed half of the increase imposed on air temperatures. This assumption was based on reported trends since 1950 of sea surface temperature rises in comparison to land based stations in South Australia (Suppiah et al. 2006).

Table 5-1 Climate change parameters for Horizon 2030

Data Type	Seasonal Variation wrt 1990				Seasonal Variation wrt 2006				Source
	Sum	Aut	Win	Spr	Sum	Aut	Win	Spr	
Temperature (^{o}C)	1.4	1.2	1.2	1.4	1.34	0.58	1.16	0.63	Suppiah *et al*. (2006)
Rainfall (%)	-9	-10	-12	-20	-26	+22	+7.4	+2.6	Suppiah *et al*. (2006)
Wind Speed (%)	7.5	3.5	3.5	3.5	4.5	2.1	2.1	2.1	CSIRO (2007)
Relative Humidity (%)	-1.5	-1.5	-2.5	-2.0	-0.9	-0.9	-1.5	-1.2	CSIRO (2007)
Solar Radiation (%)	0.0	1.0	3.5	1.5	0.0	0.6	2.1	0.9	CSIRO (2007)
Long Wave Radiation	Computed from air temperature and assumed baseline cloud cover								Derived
Mean Sea Level Rise (m)	Assumed linear 0.59 m increase from 1990 to 2100								CSIRO (2007)
Sea Surface Temperature (^{o}C)	Assumed half of air temperature increase								Suppiah *et al*. (2006)
Sea Surface Salinity	Not changed								N/A

Table 5-2 Climate change parameters for Horizon 2070

Data Type	Seasonal Variation wrt 1990				Seasonal Variation wrt 2006				Source
	Sum	Aut	Win	Spr	Sum	Aut	Win	Spr	
Temperature (^{o}C)	4.3	3.8	3.8	4.1	4.24	3.18	3.76	3.33	Suppiah *et al*. (2006)
Rainfall (%)	-25	-30	-35	-60	-39	-5.2	-21	-49	Suppiah *et al*. (2006)
Wind Speed (%)	15	10	5	12.5	12	8	4	10	CSIRO (2007)
Relative Humidity (%)	-2.5	-3.0	-3.5	-3.5	-2.0	-2.4	-2.8	-2.8	CSIRO (2007)
Solar Radiation (%)	3.5	3.5	10	3.5	2.8	2.8	8.0	2.8	CSIRO (2007)
Long Wave Radiation	Computed from air temperature and assumed baseline cloud cover								Derived
Mean Sea Level Rise (m)	Assumed linear 0.59 m increase from 1990 to 2100								CSIRO (2007)
Sea Surface Temperature (^{o}C)	Assumed half of air temperature increase								Suppiah *et al*. (2006)
Sea Surface Salinity	Not changed								N/A

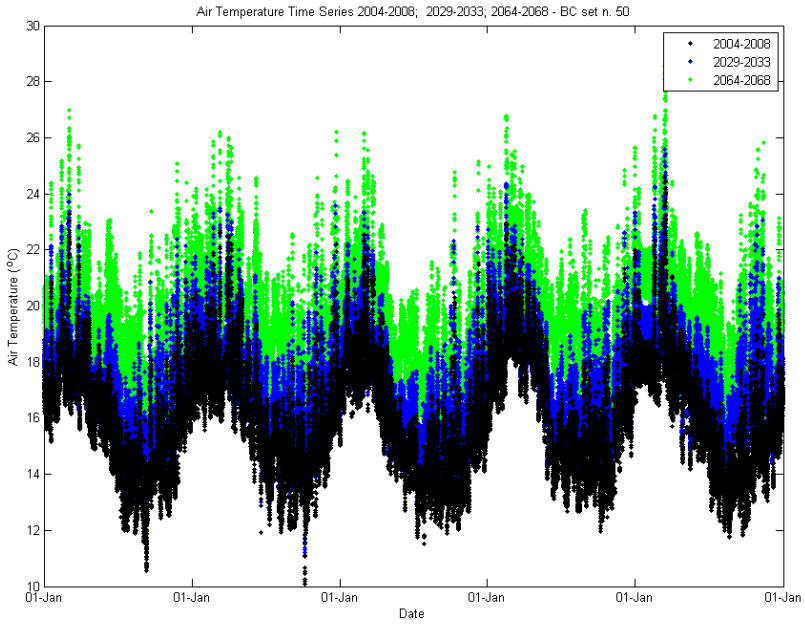

Figure 5-3 Example of air temperature and associated imposed climate change at different time horizons: boundary condition set n. 50

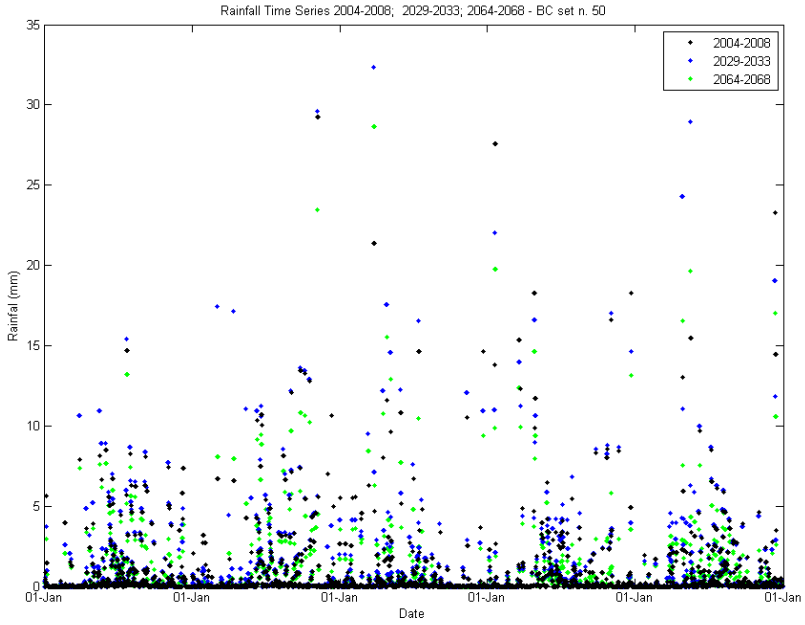

Figure 5-4 Example of air temperature and associated imposed climate change at different time horizons: boundary condition set n. 50

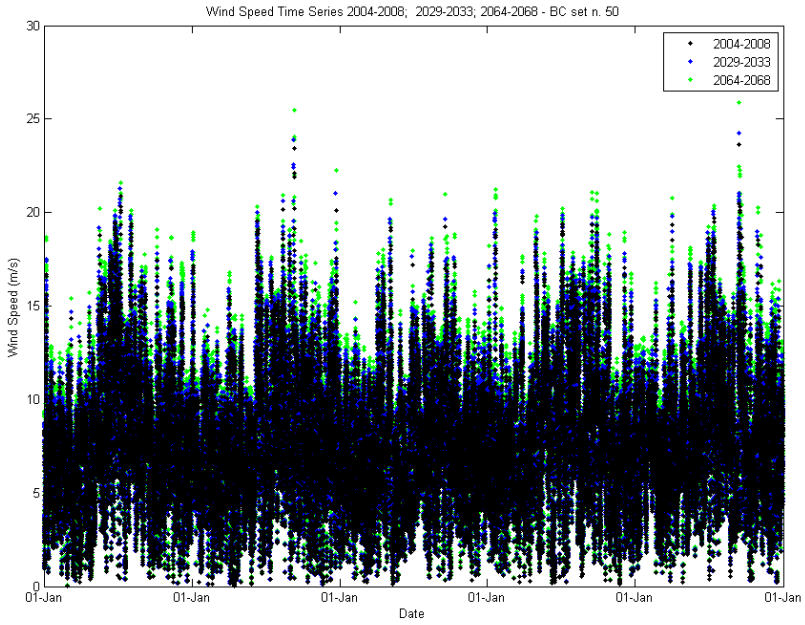

Figure 5-5 Example of wind speed and associated imposed climate change at different time horizons: boundary condition set n. 50

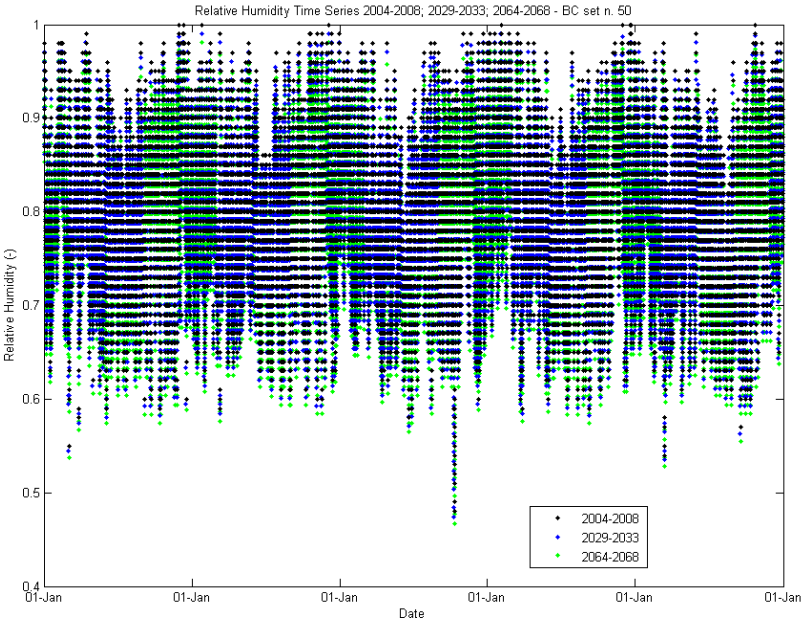

Figure 5-6 Example of relative humidity and associated imposed climate change at different time horizons: boundary condition set n. 50

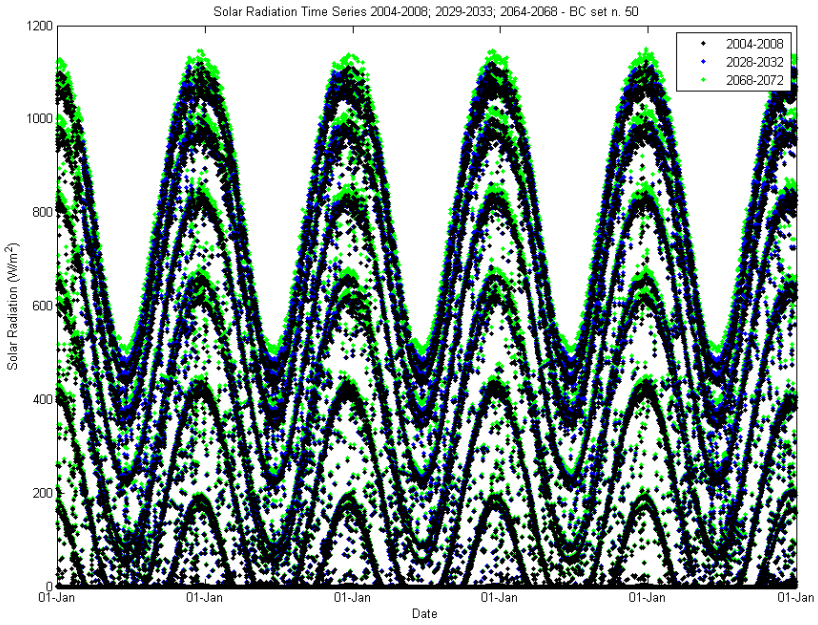

Figure 5-7 Example of solar radiation and associated imposed climate change at different time horizons: boundary condition set n. 50

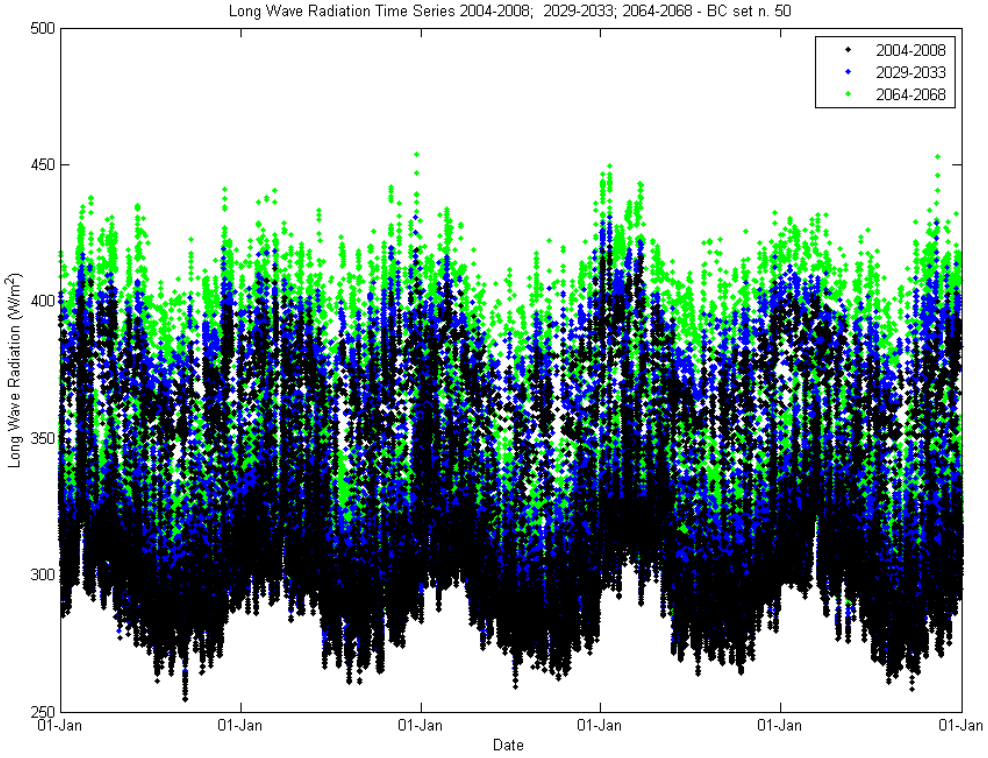

Figure 5-8 Example of long wave radiation and associated imposed climate change at different time horizons: boundary condition set n. 50

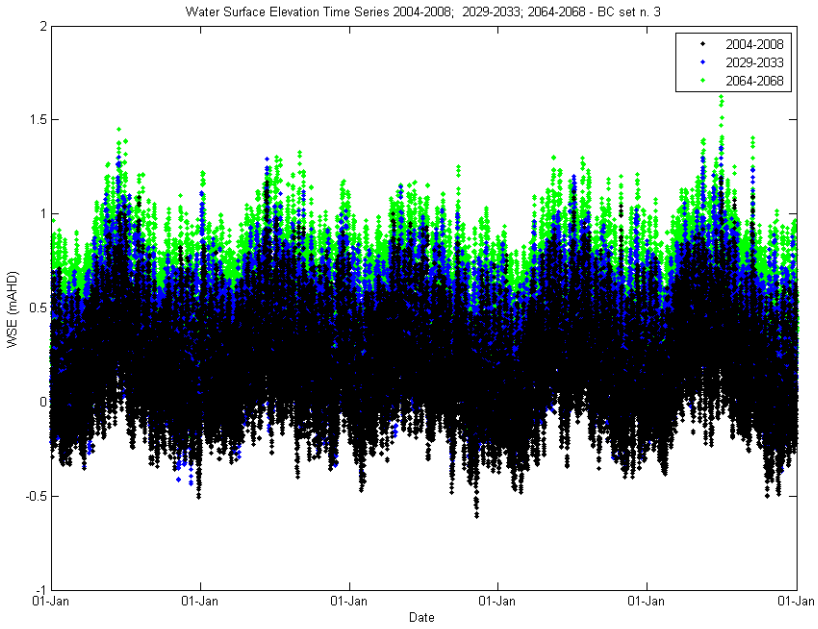

Figure 5-9 Example of water surface elevations and associated imposed climate change at different time horizons: boundary condition set n. 3

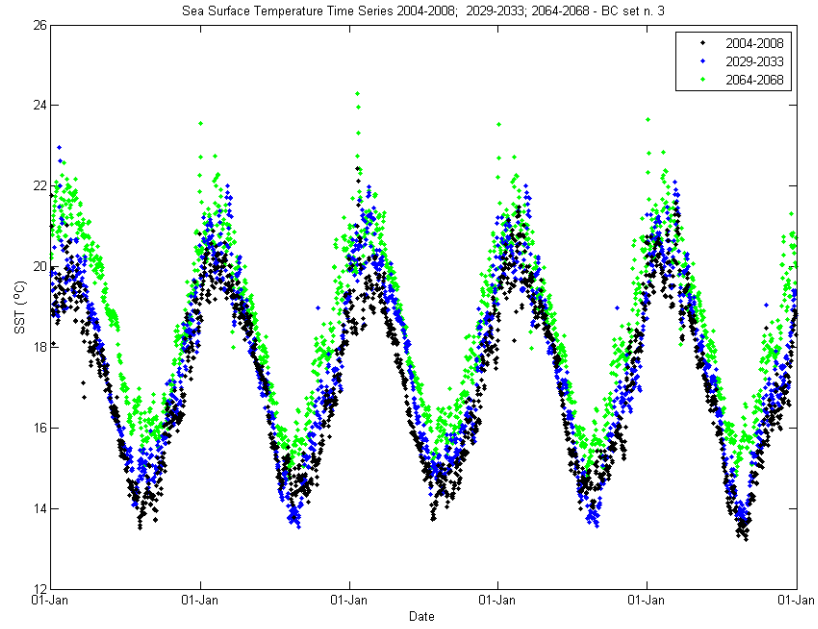

Figure 5-10 Example of sea surface temperature and associated imposed climate change at different time horizons: boundary condition set n. 3

5.2 Simulations

Similarly to the simulations presented in Section 4 above, two simulation sets for the period between 2004 and 2072 were performed, accounting for scenarios with and without the proposed desalination plant discharges. Again, for the scenario accounting for the proposed desalination plant discharge, yearly average discharge rates were assumed throughout the simulation. The characteristics of the proposed desalination plant discharge are summarised in Table 5-3.

Table 5-3 Assumed proposed desalination plant discharges in the simulations

Simulation Code	Period (Nov to Nov)	Intake Rate m^3/s	Outfall Rate m^3/s
B+C	2004-2072	0.00	0.00
B+C+D	2004-2072	4.95	2.79

5.3 Results

Similarly to Section 4, results were assessed for two different areas representing the Northern Spencer Gulf and the entire Spencer Gulf, allowing comparisons for the relative effects of the changes imposed by climate change and desalination alone, as well as the combined effect.

Figure 5-11 to Figure 5-14 show the time evolution of the Northern Spencer Gulf average salinities from simulations with and without imposed climate change, and with and without the proposed desalination plant. The seasonal aspects of the salinity in the Northern Gulf were not disrupted with the imposed climate change to the time 2070 time horizon, such that the annual cycle of salt accumulation in summer months and salt ejection in winter were still operating. Salinities, though, increased considerably, particularly between the 2030 and 2070 time horizons.

These salinity increases under the climate change scenarios are due to increased evaporation resulting from the modulated atmospheric forcing. This increased evaporation (note evaporation is negative as it represents an outward flux from the model perspective) is shown as a difference with respect to the baseline (simulation B) for the two future horizons in Figure 5-15 to Figure 5-16. (i.e. (B+C) – B). The climate-driven salinity increases (B+C) are greater than those due to desalination alone (B+D).

These modelling results indicate that the projected changes would not alter the seasonal Northern Gulf salinity dynamics, as the changes did not modify the inherent physics of the salt ejection mechanism (see Nunes-Vaz et al. 1990, SEIS Appendix 17.5.2). However, results indicated that the Northern Gulf would experience an increase in salinity.

Similarly to the scenarios without climate change, the additional effects of the brine discharge on a climate change scenario did not produce continuously increasing salinities with time. This is illustrated in the cumulative distributions presented in Figure 5-17 for the entire time series (2004 to 2072) and percentiles for past (2004 to 2008) and future time horizons (2028 to 2032 and 2068 to 2072). No significant change in the difference between salinity percentiles (with and without the proposed discharge) can be distinguished for different periods. These were maintained always

between 0.02 and 0.09, with exception for the 90th and 100th percentiles in the horizon 2068-2072, for the means and any of the presented percentiles. The difference in these two percentiles were 0.11-0.12, which are however not significantly different from 0.10. The modelling results therefore indicated that the effects of the desalination discharge in the Northern Spencer Gulf salinities are within the range 0.06 to 0.12 under a scenario of climate change.

The effects of the proposed desalination plant discharge on salinity can also be contrasted to the imposed climate change in Figure 5-17. The effects of the desalination plant were about the same order as the effects of climate change in the horizon 2028-2032 (i.e. black and cyan lines are evenly matched) but a substantial increase in salinity results from the imposed climate change on the horizon 2068-2072 (i.e. separation between the climate change and the baseline climate data sets lines).

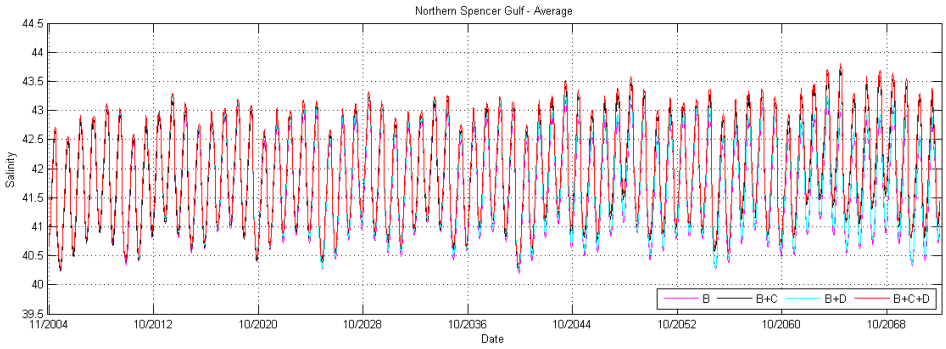

Figure 5-11 Modelled Northern Spencer Gulf averaged salinities for different climate scenarios and with and without the proposed desalination plant outfall discharge for the 2004 to 2072 period

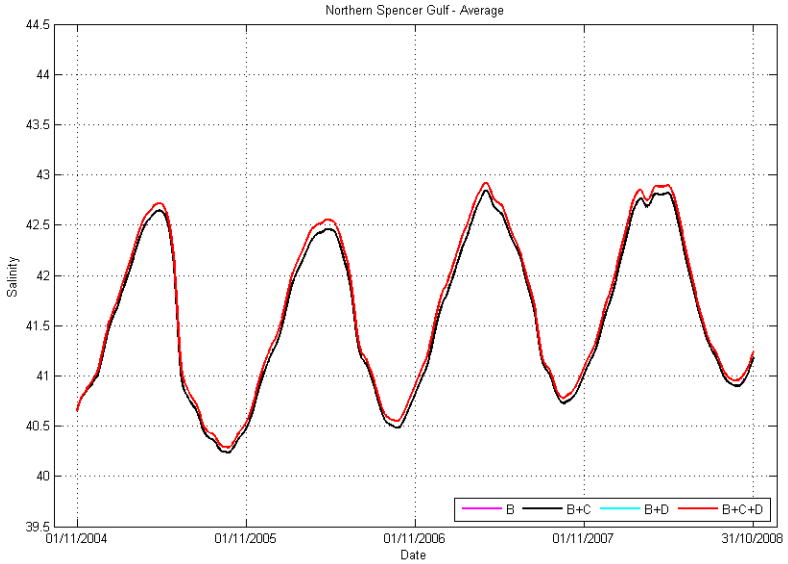

Figure 5-12 Modelled Northern Spencer Gulf averaged salinities for different climate scenarios and with and without the proposed desalination plant outfall discharge for the 2004 to 2008 period

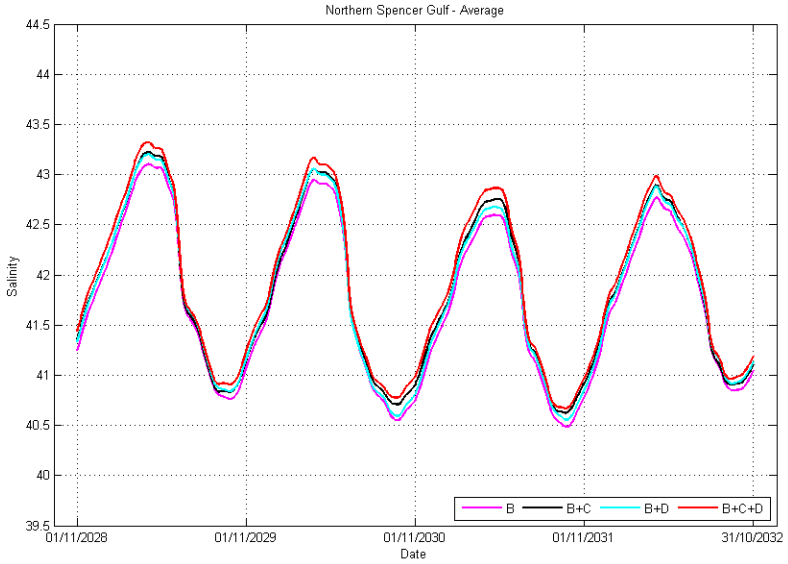

Figure 5-13 Modelled Northern Spencer Gulf averaged salinities for different climate scenarios and with and without the proposed desalination plant outfall discharge for the 2028 to 2032 period

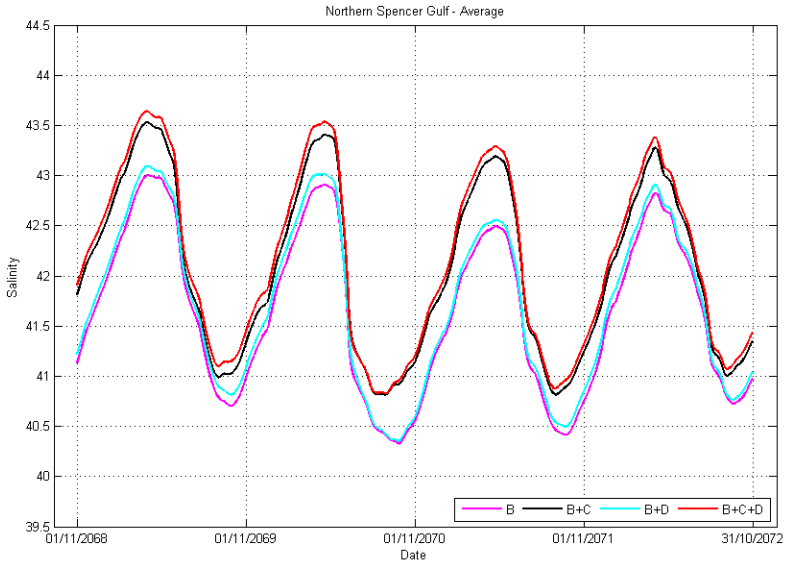

Figure 5-14 Modelled Northern Spencer Gulf averaged salinities for different climate scenarios and with and without the proposed desalination plant outfall discharge for the 2068 to 2072 period

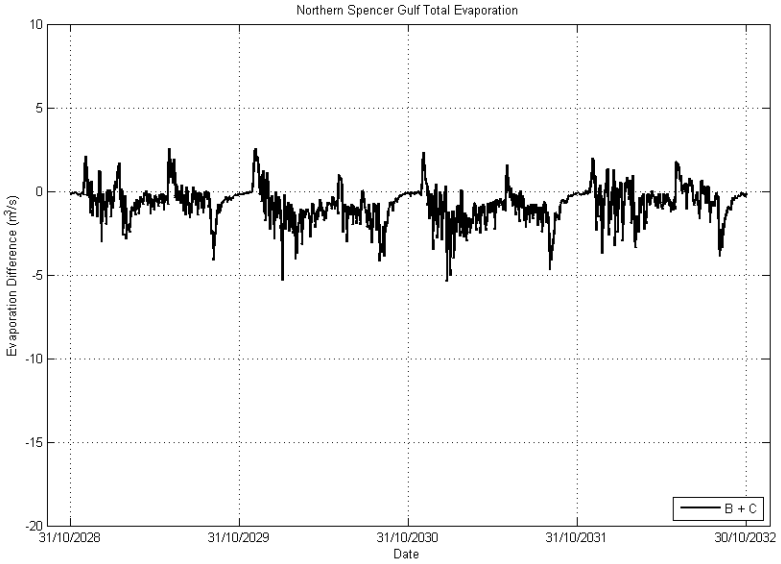

Figure 5-15 Difference with respect to the baseline for modelled Northern Spencer Gulf evaporation rates for climate change scenarios and with the proposed desalination plant outfall discharge for the 2028 to 2032 period

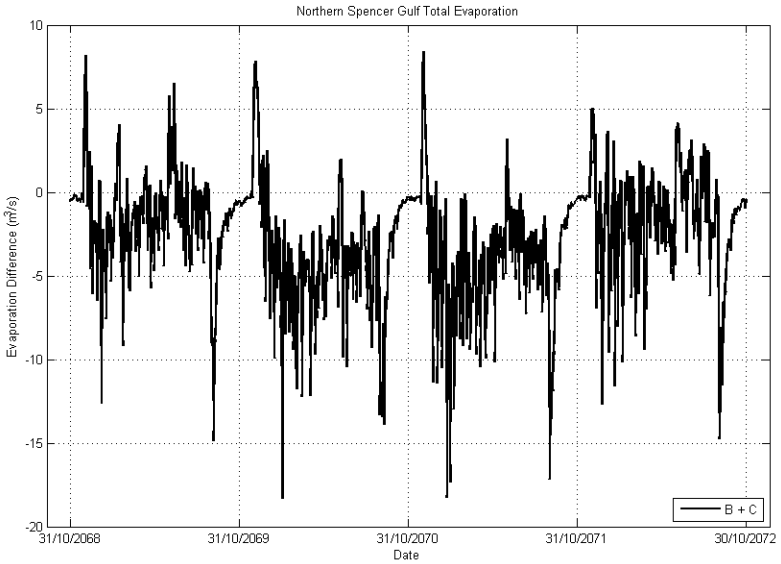

Figure 5-16 Difference with respect to the baseline for modelled Northern Spencer Gulf evaporation rates for climate change scenarios and with the proposed desalination plant outfall discharge for the 2068 to 2072 period

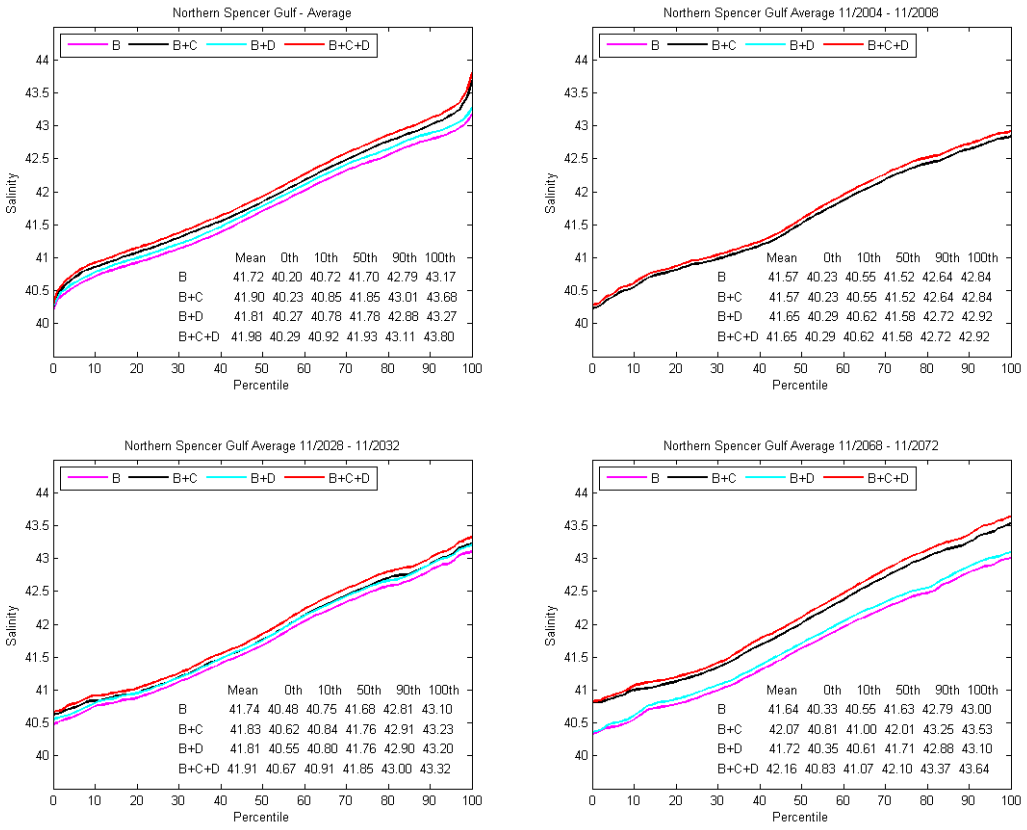

Figure 5-17 Modelled cumulative distributions of the Northern Spencer Gulf averaged salinities for different climate scenarios, and with and without the proposed desalination plant outfall discharge. Top left panel: 2004 to 2072 period; top right panel: 2004-2008 period; bottom left panel: 2028-2032 period; Bottom right panel: 2068-2072 period.

Over the entire Spencer Gulf, the effects of climate change strongly dominated over the effects of the proposed desalination plant discharge alone (Figure 5-18 to Figure 5-21). The cumulative distributions of modelled average Spencer Gulf salinities shows that by the 2070 horizon, the effects of climate change would induce an average Spencer Gulf salinity increase between 0.23 and 0.30, whilst the effects of the desalination plant were to increase the average Gulf salinity by 0.01. These results reflect the relative magnitude of the proposed desalination plant discharge with the natural evaporation and rainfall cycle. The resulting modelled water balances presented in Table 5-4 show that on average the difference between desalination plant extraction and return corresponds to less than 3% of the difference between evaporation and rainfall over Spencer Gulf. Resulting salt balances are presented in Table 5-5.

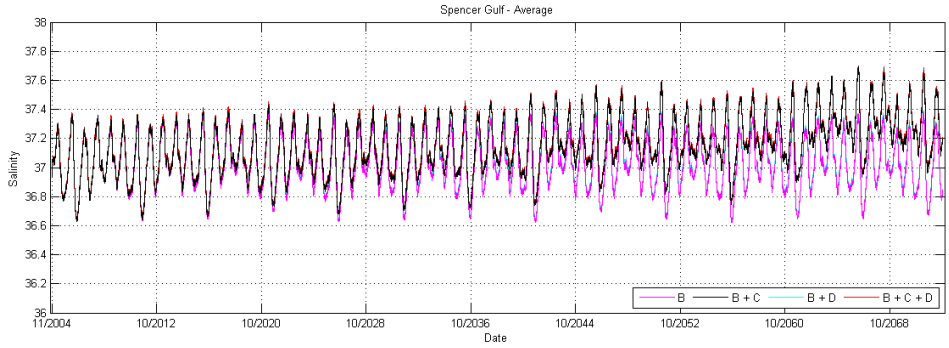

Figure 5-18 Modelled Spencer Gulf averaged salinities for different climate scenarios and with and without the proposed desalination plant outfall discharge for the 2004 to 2072 period

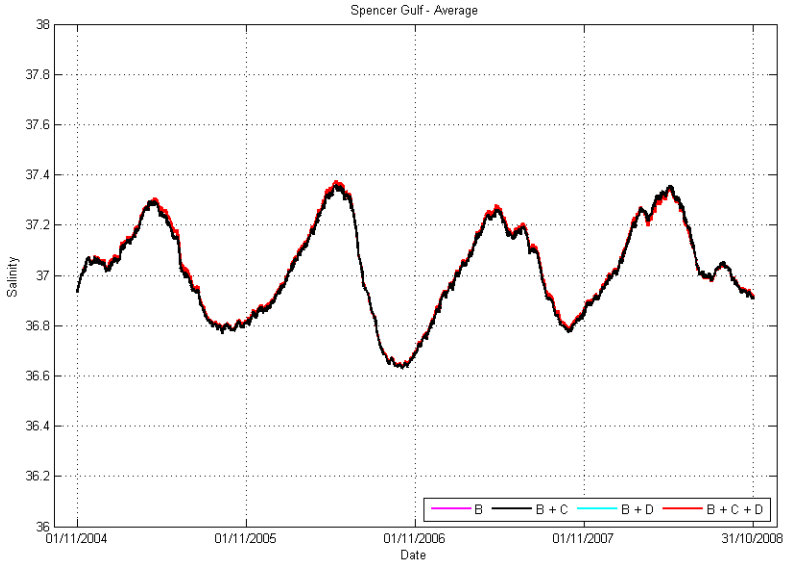

Figure 5-19 Modelled Spencer Gulf averaged salinities for different climate scenarios and with and without the proposed desalination plant outfall discharge for the 2004 to 2008 period

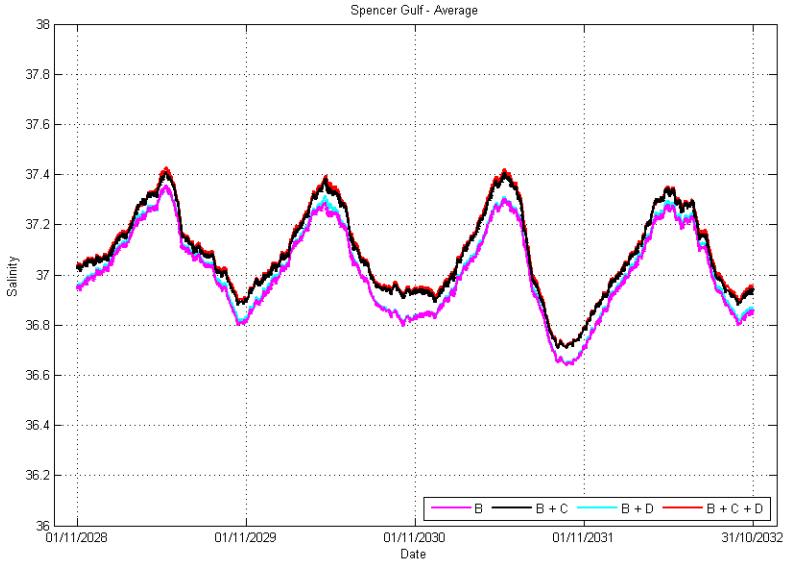

Figure 5-20 Modelled Spencer Gulf averaged salinities for different climate scenarios and with and without the proposed desalination plant outfall discharge for the 2028 to 2032 period

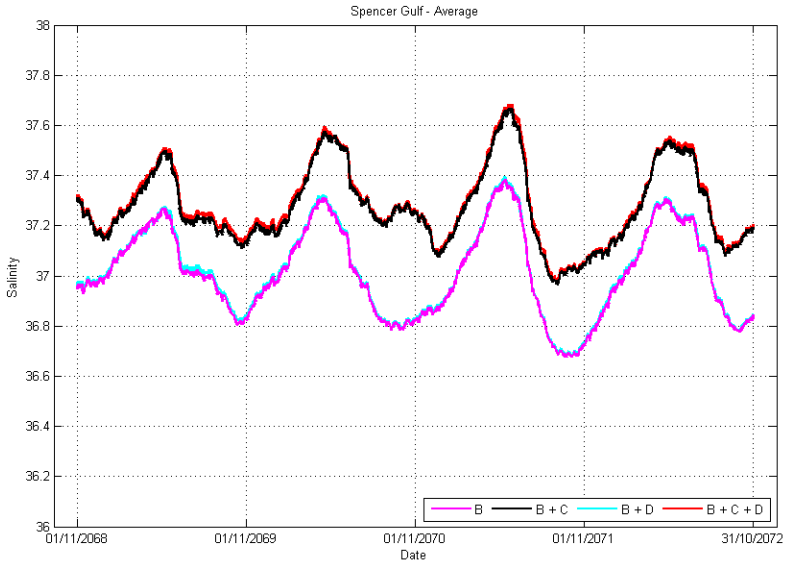

Figure 5-21 Modelled Northern Spencer Gulf averaged salinities for different climate scenarios and with and without the proposed desalination plant outfall discharge for the 2068 to 2072 period

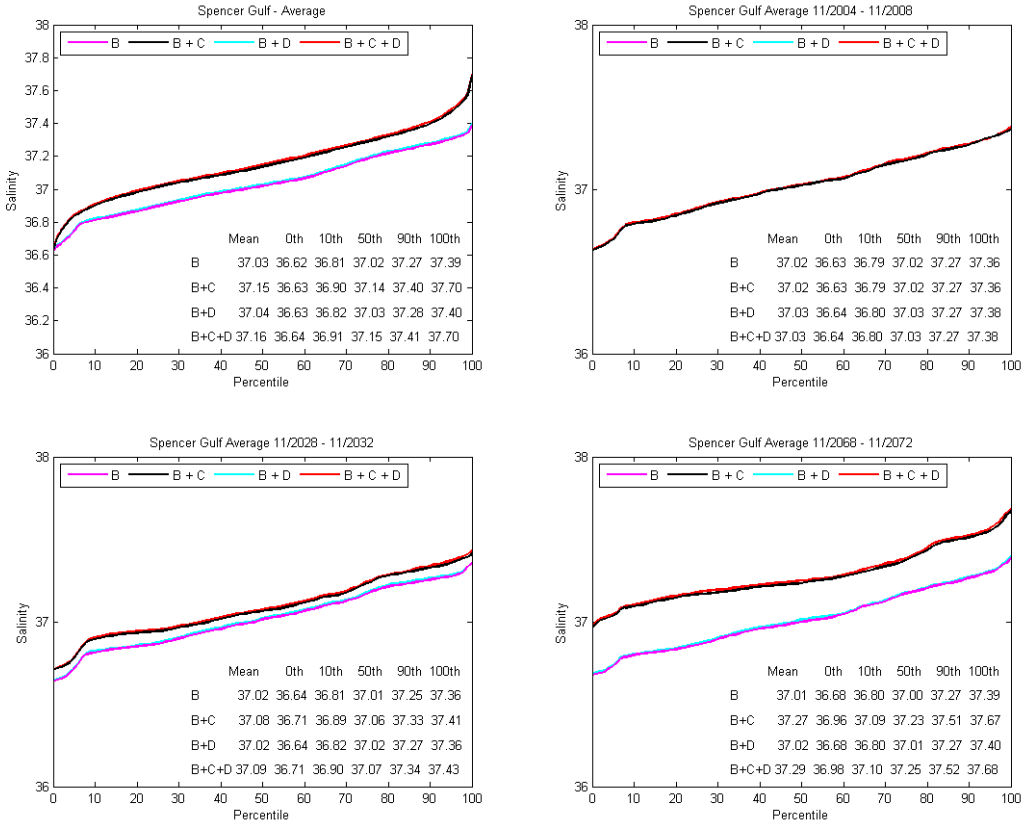

Figure 5-22 Modelled cumulative distributions of the Spencer Gulf averaged salinities for different climate scenarios, and with and without the proposed desalination plant outfall discharge. Top left panel: 2004 to 2072 period; top right panel: 2004-2008 period; bottom left panel: 2028-2032 period; Bottom right panel: 2068-2072 period.

Table 5-4 Simulated water balance with and without the effect of the proposed desalination plant

Salt Flux Item	B: 2004-2072 (Average)	B+D: 2004-2072 (Average)	B+C: 2004-2072 (Average)	B+C+D: 2004-2072 (Average)
	Gl/an	Gl/an	Gl/an	Gl/an
Tidal Influx	+7,280,000	+7,270,000	+7,270,000	+7,260,000
Tidal Eflux	-7,260,000	-7,250,000	-7,250,000	-7,250,000
Desal. Return	0.00	+88	0.00	+88
Desal. Intake	0.00	-156	0.00	-156
Evaporation	-30,160	-30,180	-30,560	-30,580
Rainfall	+6,920	+6,920	+6,860	+6,860
Other inflows	+5	+5	+5	+5

Table 5-5 Simulated salt fluxes with and without the effect of the proposed desalination plant and with and without the effect of climate change. Salinity values were assumed to be g/L.

Salt Flux Item	B: 2004-2072 (Average)	B+C: 2004-2072 (Average)	B+D: 2004-2072 (Average)	B+C+D: 2004-2072 (Average)
	Gt/an	Gt/an	Gt/an	Gt/an
Tidal Influx	+261	+261	+261	+261
Tidal Eflux	-261	-261	-261	-261
Desal. Return	0.00	0.00	+0.01	+0.01
Desal. Intake	0.00	0.00	-0.01	-0.01
Other inflows	+0.00	+0.00	+0.00	+0.00
Desalination intake and return salinities do not balance due to the constant 75 salinity assumed in the return water compared to the ambient salinities used in the intake calculations.				

6 DISSOLVED OXYGEN SIMULATIONS

In order to assess the likely dissolved oxygen dynamics associated with the proposed SEIS diffuser design, the high resolution ELCOM model (as presented in Appendix 17.5.2 of the SEIS) was augmented to include direct simulation of dissolved oxygen via activation of the water quality model CAEDYM (Computational Aquatic Ecosystem Dynamics Model).

CAEDYM is a process-based model of the major biogeochemical processes influencing water quality. It optionally models inorganic particles, oxygen, organic and inorganic nutrients (C, N, P and Si), multiple phytoplankton and zooplankton groups, fish and bacteria. Recent developments also include optional modules for benthic organisms (e.g. clams, macroalgae), pathogens and microbial indicator organisms, and a generic geochemical module capable of simulating pH, aqueous speciation (including metals), precipitation/dissolution reactions and sediment diagenesis. CAEDYM has been applied to a variety of aquatic systems including wetlands, lakes/reservoirs, rivers, estuaries and the coastal ocean (http://www.cwr.uwa.edu.au/software1/models/caedym/caedym.php). Specifically, ELCOM-CAEDYM (as used in this study) has been applied in the Australian context to this same matter of investigating dissolved oxygen dynamics in the vicinity of brine return water discharges (Okely *et al.*, 2006) so its use in this regard is established.

6.1 Model Setup

The high resolution ELCOM model was used to simulate dissolved oxygen dynamics in the vicinity of the diffuser. Individual setup elements are described below.

6.1.1 Simulation Periods

Two contrasting simulation periods were selected for this analysis so as to capture the potential seasonality of local dissolved oxygen dynamics. The periods were also selected to coincide with the small amplitude neap tides (dodge tides) that occur each year in May and November. The periods selected were as follows:

- Spring: 15/11/2008 01:00 to 24/11/2008 16:00
- Autumn: 06/05/2008 12:00 to 16/05/2008 15:00

Within these periods were dodge tides, and the smallest tidal elevation changes within these dodge tides were the following one day periods:

- Spring: 21/11/2008 14:00 to 22/11/2008 14:00 (tidal range approximately 0.30 metres); and
- Autumn: 14/05/2008 09:26 to 15/05/2008 09:26; (tidal range approximately 0.33 metres).

These periods are presented in Figure 6-1 and Figure 6-2, respectively and were used for data extraction purposes.

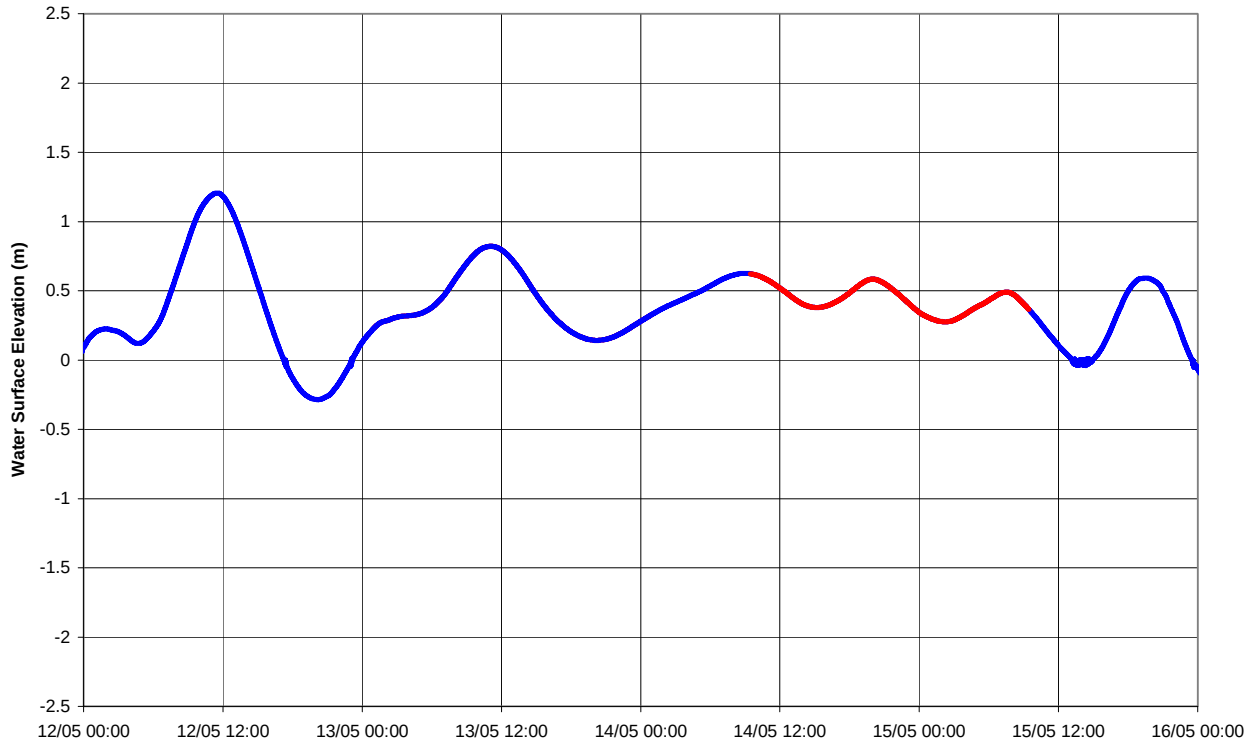

Figure 6-1 Autumn dodge tide (central day shown in red)

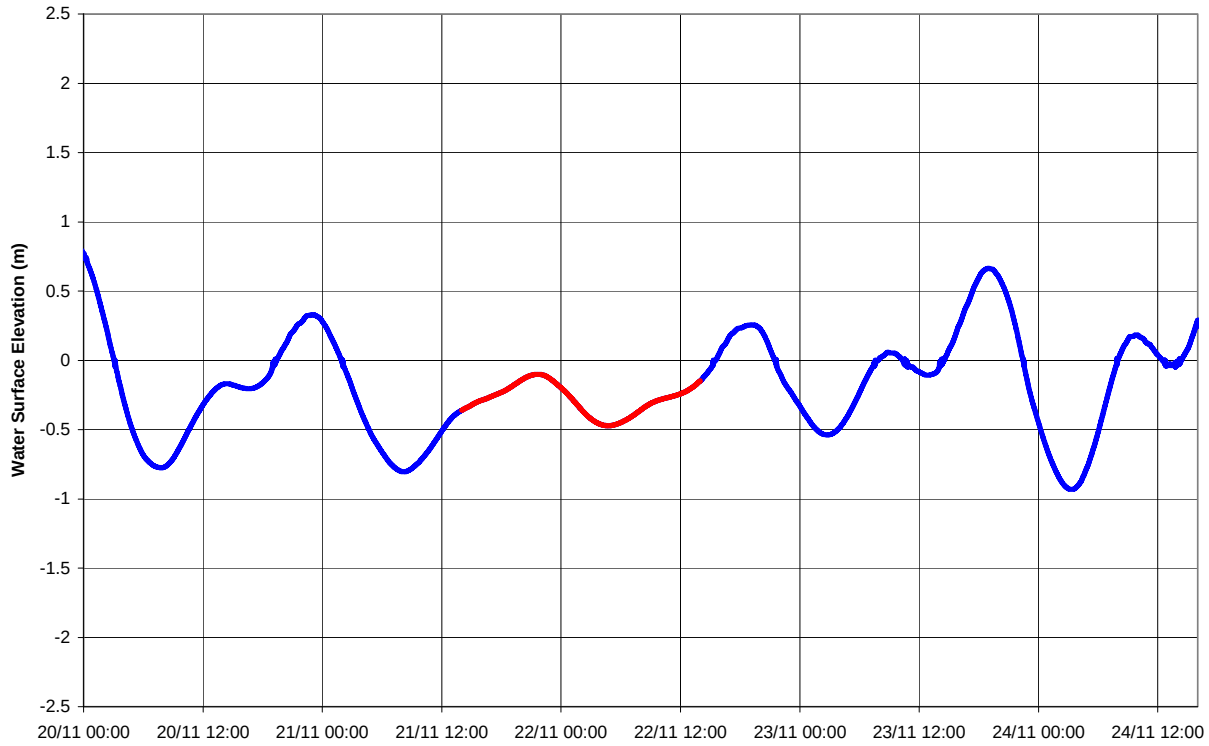

Figure 6-2 Spring dodge tide (central day shown in red)

6.1.2 Initial Conditions

6.1.2.1 Salinity

The simulations described here were hot started in terms of the specification of the initial salinity field. Specifically, this field was set by interrogating the low resolution model at the respective autumn and spring ELCOM-CAEDYM starting times, with the interrogated low resolution model having been run over a preceding multi-annual period. Depth averaged (spatially variant) low resolution salinities were extracted and interpolated to the high resolution model domain to provide initial salinity fields. This approach ensured that the initialisation of the autumn and spring high resolution simulations captured the spatial salinity variations characterising the Gulf at these times.

6.1.2.2 Temperature

The simulations were initialised for water temperature using the same technique as for salinity.

6.1.2.3 Dissolved Oxygen

The initial dissolved oxygen fields were set using the data presented in Johnson (1981). These data include measurements of water column dissolved oxygen at several locations (including Pt Lowly), depths and seasons throughout Spencer Gulf, and span the years 1975 to 1978. The data from Pt Lowly was analysed in terms of observed percent saturation dissolved oxygen and are shown in Figure 6-3. The horizontal axis is a 'day of year', and this was selected to facilitate identification of any seasonal trends. The figure shows that in general, the waters around Pt Lowly are very well oxygenated, with the minimum observed percentage saturation being approximately 92%.

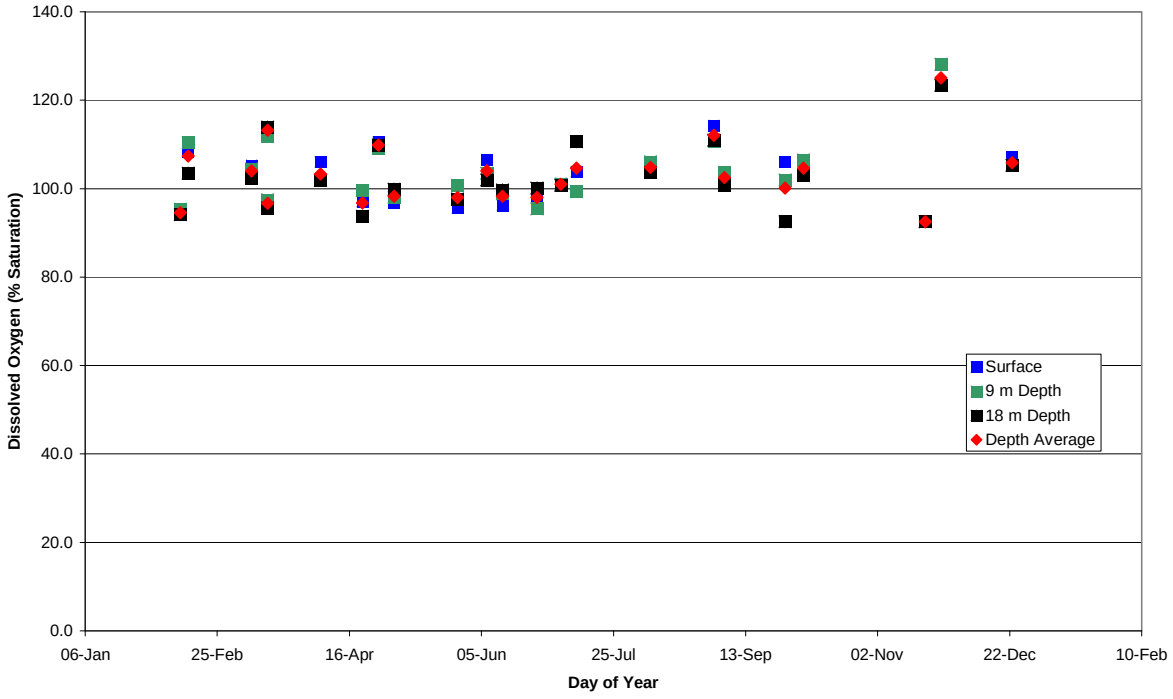

Figure 6-3 Johnson (1981) dissolved oxygen (percentage saturation) measurements at Pt Lowly

In order to adopt a conservative approach in the ELCOM-CAEDYM simulations, a background percentage saturation of approximately 80% was selected. This value is well below any observations of Johnson (1981) at Pt Lowly, however since the diffused return water mixes with the ambient water column prior to hitting the seabed, this adopted percentage saturation provided a 'worst case' scenario for both the autumn and spring simulations. Once this saturation value had been adopted, the dissolved oxygen concentrations in mg/L were computed from the initial salinity and temperature fields described above, and used to initialise CAEDYM.

6.1.2.4 Model Spin Up

In addition to initialising each high resolution model with the salinity, temperature and dissolved oxygen fields as described above, the full high resolution ELCOM-CAEDYM models were also spun up for approximately a one (1) week period preceding the respective autumn and spring dodge tides of interest. This spin up allowed for the localised behaviour of the return water plume to be established in three dimensions.

6.1.3 Boundary Conditions

6.1.3.1 Return Water

The quality of the return water entering the ELCOM-CAEDYM model (as a mixed quantity) was set using extracted timeseries from the base case (no return water) high resolution simulations. Specifically, the depth average temperature, salinity and dissolved oxygen concentrations above the diffuser location in each base case (autumn and spring) were extracted and combined with the return water in a dynamically varying ratio set by the CFD study and the background tidal velocities. This used the same methodology as described in previous sections, so is not repeated here. The assumed raw (i.e. at diffuser nozzle) return water quality was provided to BMT WBM and was:

- Salinity: 75 g/L;
- Temperature: Ambient at the intake site, plus 1 degree Celsius (this also varied dynamically according to the simulated temperature at the intake site in each season); and
- 100% saturation dissolved oxygen at the given temperature and salinity.

Depth average information was used firstly to be consistent with the previously adopted methodology, but also to capture the fact that the discharge plume, on exit from the diffuser, mixes with a large fraction of the water column.

6.1.3.2 Atmospheric Forcing

The same atmospheric forcing data used in the high resolution simulations was applied to the ELCOM-CAEDYM simulations. Full water column – atmosphere interaction was allowed, as was the case for all other simulations described in this report.

6.1.4 CAEDYM Configuration

CAEDYM was configured to simulate the following oxygen dynamics:

- Atmospheric exchange; and

- Sediment oxygen demand (SOD).

Atmospheric exchange in CAEDYM is based on the model of Wanninkhof (1992) and the flux equation of Riley and Skirrow (1974). A simple static sediment oxygen demand (SOD) model is employed within CAEDYM that uses a Michaelis-Menton function given by

$$SOD = SOD_{MAX}\left(\frac{DO}{K_{SOD} + DO}\right)$$

where SOD_{MAX} is the maximum demand, K_{SOD} is a half saturation constant and DO is the overlying dissolved oxygen concentration.

Lauer (2005) was used to set the value of SOD_{MAX} within the ELCOM-CAEDYM simulations. Lauer (2005) sampled SOD at 6 locations within Spencer Gulf Figure 6-4) across several seasons. No measurements were made directly off Pt Lowly, however the site closest (Western Shoal) showed little seasonal variation in SOD, with typical values around 400 to 500 $\mu mol.m^{-2}.h^{-1}$ (Lauer 2005, Figure 5-7). Despite this, other sites throughout the Gulf exhibited much larger SOD. As such, and with the overall intent to be conservative, the maximum SOD observed by Lauer (2005) at sites within the main body of the Gulf, and across all seasons, was adopted for the current simulations. The adopted SOD was thus set at 0.921 g/m^2/day. The half saturation constant (KSOD) was set to 0.5.

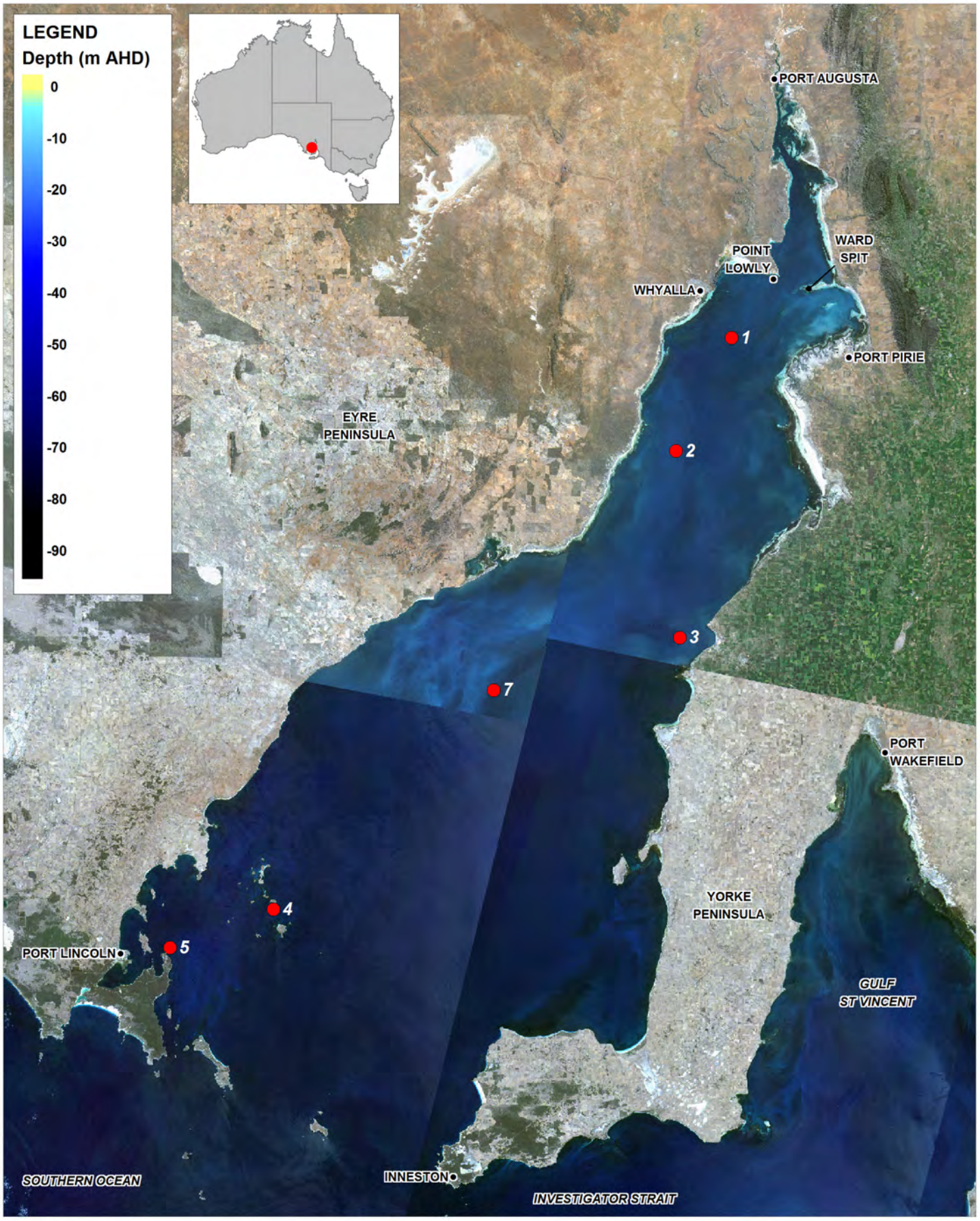

Title:

Lauer (2005) SOD Sampling Sites (estimated from Lauer (2005) Figure 5.1)

Figure: 6-4

Rev: A

N

0 30 60km

Approx. Scale

BMT WBM

www.bmtwbm.com.au

Filepath :

This ELCOM-CAEDYM setup was reviewed by CWR staff to ensure accuracy and consistency in the application of CAEDYM with other Australian studies.

6.2 Model Execution

Four simulations were executed as follows:

- Autumn without return water discharge;
- Autumn with return water discharge;
- Spring without return water discharge; and
- Spring with return water discharge.

Comparison of these allowed for the assessment of the return water discharge on local dissolved oxygen dynamics.

6.3 Results

The following results are presented in the following sections:

1 Bottom sheet dissolved oxygen. These sheets show a snapshot of bottom layer predicted dissolved oxygen concentrations at the end of the red dodge tide periods shown in Figure 6-1 and Figure 6-2., with base case (no return water discharge) and brine discharge results presented in parallel to facilitate comparison

2 Mid depth sheet dissolved oxygen. These sheets show a snapshot of mid depth layer predicted dissolved oxygen concentrations at the same time as above, again with base case (no return water discharge) and brine discharge results presented in parallel to facilitate comparison.

3 Vertical profiles of dissolved oxygen. These profiles span the entire simulation period for both base case and discharge scenarios, and are located 100 and 500 metres upstream and downstream from the diffuser. Difference contours (i.e. desalination case subtract base case) of these curtains are also provided.

4 Vertical curtain of dissolved oxygen. This curtain shows a snapshot of dissolved oxygen at the end of each one day dodge tide period (as defined above), with base case (no return water discharge) and brine discharge results presented in parallel to facilitate comparison. The curtain runs directly perpendicular to the alignment of the proposed diffuser, for several hundred metres either side of the diffuser alignment.

All results are presented as milligrams per litre of dissolved oxygen.

6.3.1 Bottom Sheets

6.3.1.1 Autumn

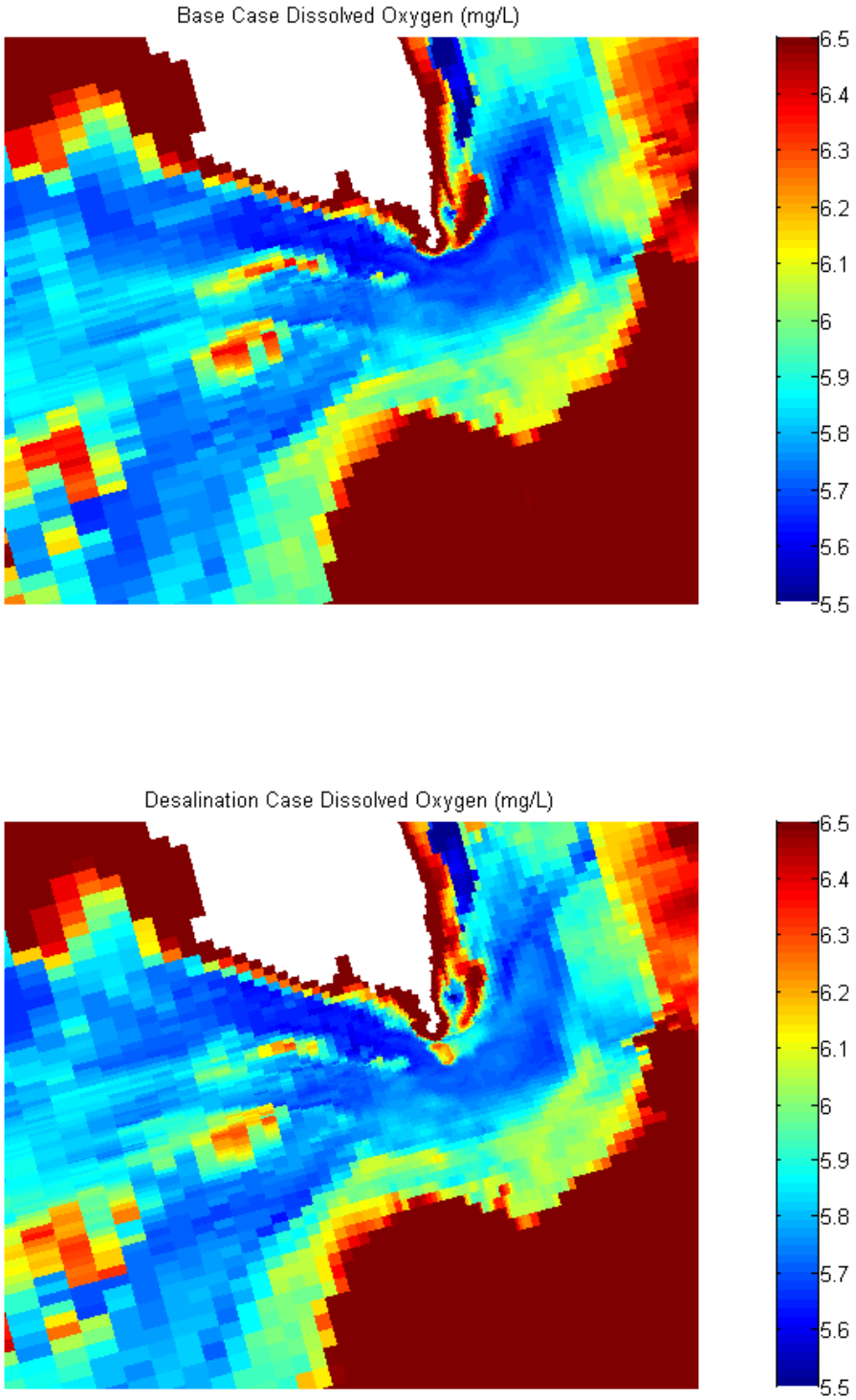

Figure 6-5 Bottom layer dissolved oxygen (mg/L) at the end of the Autumn dodge period

6.3.1.2 Spring

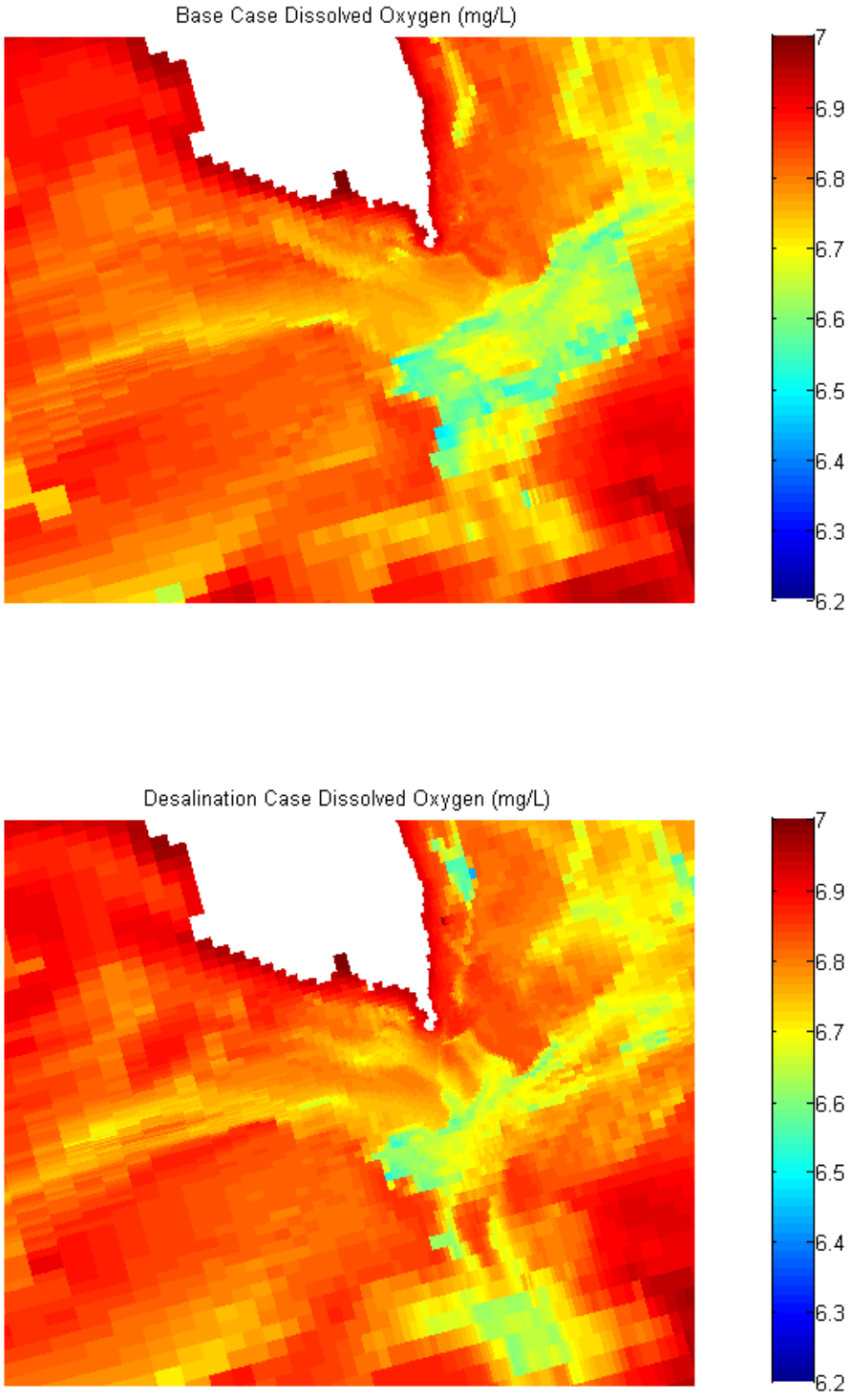

Figure 6-6 Bottom layer dissolved oxygen (mg/L) at the end of the Spring dodge period

6.3.2 Mid Depth Sheets

6.3.2.1 Autumn

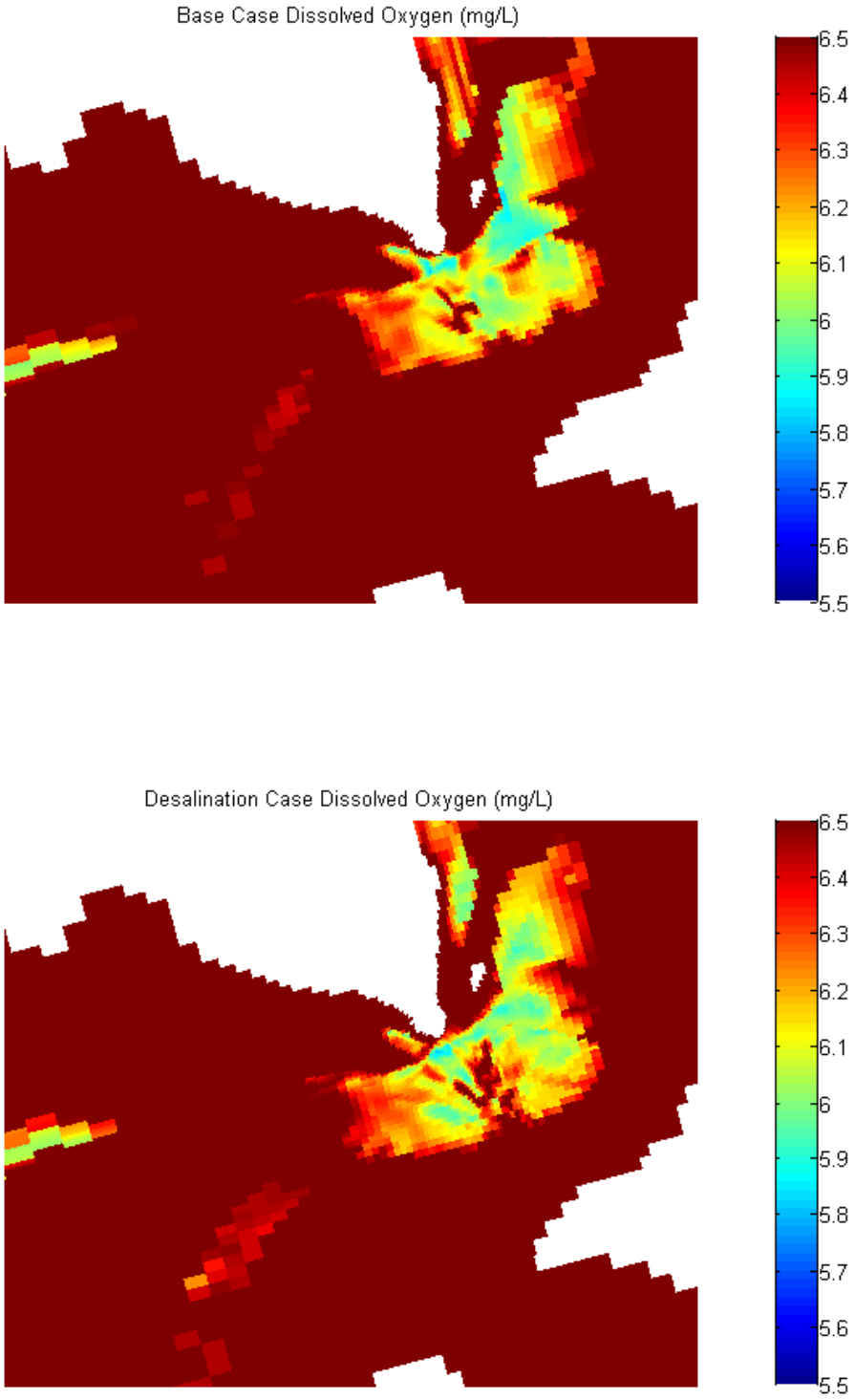

Figure 6-7 Mid depth dissolved oxygen (mg/L) at the end of the Autumn dodge period

6.3.2.2 Spring

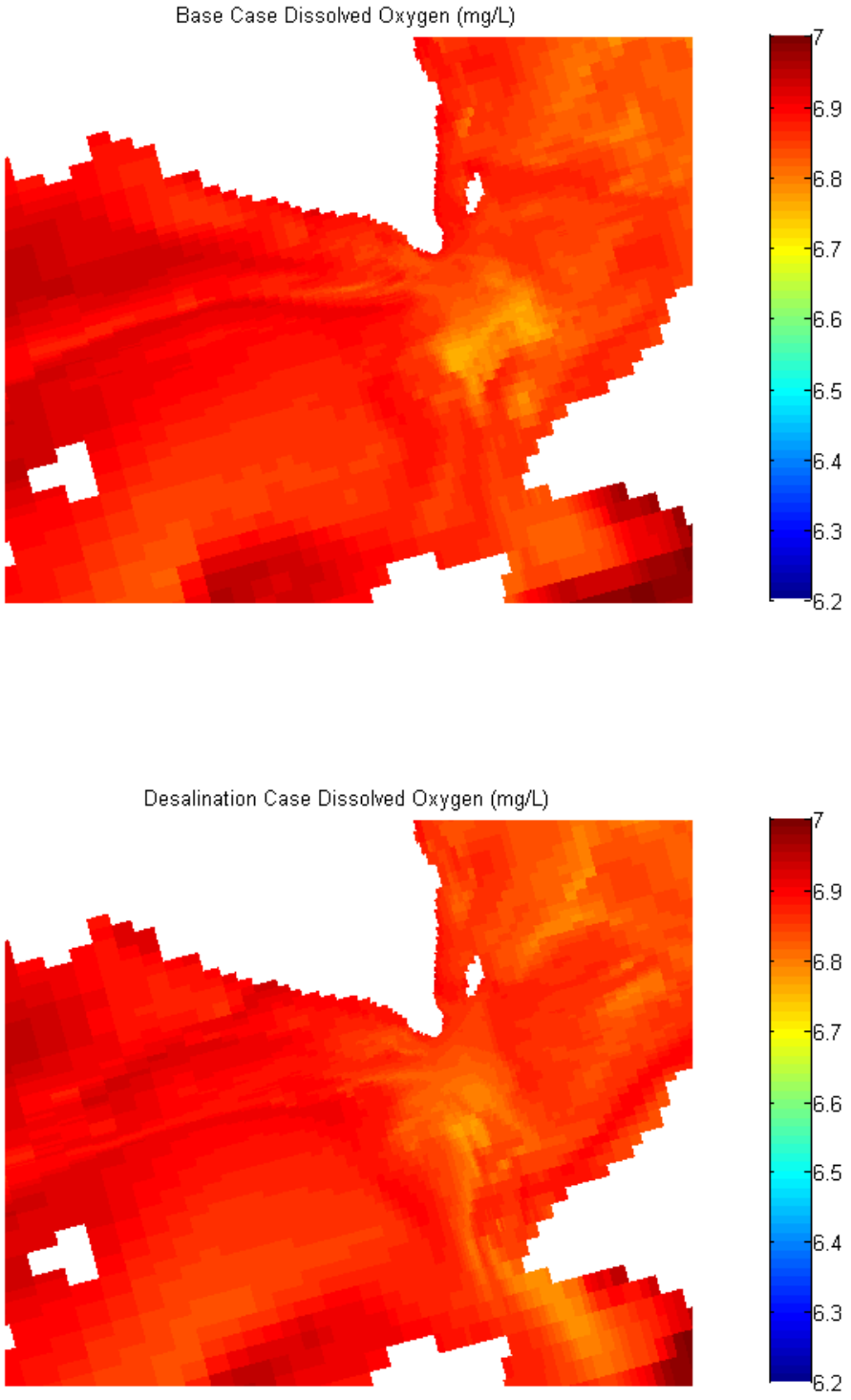

Figure 6-8 Mid depth dissolved oxygen (mg/L) at the end of the Spring dodge period

6.3.3 Profiles

6.3.3.1 Autumn 100 Metres Upstream

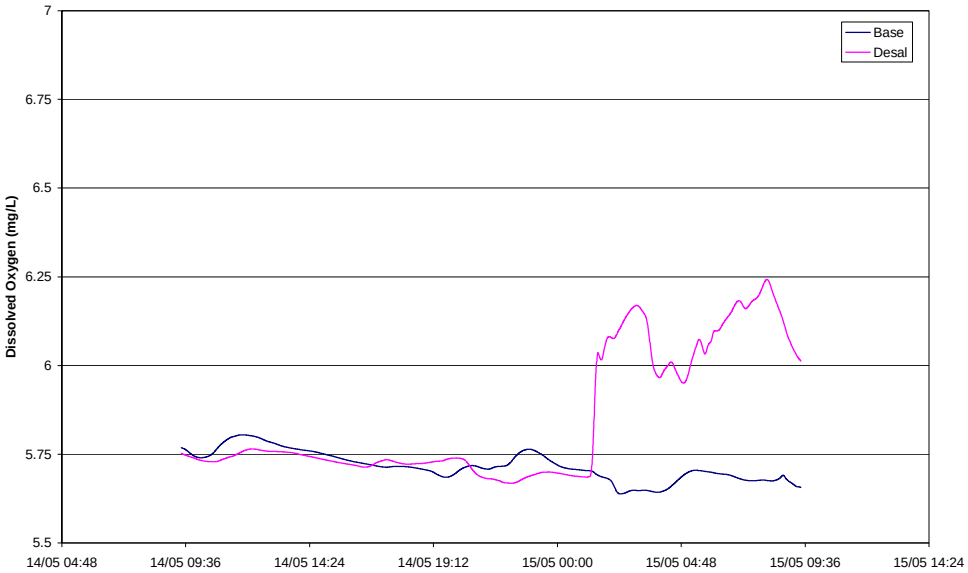

Figure 6-9 Profile dissolved oxygen (mg/L) - 100 metres upstream, Autumn

6.3.3.2 Autumn 100 Metres Downstream

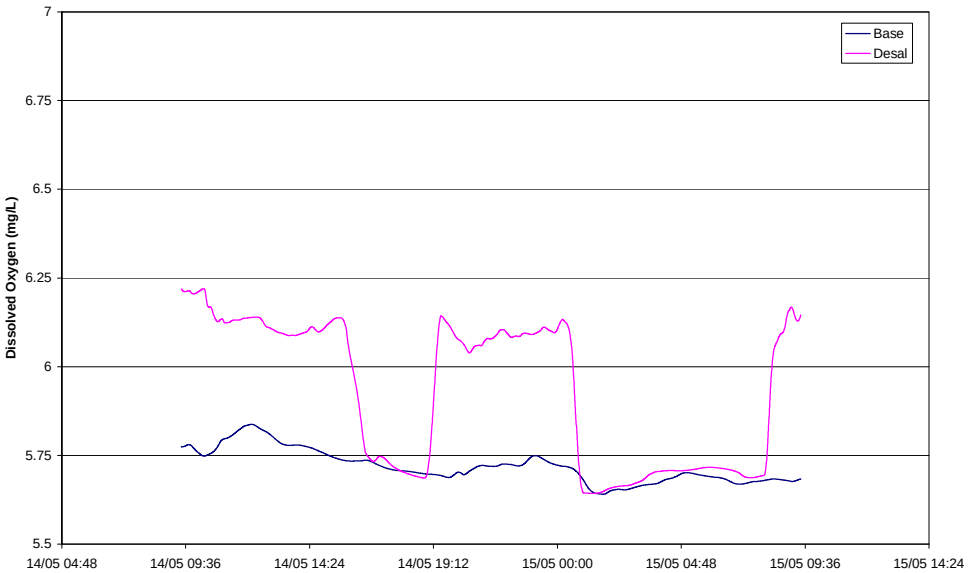

Figure 6-10 Profile dissolved oxygen (mg/L) - 100 metres downstream, Autumn

6.3.3.3 Autumn 500 Metres Upstream

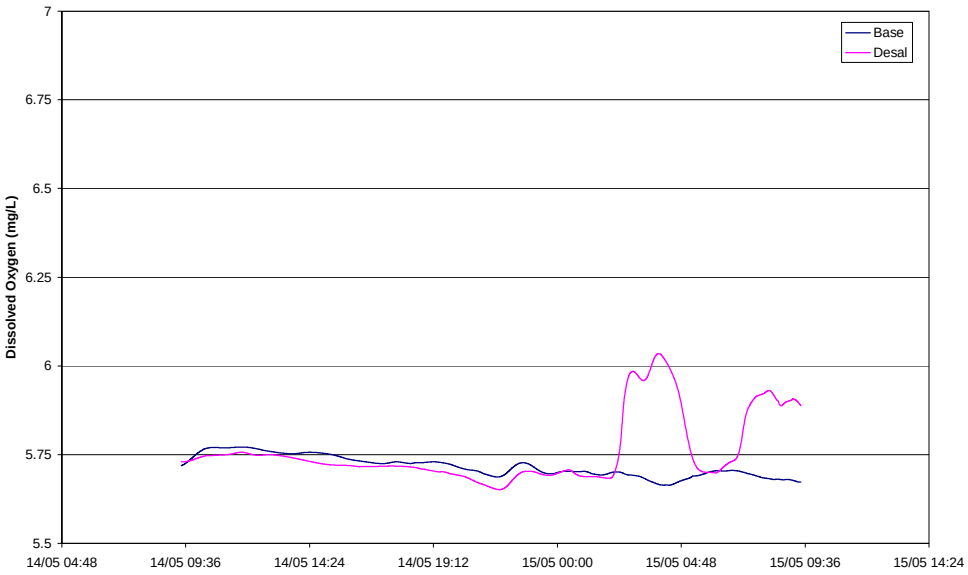

Figure 6-11 Profile dissolved oxygen (mg/L) - 500 metres upstream, Autumn

6.3.3.4 Autumn 500 Metres Downstream

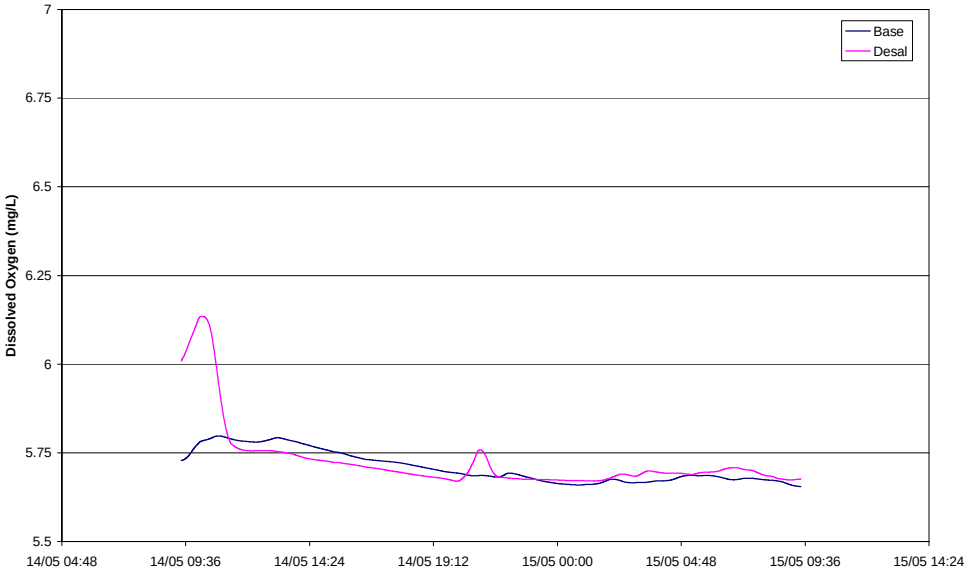

Figure 6-12 Profile dissolved oxygen (mg/L) - 500 metres downstream, Autumn

6.3.3.5 Spring 100 Metres Upstream

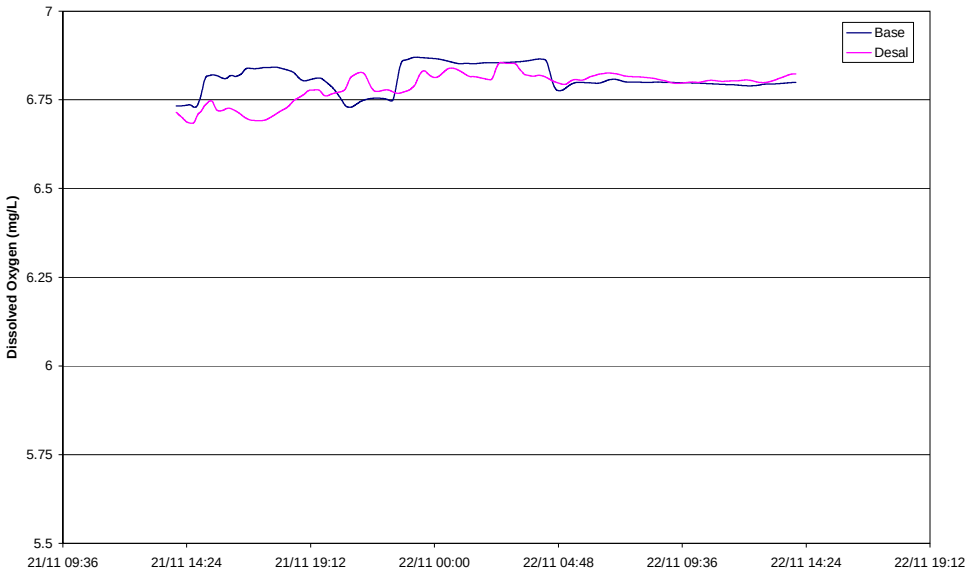

Figure 6-13 Profile dissolved oxygen (mg/L) - 100 metres upstream, Spring

6.3.3.6 Spring 100 Metres Downstream

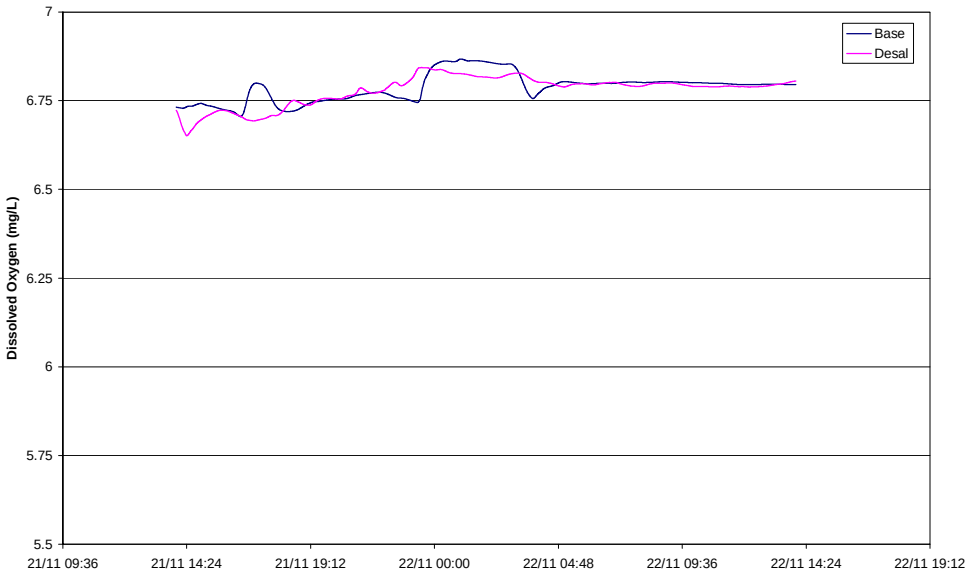

Figure 6-14 Profile dissolved oxygen (mg/L) - 100 metres downstream, Spring

6.3.3.7 Spring 500 Metres Upstream

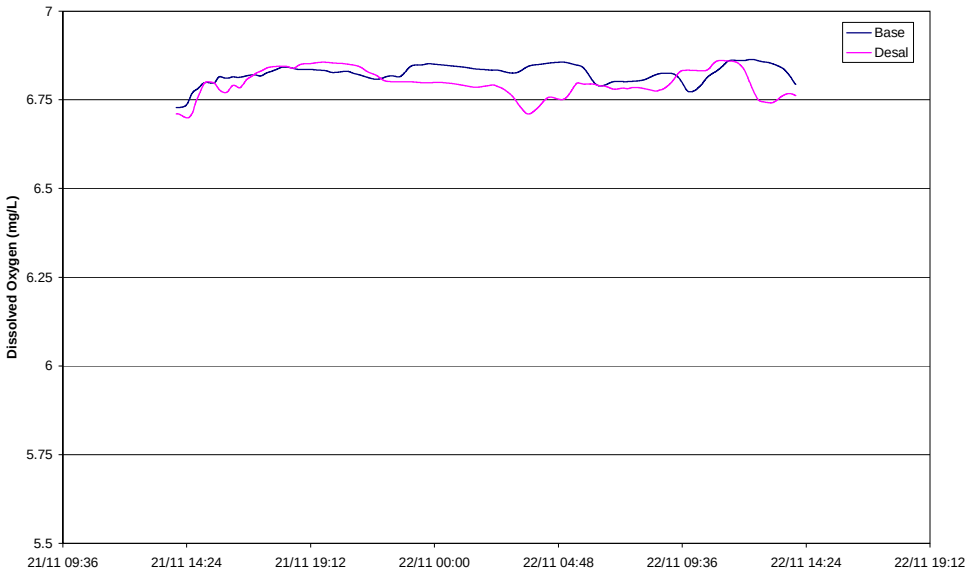

Figure 6-15 Profile dissolved oxygen (mg/L) - 500 metres upstream, Spring

6.3.3.8 Spring 500 Metres Downstream

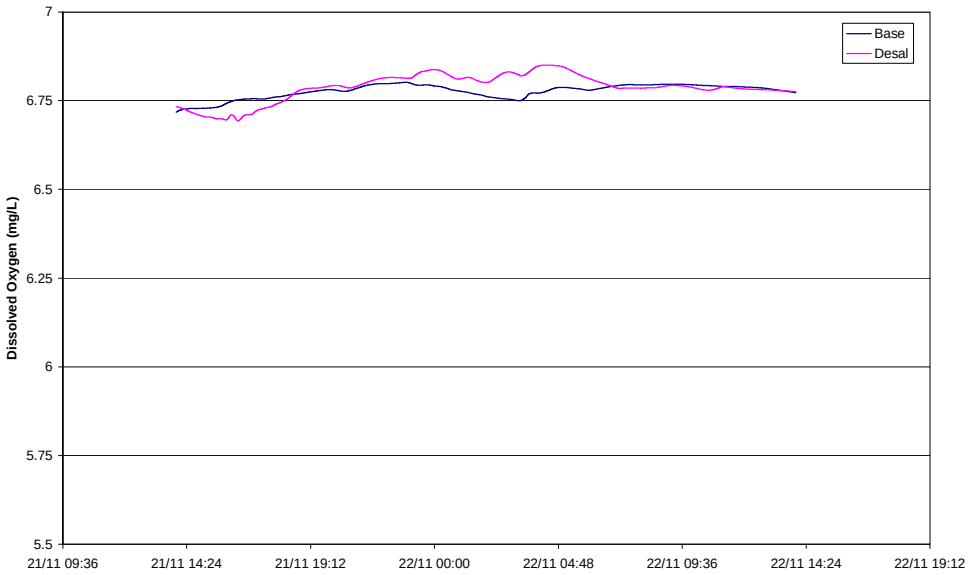

Figure 6-16 Profile dissolved oxygen (mg/L) - 500 metres downstream, Spring

6.3.4 Curtain

6.3.4.1 Autumn

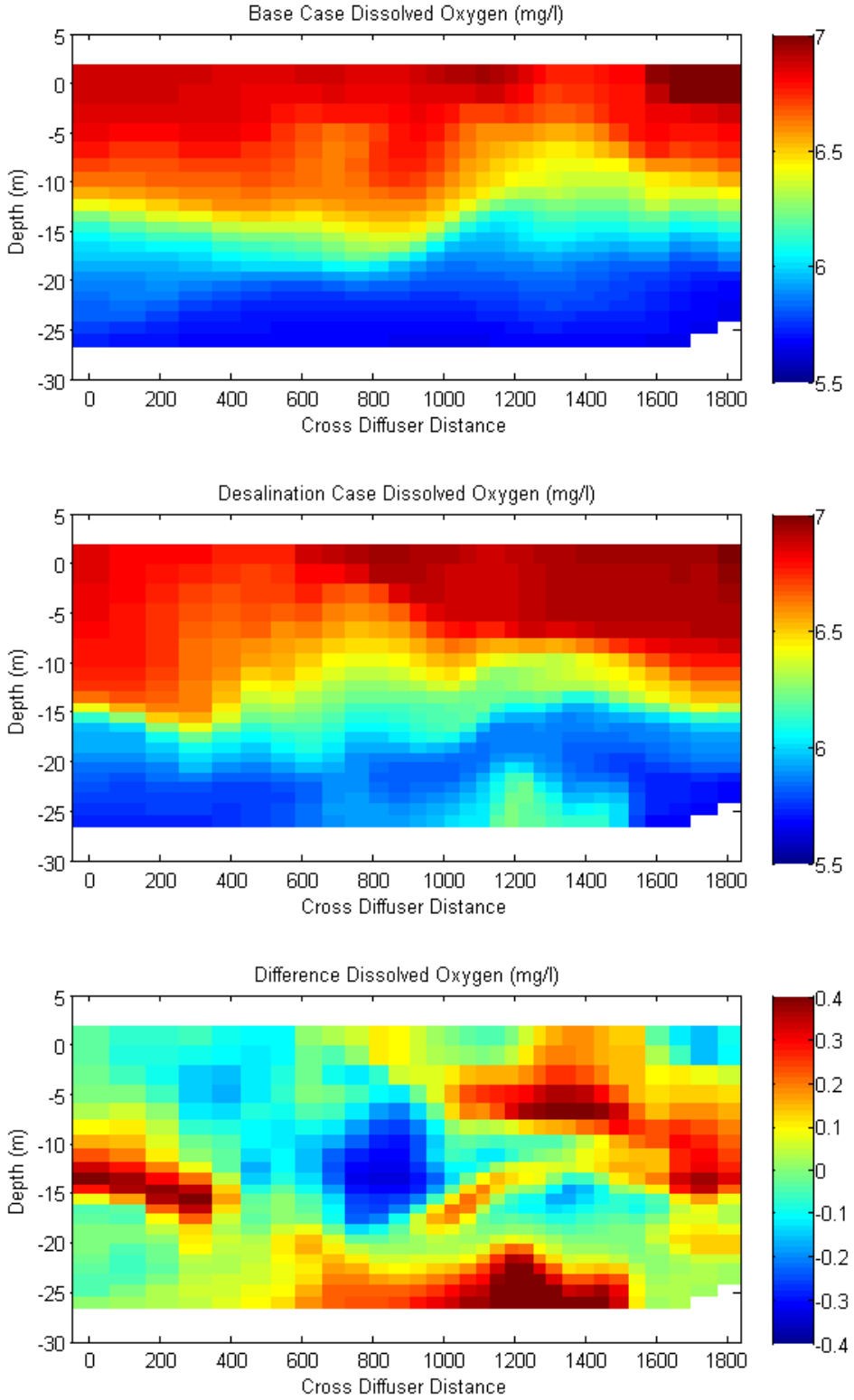

Figure 6-17 Transverse curtain dissolved oxygen (mg/L) at the end of the Autumn dodge period

6.3.4.2 Spring

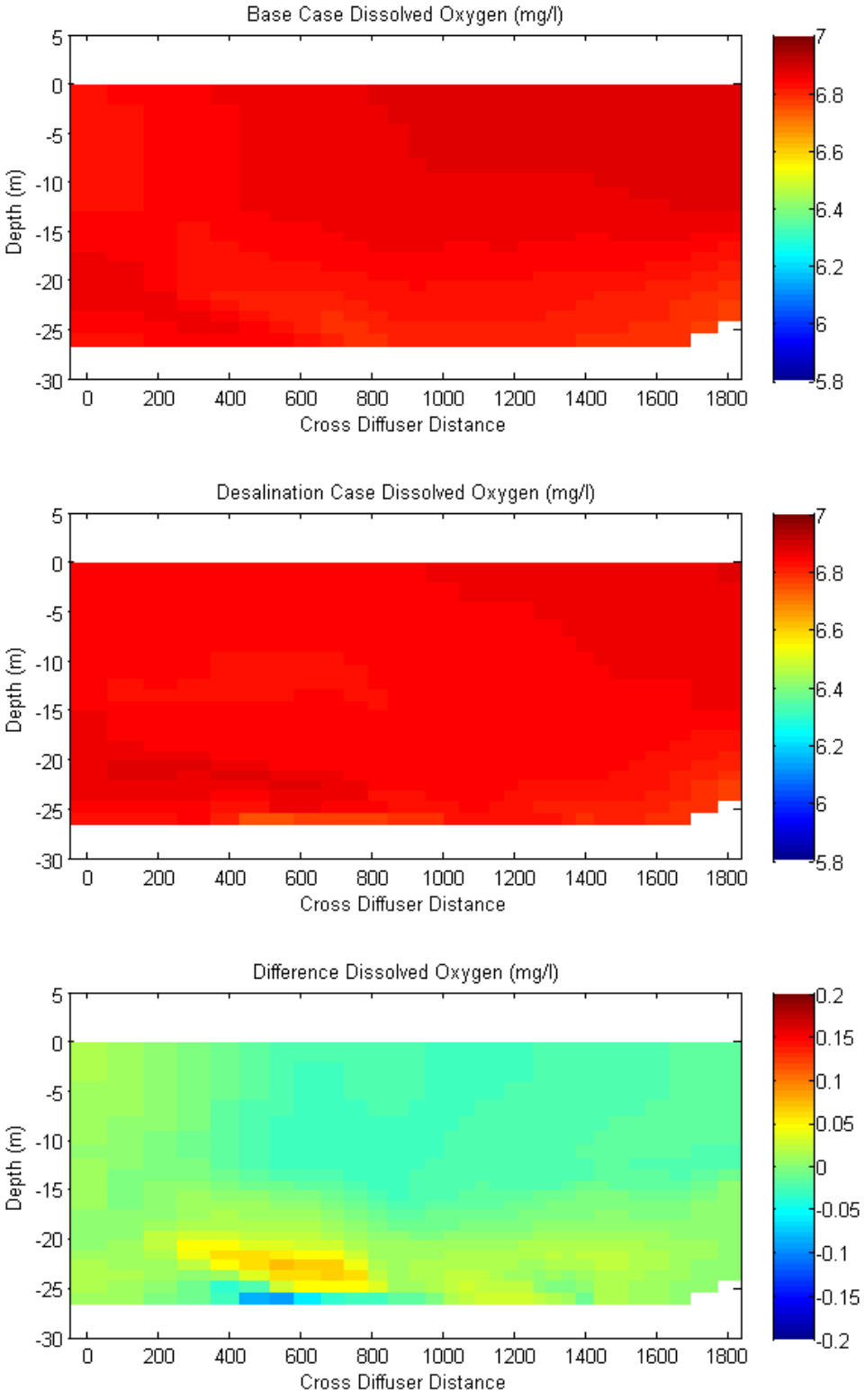

Figure 6-18 Transverse curtain dissolved oxygen (mg/L) at the end of the Spring dodge period

There is no evidence in the model results to suggest that significant deoxygenation of bottom waters occurs during the simulated times. This appears to be the case even with the adoption of the conservative assumption that the greatest sediment oxygen demand measured in Lauer (2005) for sites in the main section of Spencer Gulf operates throughout the entire model domain. In some cases the model shows that the brine discharge acts as an effective conduit for delivery of well-oxygenated mid-depth waters to the bed, thus occasionally increasing dissolved oxygen at depth.

7 UPWELLING ANALYSES

The potential for upwelling of mixed return water was addressed as part of the DEIS. The matter has been re-examined here using the upgraded modelling tools developed as part of the SEIS process, and this analysis is described below.

7.1 Background

The process of upwelling is well established in the literature (recently, Shintani *et al.*, 2010). The basic principle of upwelling, is that in a closed system (e.g. a lake), wind blowing in one direction can induce a return current in the opposite direction at depth. In a stratified water body, wind action can also induce thermocline (or pycnocline) tilt and result in delivery of bottom waters to the surface at the upwind end of the domain. This process of causing deep waters to move upwards under the action of a surface wind is known as upwelling.

The intent of this report is not to review or explain this process in detail, but rather to investigate its applicability to the case of return water discharge from Pt Lowly, and the reader is referred to Shintani *et al.* (2010) and included references for a mathematical description of the dynamics of upwelling.

In order to undertake this investigation, a series of numerical simulations have been executed using the high resolution model, or a derivative. The analyses are designed to move from the most simplistic through to ones representing real world conditions. As such, the following simulations are presented:

1 A two-dimensional (i.e. vertically and longitudinally resolved but laterally constrained – a vertical slice model) simulation;

2 A three-dimensional version of 1, with the lateral constraint removed so that water can flow into and out of the model through its sides, but maintaining the vertical slice geometry. This is referred to as a quasi three-dimensional model;

3 A fully three dimensional model (i.e. using real world bathymetry) with a range of wind forcing regimes but no tidal forcing (i.e. completely slack water); and

4 A fully three dimensional model with tidal forcing turned on and the Autumn dodge tide described in 6.1.1 simulated, with (to allow comparison) the wind forcing from 3 applied instead of the actual wind forcing.

These simulations and their results are described below.

7.2 Two-Dimensional Model

The first model applied here is that of a vertical slice two-dimensional domain. The nature of this domain is such that it can only simulate vertical and longitudinal (i.e. on the alignment of wind forcing) processes, and prohibits lateral water motion. That is, water within the domain is unable to move in any direction other than directly with (or against) the orientation of the applied wind field.

7.2.1 Model Domain

To affect this simulation, the high resolution ELCOM model described above and elsewhere was truncated to cover a transect that (approximately) spanned Spencer Gulf from Port Bonython to the eastern shore. The location of this transect is shown in Figure 7-3.

To do so, three dimensional bathymetry was removed from the entire high resolution ELCOM model domain outside a narrow band of cells set along the alignment shown in Figure 7-3. This is the equivalent of building solid 'walls' on each side of the alignment and preventing water flowing through the walls. In doing so, all currents are effectively forced to flow along the alignment. The vertical slice bathymetry is presented in Figure 7-1 and Figure 7-2.

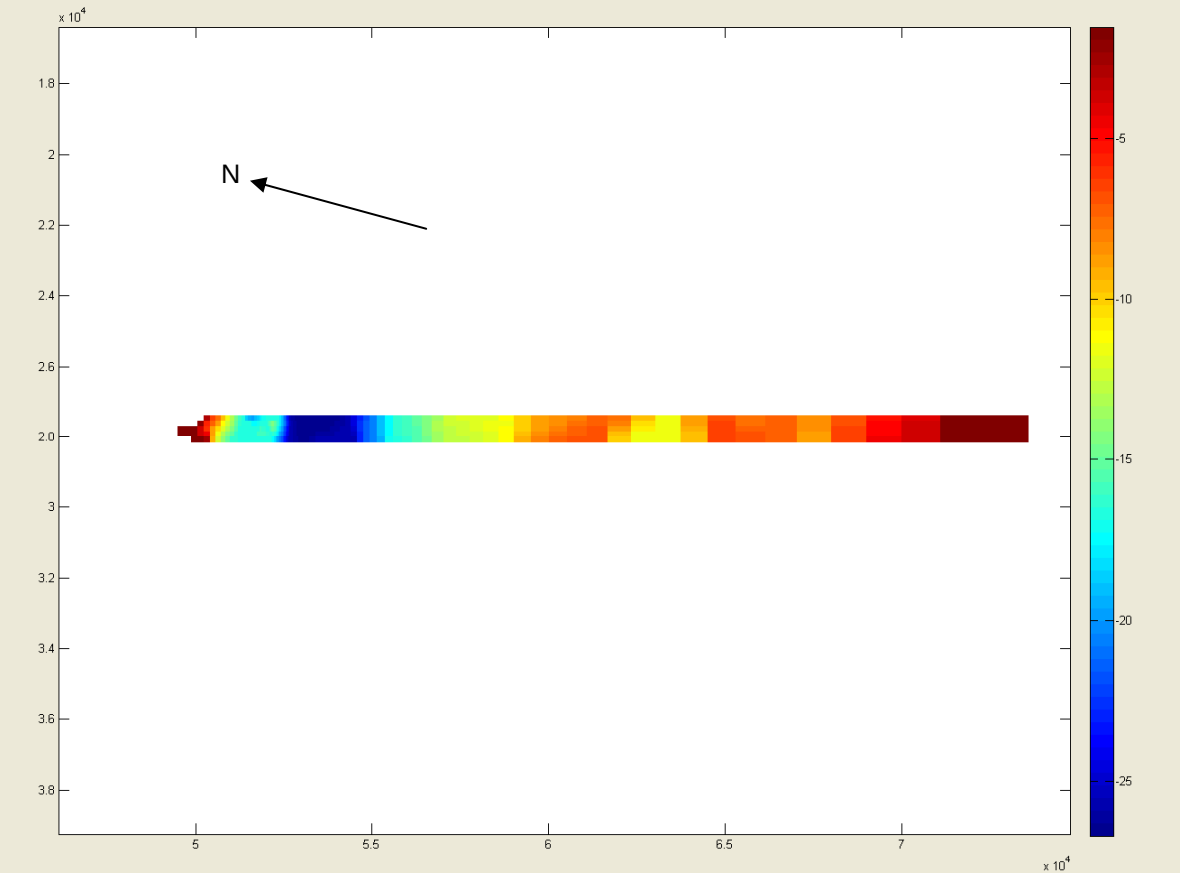

Figure 7-1 Two-Dimensional model bathymetry – plan view

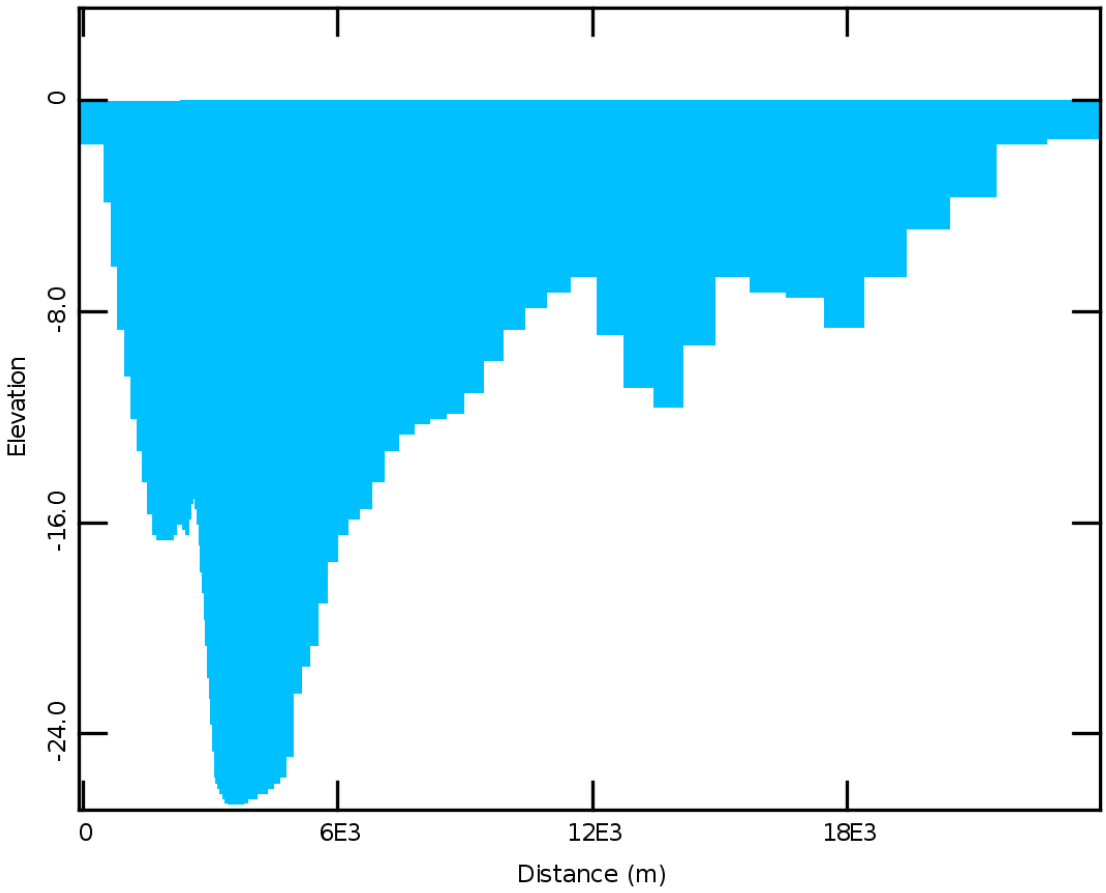

Figure 7-2 Two-Dimensional model bathymetry – profile view

The slice is five cells 'wide' (approximately 600 metres) so that any effect of the solid side walls in terms of viscous drag is minimised. The domain is approximately 20 kilometres 'long', and despite being artificially laterally constrained, the bathymetry is real within the section of the slice. The short sides (i.e. at Port Bonython and the eastern shore) are also closed and are set to land. This creates a closed box on all sides.

7.2.2 Vertical Resolution

In order to allow resolution of any upwelling processes, the previously described high resolution ELCOM model was augmented to include a vertical resolution of 20 cm at all depths throughout the domain. This was applied equally throughout the domain.

7.2.3 Timestep

To complement the above increase in vertical resolution, the timestep in this simulation was reduced from 24 to 5 seconds.

7.2.4 Longitudinal Resolution

The model resolution 'along' the box from Port Bonython to the eastern shore varies from 40 metres to several hundred metres, reflecting the overall (complete) high resolution model domain.

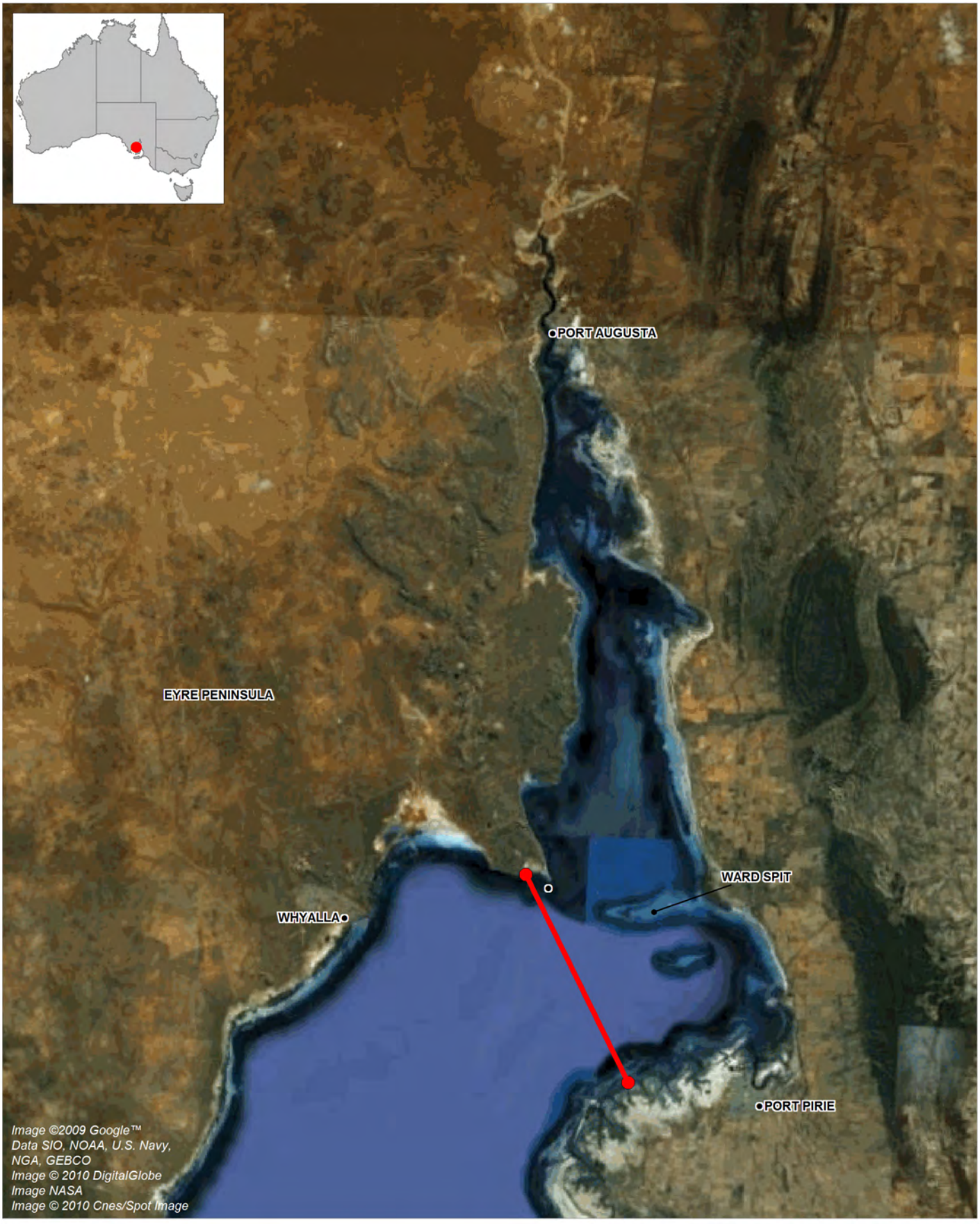

Title:

Plan Location of Two-Dimensional Model

Figure: **7-3**

Rev: **A**

BMT WBM endeavours to ensure that the information provided in this map is correct at the time of publication. BMT WBM does not warrant, guarantee or make representations regarding the currency and accuracy of information contained in this map.

N

0 10 20km

Approx. Scale

BMT WBM

www.bmtwbm.com.au

Filepath :

Initial Condition

The initial condition in salinity was set as a linear increase from ambient to a 1.52 g/kg anomaly at the bed, over the bottom 5 metres. Ambient was assumed to be 43 g/L. As such, this linear salinity field provides a maximum salinity at the bottom of 44.52 g/L, which is the result of a 20:1 dilution of 75g/L brine. Temperature was set to a uniform value of 20 C.

7.2.6 Wind Forcing

The wind direction in the ELCOM model was set to be parallel to the mode orientation in Figure 7-3, i.e. blowing along the longitudinal axis of the model. The wind speed was set to a constant at 15 m/s.

7.2.7 Tidal Forcing

The two-dimensional nature of this model precludes application of tidal flows perpendicular to the plane of the model. As such, tidal currents are effectively shut off in this simulation.

7.2.8 Simulation Period

The ELCOM model was executed for 2 days under the above forcing.

7.2.9 Results

The two figures below present the salinity colour contours of the vertical slice model overlain with velocity vectors at just after initialisation (referred to as zero hours) and 6 hours into the simulation. The top panel in each is a curtain running from Port Bonython to the eastern shore, and the panels under that in each figure are surface and bottom salinities (with velocity arrows), respectively. Salinity colour contours have been truncated at 43.4g/L (i.e. all salinities above this value appear the same colour of red) in the figures to allow visualisation of upwelling. As such, the red colour in the salt initialisation figure does represent salt at 45 g/L, despite appearing red.

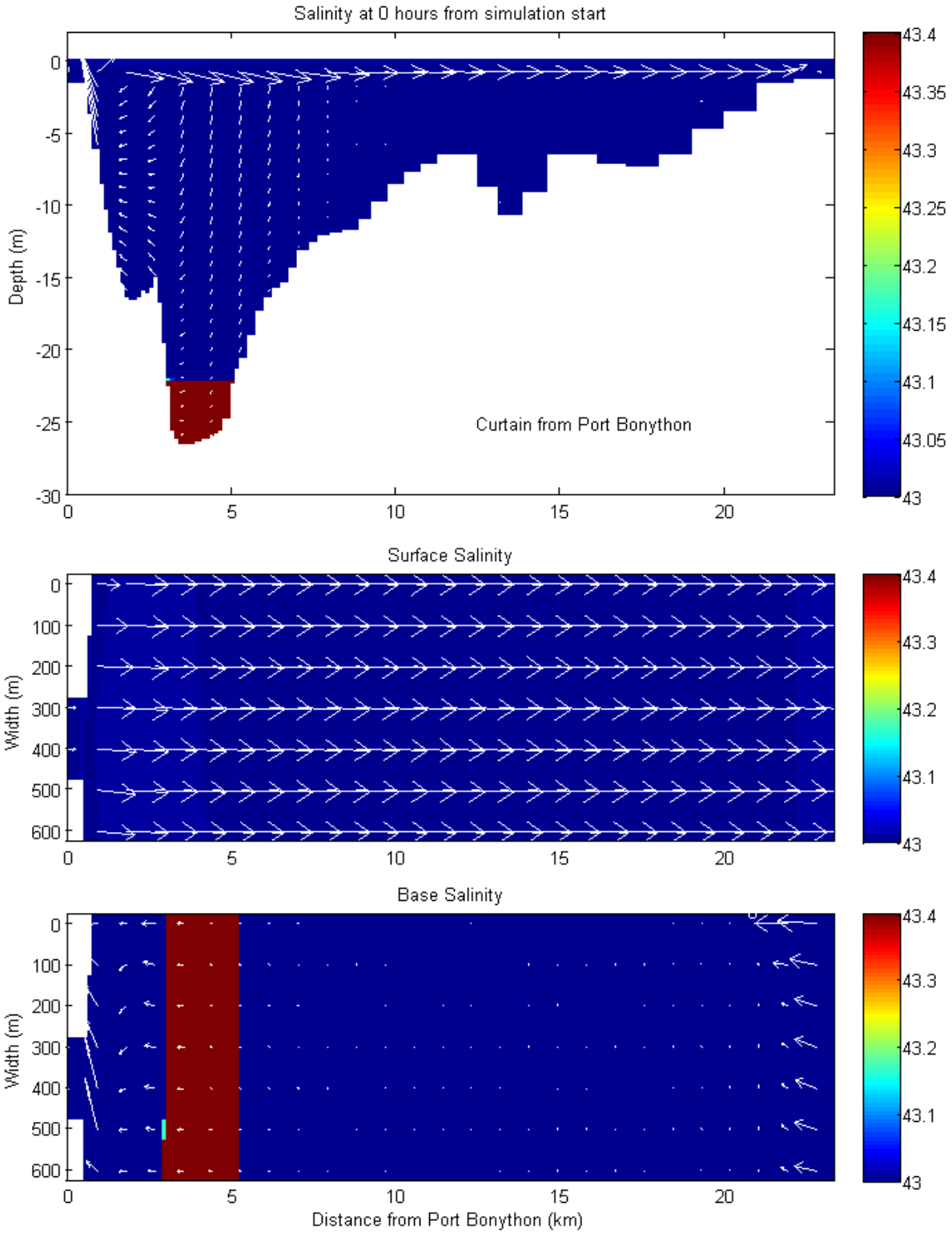

Figure 7-4 Salinity and velocities immediately following initialisation

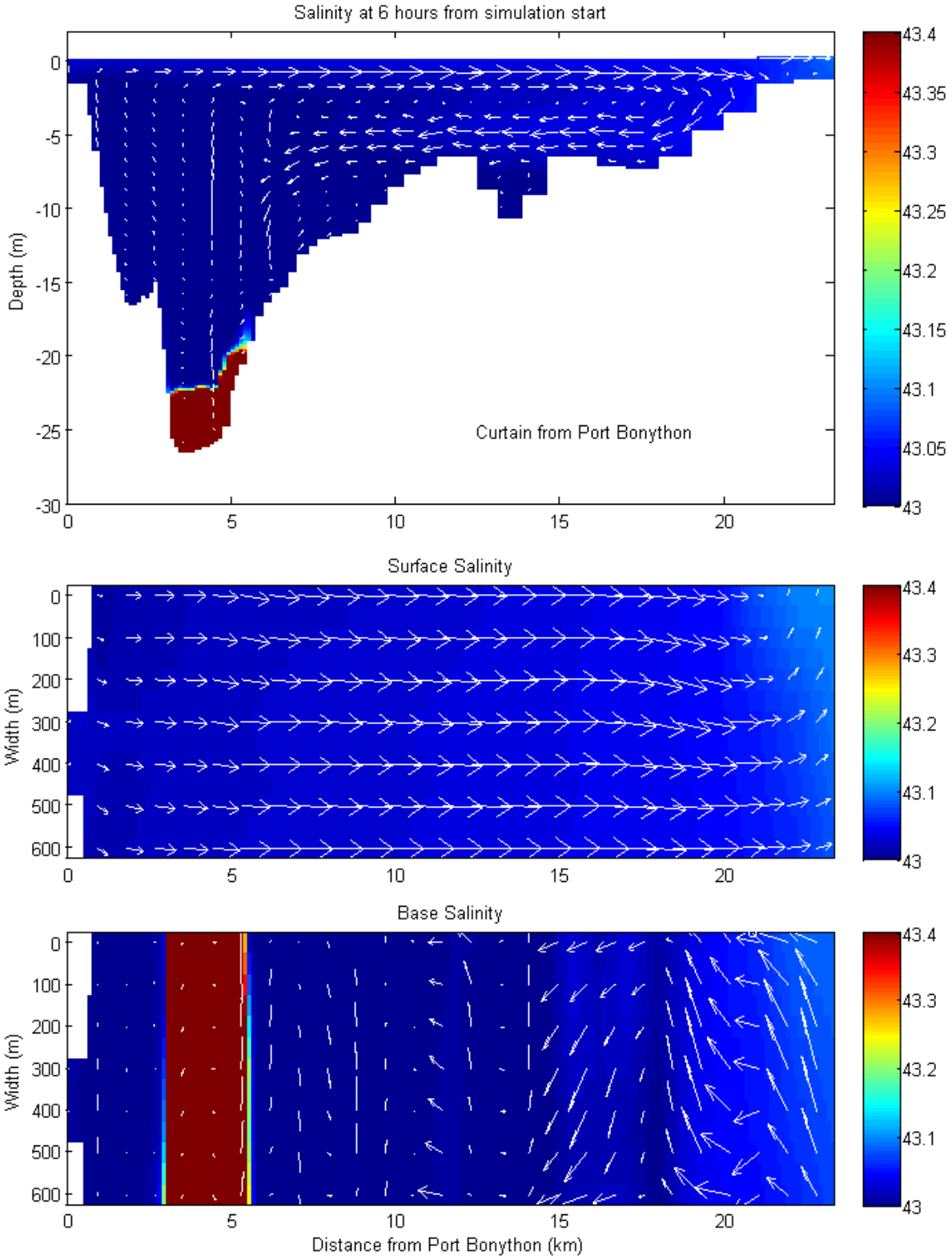

Figure 7-5 Salinity and velocities 6 hours following initialisation

The figures demonstrate that after 6 hours the two-dimensional model predicts that a significant upwelling circulation has developed, with surface and bottom waters travelling in opposite directions.

The brine pool in the model also appears to feel the influence of this circulation. Figure 7-6 presents the same data, but at 27.3 hours from initialisation.

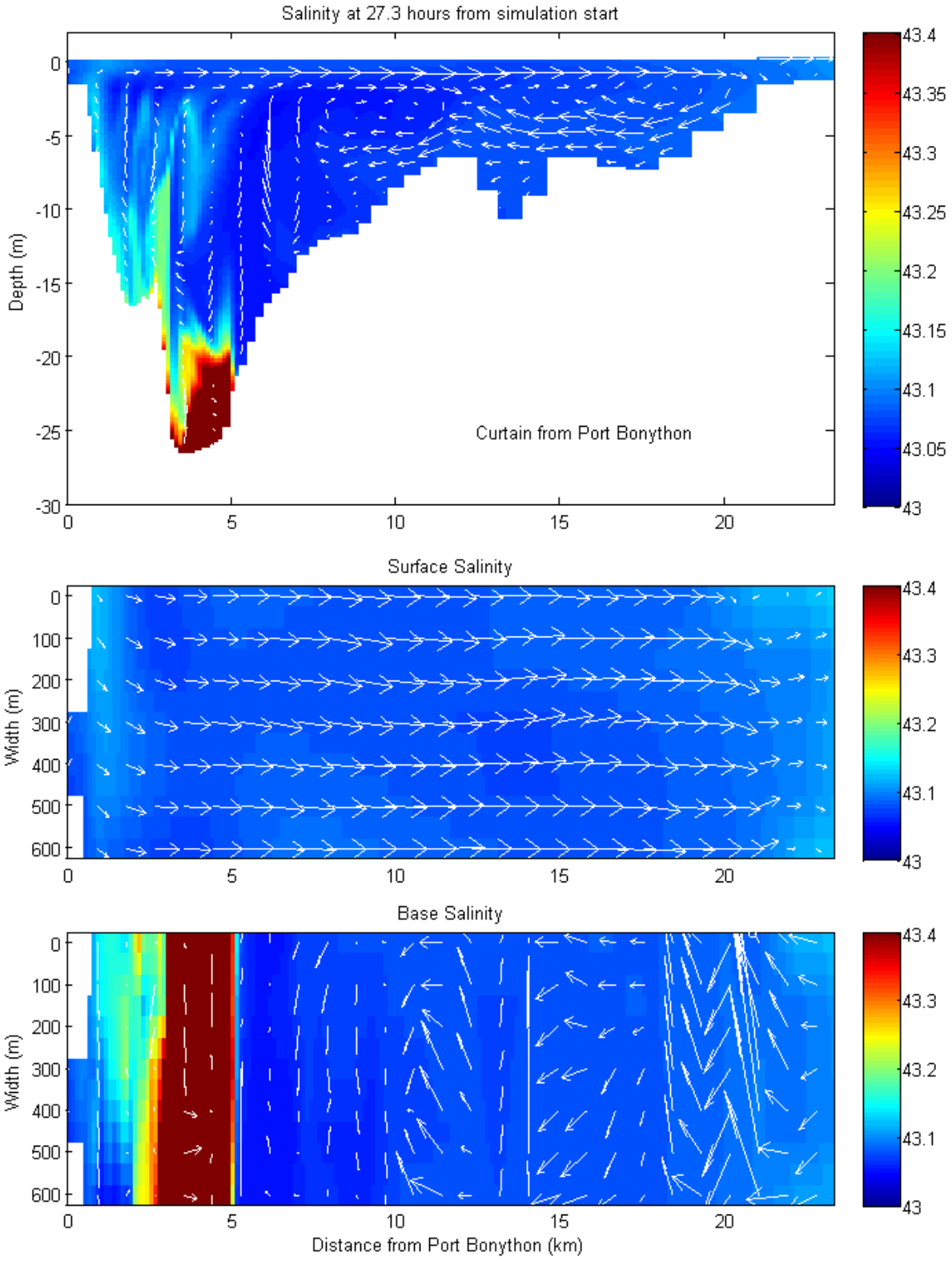

Figure 7-6 Salinity and velocities 27.3 hours following initialisation

The figure shows that the brine pool, in this simulation, has a propensity to be advected towards the shore at Port Bonython as a result of the upwelling circulation. .

Although the above figures do show upwelling to occur, it is evident that the nature of the model schematisation has caused this upwelling result, rather than the operation of a real physical process relevant to Spencer Gulf. Specifically, no other result is physically possible within this two-dimensional model framework. The underlying reason for this is the presence of the 'solid walls' along the longitudinal model boundaries: these walls militate that a parcel of surface water advected by the wind from Port Bonython has no other option on reaching the eastern shore but to travel to the bottom of the water column at that point and make a direct path back to Port Bonython along the seabed joining the ends of the two dimensional model. In short, the water parcel has no alternative but to participate in upwelling, and as such it is no surprise that the cut down two-dimensional ELCOM model predicts upwelling to occur – no other result was possible than the development of the long-established two dimensional upwelling phenomenon.

This result is consistent with, and supports, the long history of research into upwelling in essentially two dimensional systems such as lakes. Application of these research outcomes to three-dimensional domains such as Spencer Gulf does, however, require further investigation, and this is provided below.

7.3 Quasi Three-Dimensional Model

In order to better assess the likely potential for upwelling at Point Lowly (although still not being completely rigorous), the model described in Section 7.2 was rerun, but with the laterally bounding 'solid walls' removed to allow water to travel in and out (i.e. in a direction perpendicular to the page) of the domain as required. As such, the model domain, vertical and longitudinal resolution, initial condition, wind forcing, tidal forcing (i.e. switched off) and simulation duration were as described in Section 7.2, with the only difference being the relaxation of the artificial prohibition of lateral flows.

7.3.1 Results

The figure below presents the salinity colour contours of the quasi three-dimensional vertical slice model overlain with velocity vectors at 6 hours into the simulation to allow direct comparison with Figure 7-5. The panels within the figure and contouring are the same as presented above.

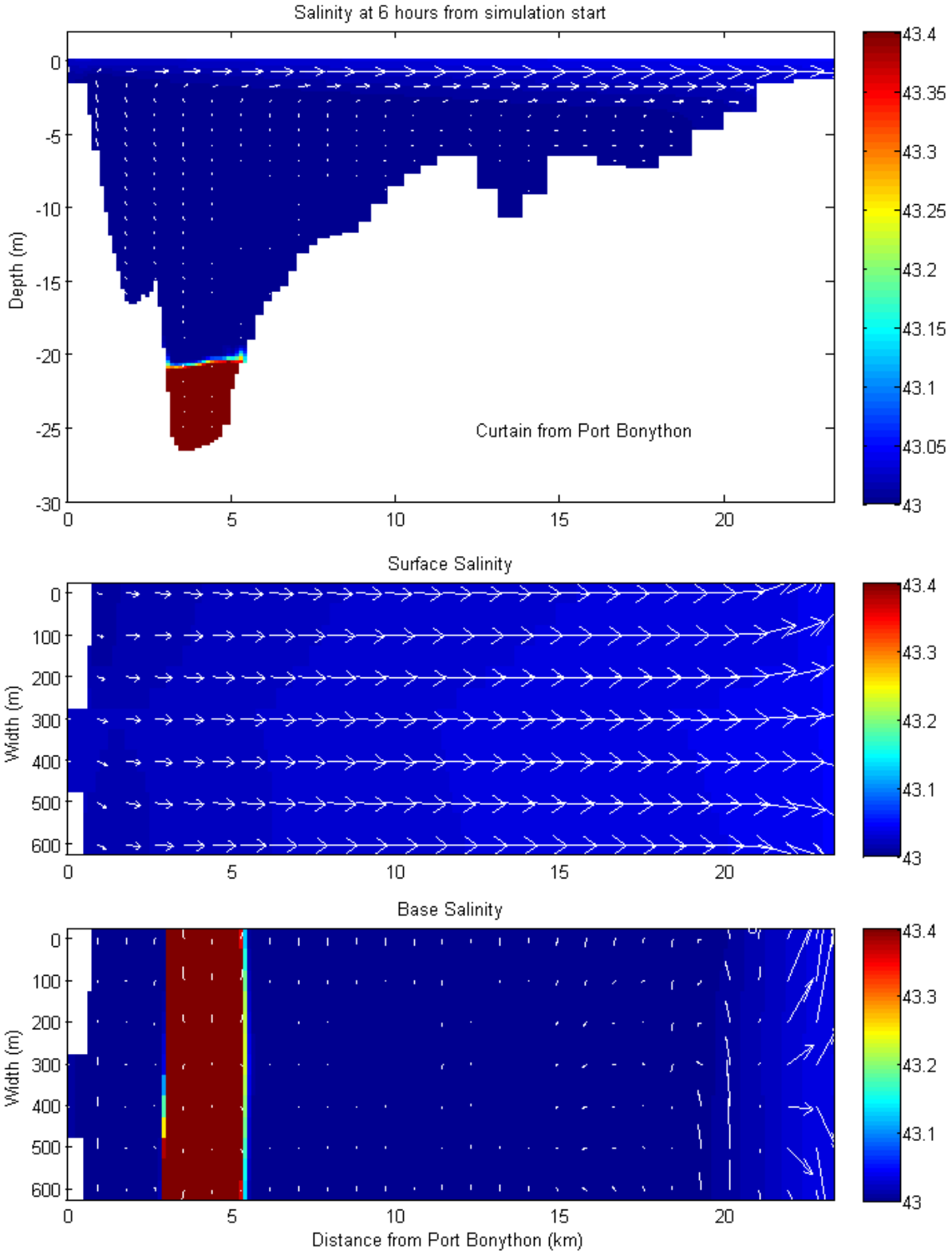

Figure 7-7 Salinity and velocities immediately following initialisation

The figure demonstrates that after 6 hours the quasi three-dimensional model predicts an absence of upwelling flows at Point Lowly. This is because, when given the opportunity, water parcels

preferentially flow laterally out of the model (at the surface and at depth) on reaching the eastern model extent. These outflows are evident in the second and third panes in Figure 7-7.

Notwithstanding that this quasi three-dimensional model is closer to reality than the first example, and shows an absence of upwelling, it is still not representative of real world conditions. These conditions would include allowing for fully three dimensional flows to occur in a well resolved domain as a result of wind and bathymetric effects, and for some degree of uniformity in the axial (out of the page) direction. The following section describes the set up and execution of such a model.

7.4 Fully Three-Dimensional Model

The high resolution model described above was used to investigate the possibility for upwelling at Point Lowly in real world (bathymetric) conditions across a suite of wind forcing regimes. The model setup and scenarios are described below.

7.4.1 Model Domain

The high resolution model domain described previously was used in these simulations.

7.4.2 Vertical Resolution

In order to reduce the influence of numerical dispersion on potential upwelling processes, the vertical resolution of the high resolution model was increased such that all layers between approximately -24 and -12 metres were 0.5 metres thick.

7.4.3 Longitudinal Resolution

The entire extents of Spencer Gulf were simulated.

7.4.4 Initial Condition

As an improvement on the previous assumptions regarding the vertical distribution of brine, this suite of simulations was set to include a representation of a brine discharge into an initially uniform salinity condition. The initial salinity was assumed to be uniformly 43 g/L, and the inflow set to a constant 44.52 g/L, corresponding to a dilution of 20:1 for a brine salinity of 75 g/L in the selected ambient conditions. It is noted that this brine concentration is near the worst case of any predictions from the DEIS (or SEIS) modelling. As such, it is conservative.

The brine discharge was allowed to enter the model for a two day period where all tides and winds were turned off, and the model interrogated over the third day when winds were turned on.

7.4.5 Wind Forcing

Three wind forcing scenarios were applied, as winds coming from the following directions:

- Westerly;
- Northerly; and
- North-Westerly.

The wind forcing for the above scenarios was set to reflect realistic wind conditions where possible, rather than have a constant velocity and direction applied. To do so, the wind records used in the high resolution model were interrogated at Point Lowly to find a period where a westerly wind reached approximately 15 m/s over one day. The period identified is shown in Figure 7-8.

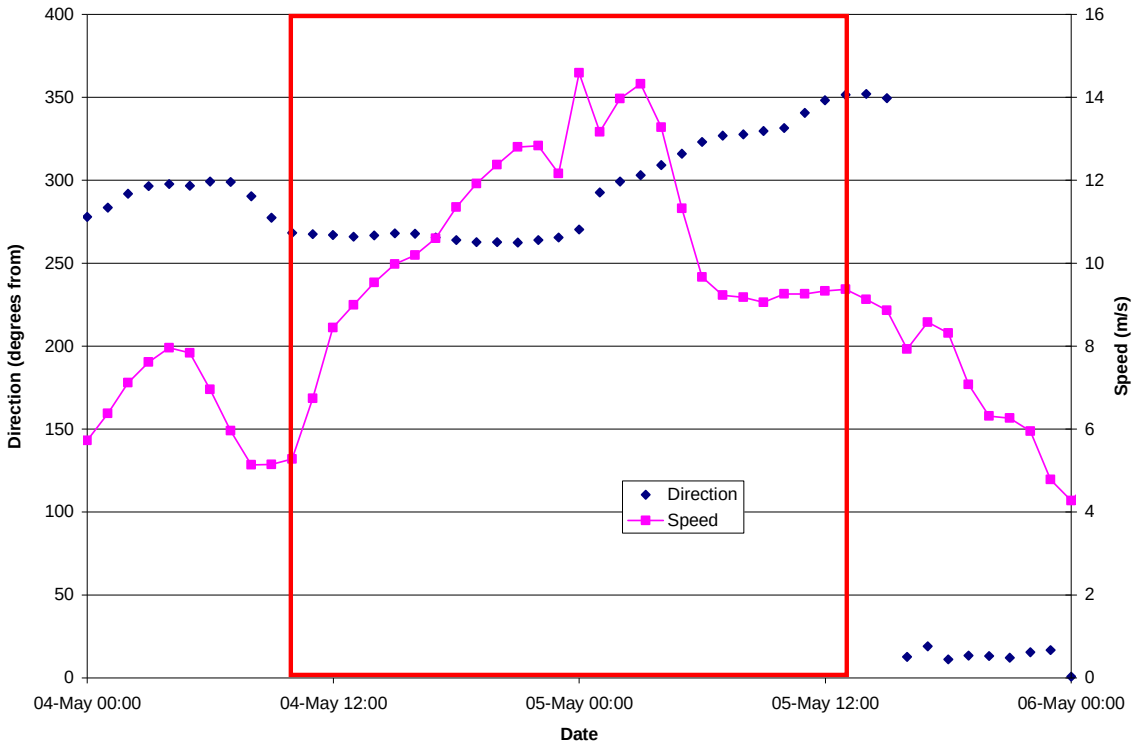

Figure 7-8 Westerly wind period (red box)

The evolution of wind speed (and direction) up to this threshold was kept as the actual records showed within the model, and not applied as a step change. The wind speeds were kept the same for the other two scenarios, with the wind directions changed manually to suit. Wind was spatially applied as s subset of the base high resolution, with three points within the domain covering this model. Specifically, the data from Point Lowly (shown above) was applied locally, and two other representative fields applied to the north and south.

7.4.6 Tidal Forcing

Water surface elevations at the boundary near Port Lincoln were set to a constant value, effectively eliminating tidal flushing from these simulations.

7.4.7 Simulation Period

Each ELCOM model was executed for a 2 day warm up period (with no tides or winds applied) to allow the brine discharge to pool. The respective wind data set was then applied for the third day.

7.4.8 Results

Each scenario's results are presented below, at times of 0, 6, 12, 18 and 24 hours into the third day. Each time presents three colour panels of dilution:

- A bottom sheet;
- A curtain running from the tip of Point Lowly (left hand side) in a south easterly direction towards Ward Spit (right hand side); and
- A zoom of the above curtain to 1500 metres offshore from Point Lowly to show the results in detail in the area of potential upwelling.

The maximum dilution presented is 85:1. Greater dilutions appear as a uniform red colour.

7.4.8.1 Westerly Wind

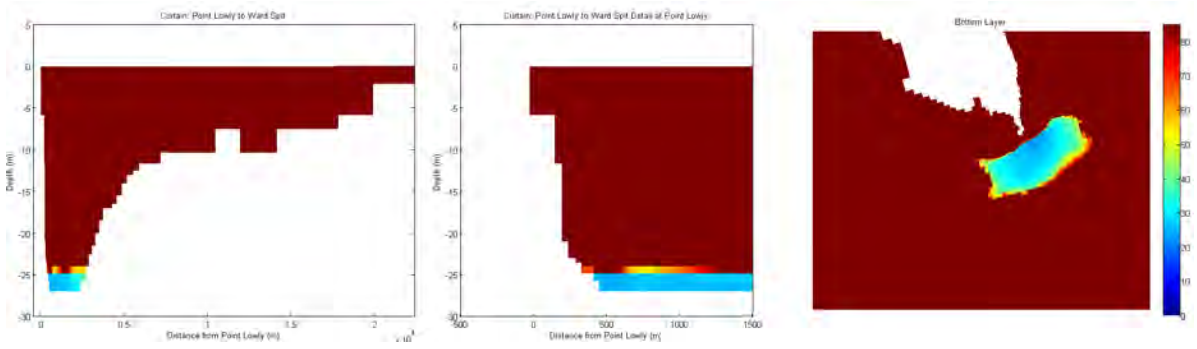

Figure 7-9 Dilution at 0 hours from wind commencement

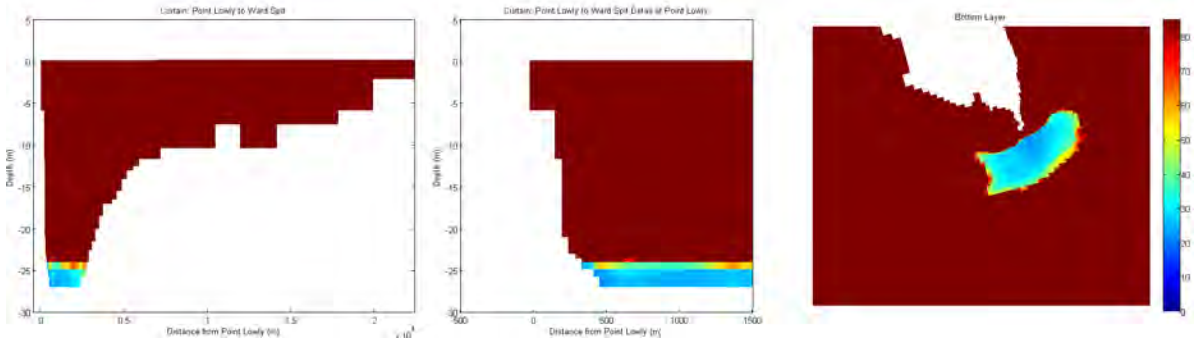

Figure 7-10 Dilution at 6 hours from wind commencement

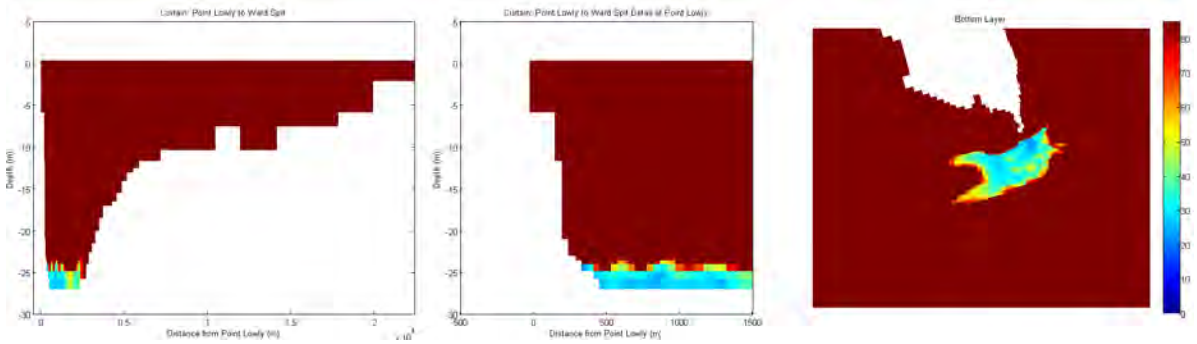

Figure 7-11 Dilution at 12 hours from wind commencement

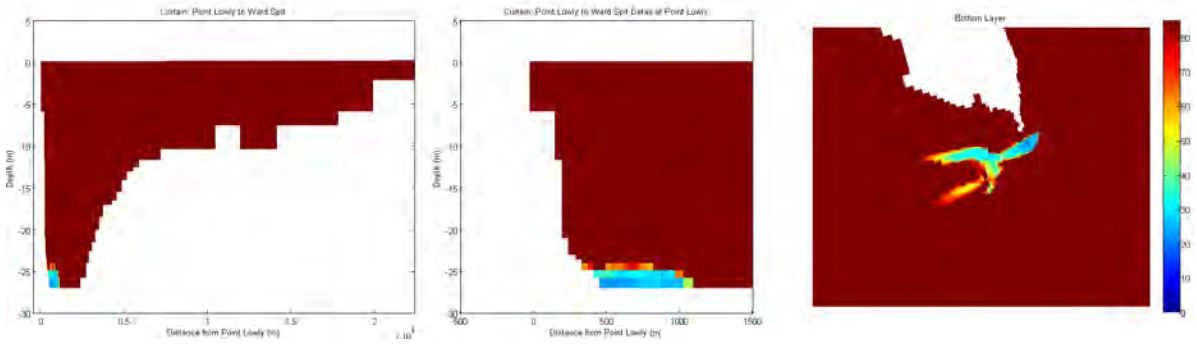

Figure 7-12 Dilution at 18 hours from wind commencement

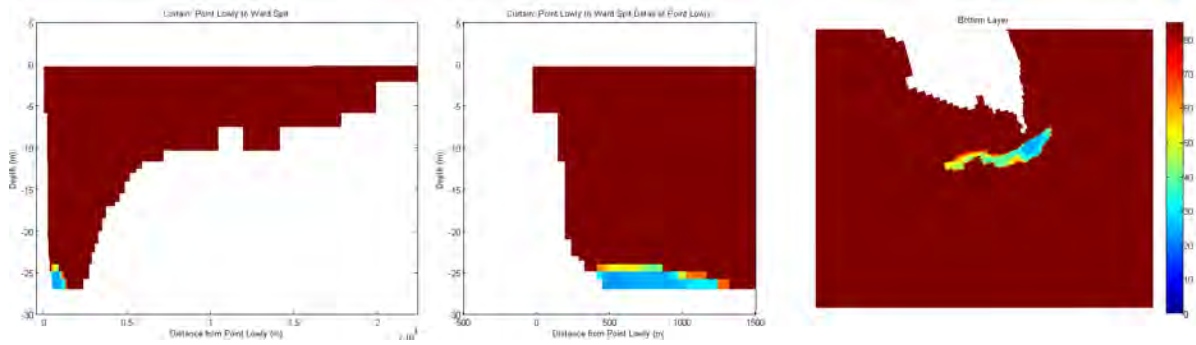

Figure 7-13 Dilution at 24 hours from wind commencement

7.4.8.2 Northerly Wind

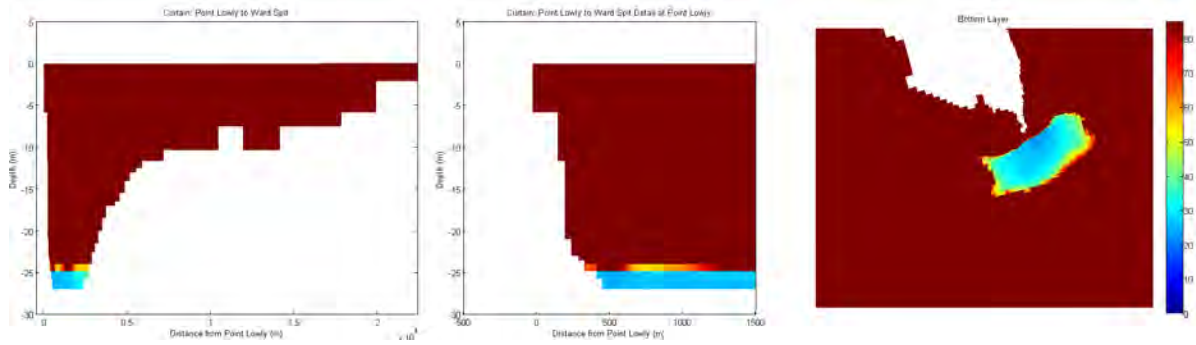

Figure 7-14 Dilution at 0 hours from wind commencement

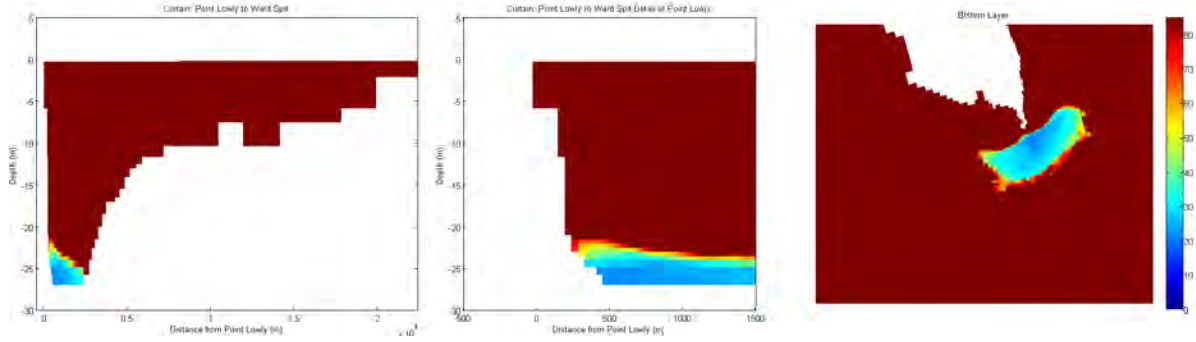

Figure 7-15 Dilution at 6 hours from wind commencement

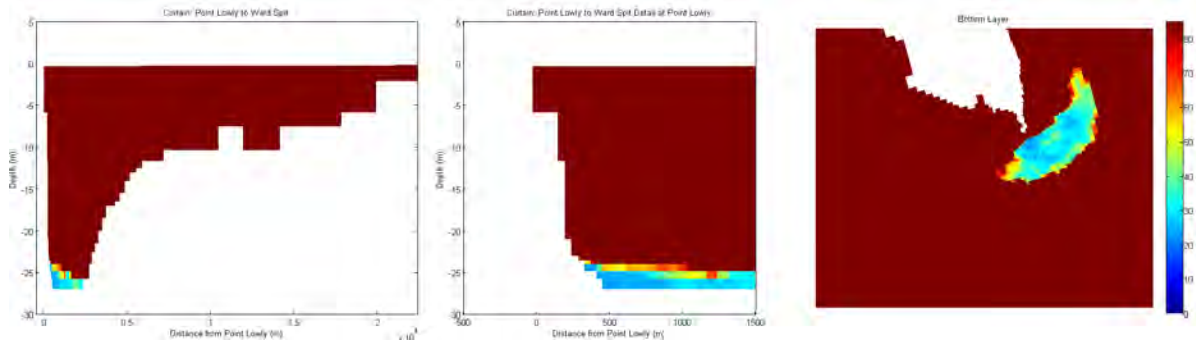

Figure 7-16 Dilution at 12 hours from wind commencement

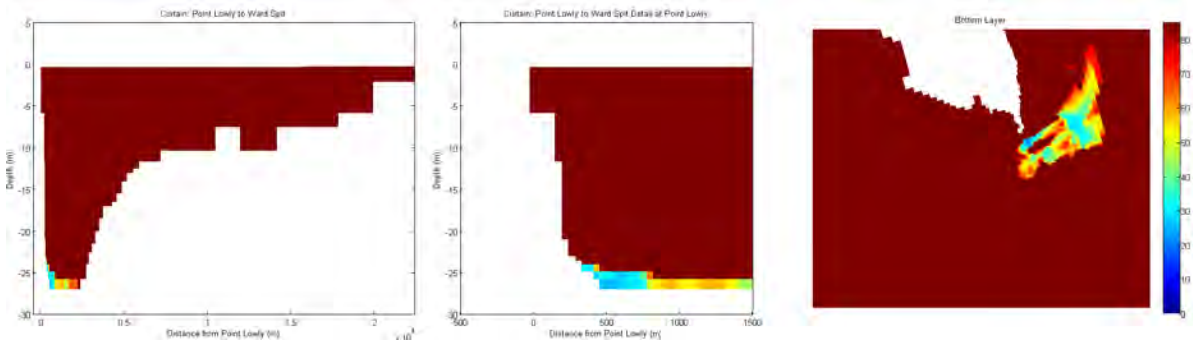

Figure 7-17 Dilution at 18 hours from wind commencement

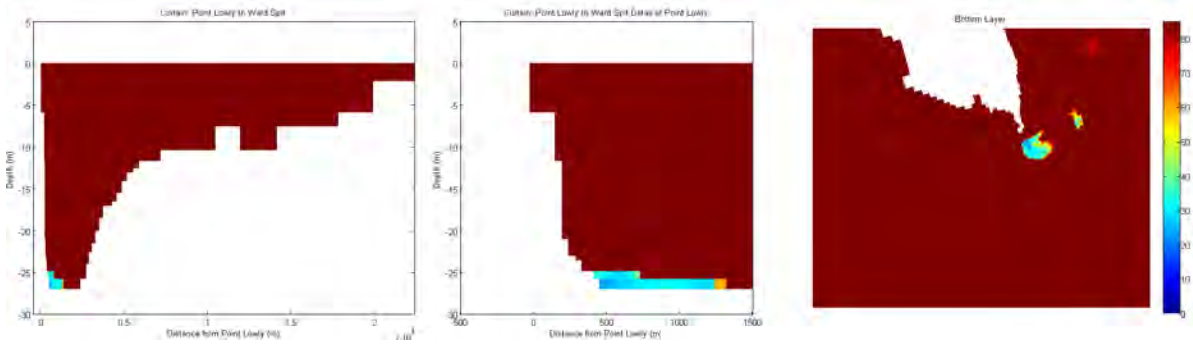

Figure 7-18 Dilution at 24 hours from wind commencement

7.4.8.3 North Westerly Wind

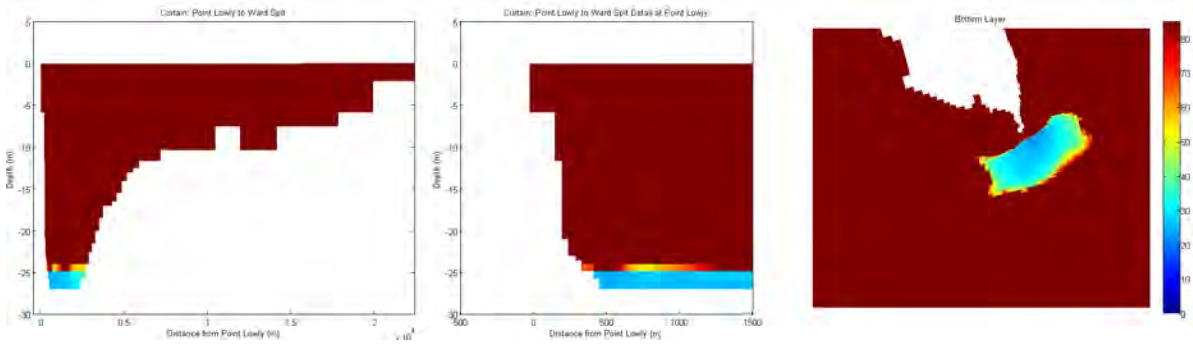

Figure 7-19 Dilution at 0 hours from wind commencement

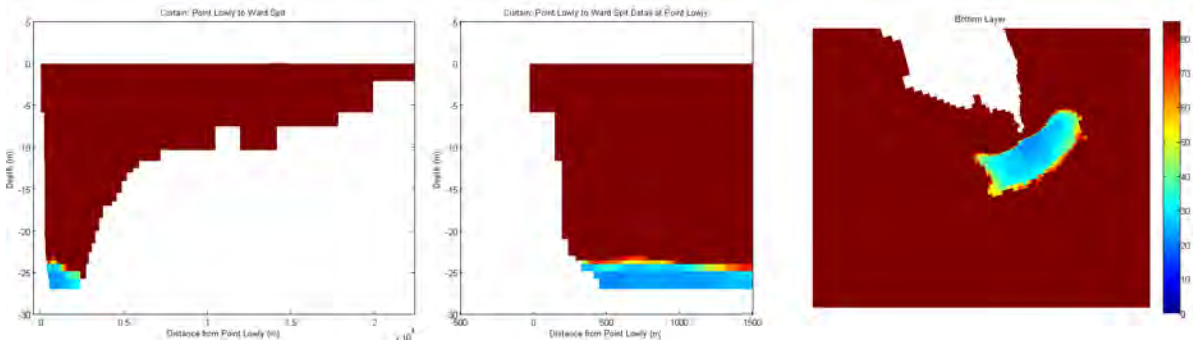

Figure 7-20 Dilution at 6 hours from wind commencement

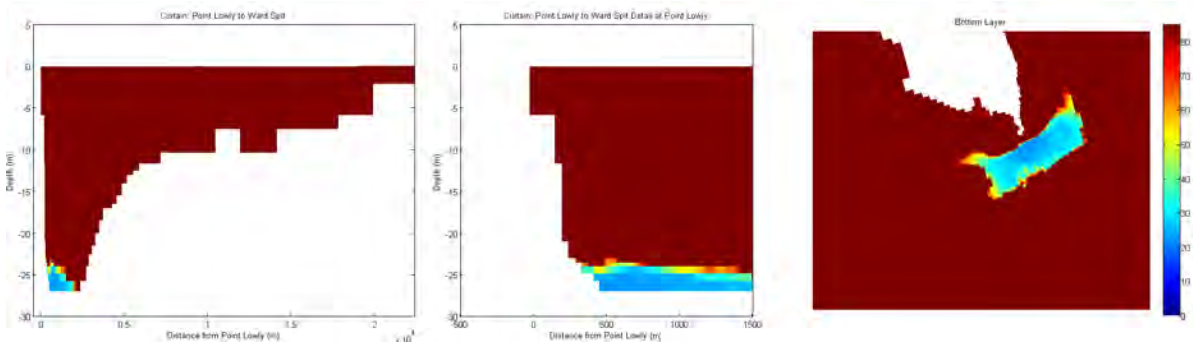

Figure 7-21 Dilution at 12 hours from wind commencement

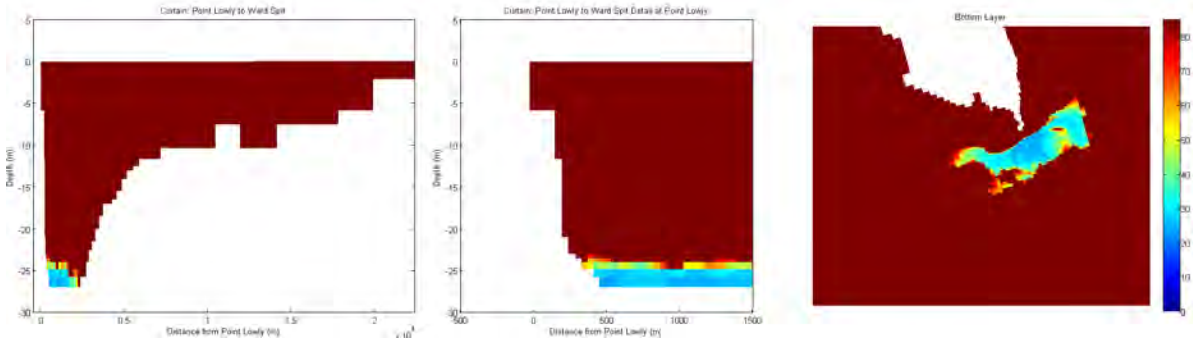

Figure 7-22 Dilution at 18 hours from wind commencement

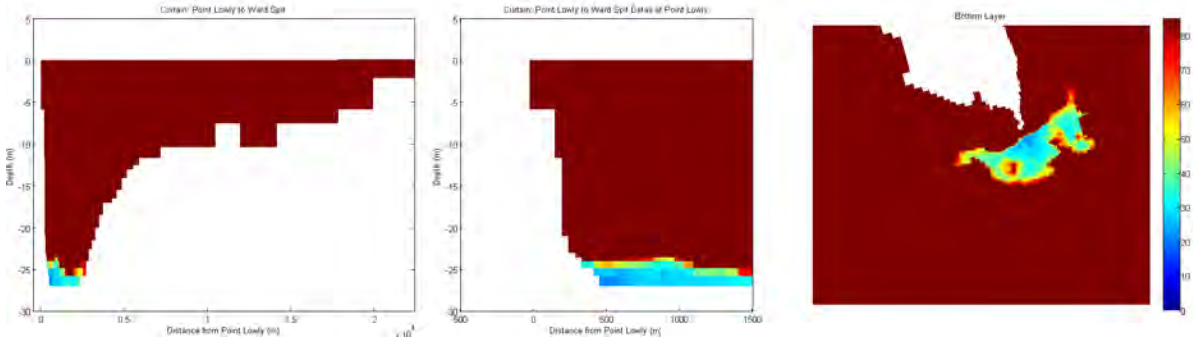

Figure 7-23 Dilution at 24 hours from wind commencement

The figures show that there is very little propensity for upwelling to occur in the fully three dimensional domain over the periods simulated. Rather than 'flowing uphill' to the shallow areas of Point Lowly as was the case in the two-dimensional model, the dense brine preferentially flows laterally away from the diffuser (at the same or similar depth to insertion) around Point Lowly to either the south (westerly wind), north (northerly wind) or both (north westerly wind) in the simulations considered here. It appears that this lateral movement is a dynamically relevant process by which brine leaves the diffuser site under the action of wind forcing, so cannot be ignored in an upwelling analysis.

On only two occasions does the brine elevate away from the bottom layer in the above simulations and in both instances the elevated brine is not bottom-attached. This implies that a process other than upwelling, such as local eddying, may be responsible for this behaviour. In any case, the dilutions characterising these vertical excursions are still greater than approximately 350:1 at 15 to 20

metres depth. No upwelling to shallow waters at biologically significant dilutions is observed under any circumstance over the simulation periods considered.

7.5 Fully Three Dimensional Model – Tides Active

In order to provide some real world context for the upwelling potential at Point Lowly, the fully three dimensional model was rerun with real tides, wind and diffuser flows. These are described below.

7.5.1 Model Domain

The high resolution model domain described previously was used in these simulations.

7.5.2 Vertical Resolution

In order to reduce the influence of numerical dispersion on potential upwelling processes, the vertical resolution of the high resolution model was increased such that all layers between approximately -24 and -12 metres were 0.5 metres thick.

7.5.3 Longitudinal Resolution

The entire extents of Spencer Gulf were simulated.

7.5.4 Initial Condition

As an improvement on the previous assumptions regarding the vertical distribution of brine, this simulation was initialised using results of the low resolution model after several years warmup. This allowed for a realistic initial salinity and temperature distribution across the depth and breadth of the domain.

The brine was introduced into the model using the same procedure described in Section 4.3.1 above, as applied to the optimised SEIS diffuser. In other words, actual dilutions predicted by the CFD modelling were used to force this model, where background salinities (to mix with the brine) were sourced from a previous (desalination plant off) simulation.

7.5.5 Simulation Period

The period simulated was one week leading up to the dodge tide in May 2008 simulated as part of the dissolved oxygen study. The brine discharge was allowed to enter the warmed up model for a one week period where all tides and winds as used in the high resolution model over 2008 were turned on, again, to simulate realistic conditions. The week period was selected as it provided a lead up to a dodge tide period, as shown previously. A one day window in the middle of the dodge tide was selected for results extraction, again to maintain consistency with previous results presentation. This day period is shown in red below.

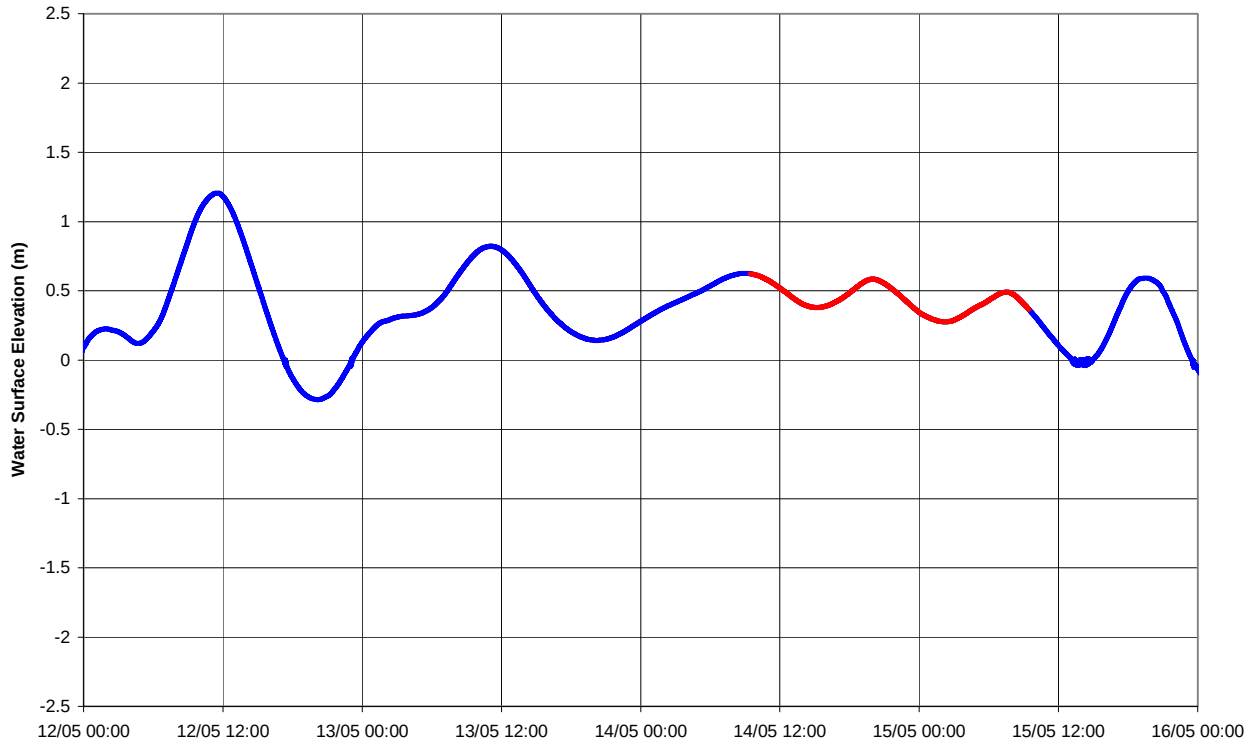

Figure 7-24 Autumn dodge tide (central day shown in red)

7.5.6 Wind Forcing

Actual wind fields for the period leading up to the dodge tide were applied to the simulation. During the one day dodge sub-period noted above, the same wind speed series shown in Figure 7-8 was applied to the model, and the wind direction (based on the results presented previously) was set to a constant north westerly direction.

7.5.7 Tidal Forcing

Water surface elevations at the boundary near Port Lincoln were set to be actual values for the week and dodge tide period identified in May 2008.

7.5.8 Results

Results are presented below in the same format as previously, namely at times of 0, 6, 12, 18 and 24 hours into the nominated dodge day. Each time presents three colour panels of dilution:

- A curtain running from the tip of Point Lowly (left hand side) in a south easterly direction towards Ward Spit (right hand side). This is not necessarily on the proposed diffuser alignment, but has been located to be coincident with areas of interest;
- A zoom of the above curtain to 1500 metre offshore from Point Lowly to show the results in detail in the area of potential upwelling; and
- A bottom sheet.

To illustrate the results of this real world simulation, dilutions were contoured to have the least restrictive ecologically relevant dilution (85:1) as the maximum.

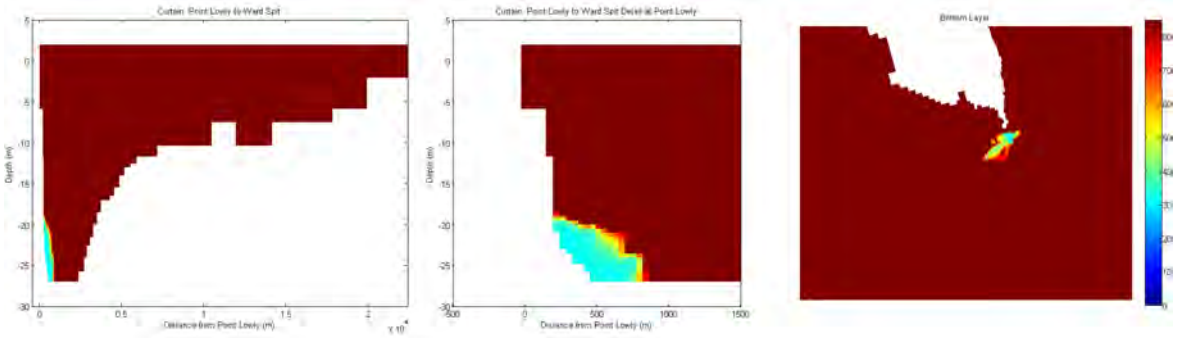

Figure 7-25 Dilution at 0 hours from wind commencement

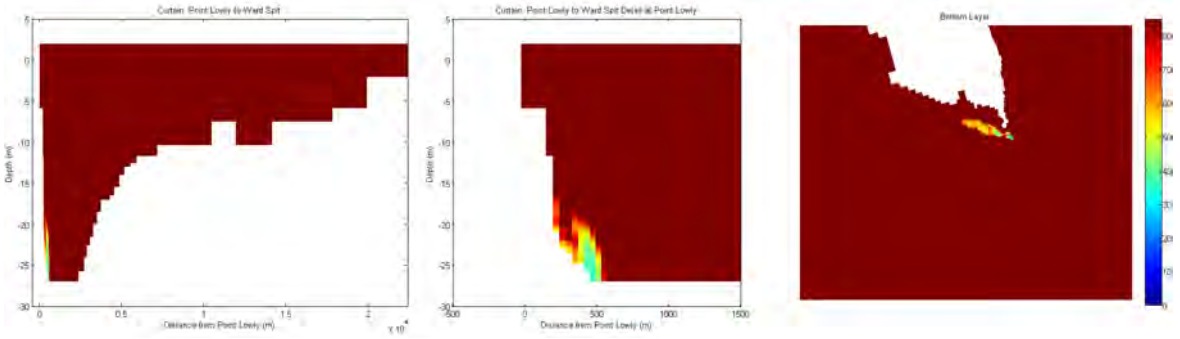

Figure 7-26 Dilution at 6 hours from wind commencement

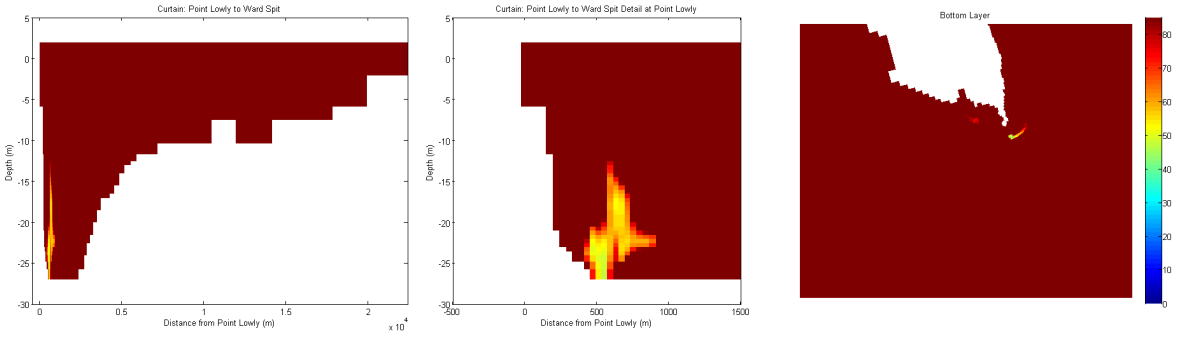

Figure 7-27 Dilution at 12 hours from wind commencement

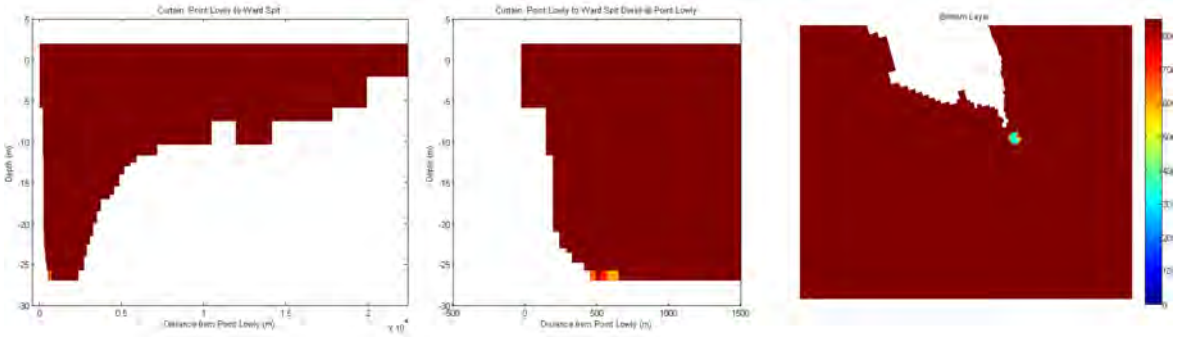

Figure 7-28 Dilution at 18 hours from wind commencement

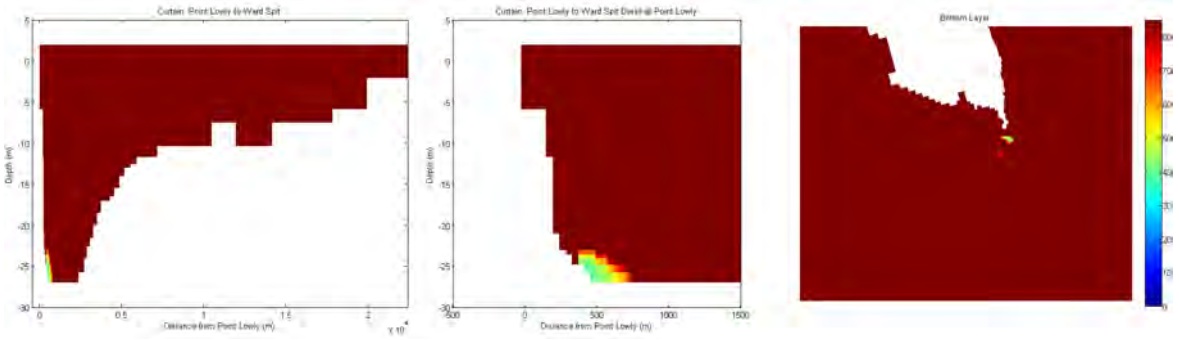

Figure 7-29 Dilution at 24 hours from wind commencement

The figures again show little propensity for upwelling to occur to an extent that ecologically relevant dilutions approach areas of interest. It is noted that the initial (0 hour) curtain plot does not necessarily indicate the presence of upwelling as the north westerly wind has not commenced at that time. In addition, the figures show that the initial brine pool for upwelling is significantly smaller in lateral and vertical extents as compared to the previous simulations where brine was injected into the model without tides for the two day period. This result suggests, as expected, that tides play a large role in diluting and evacuating the brine pool from Point Lowly, even during the lead up to, and commencement of the dodge tide simulated here.

8 REFERENCES

Cardno Lawson Treloar (2008) *Near Field Dilution and Outfall Hydraulics Investigations – Adelaide Desalination Plant*. Report Prepared for Connell Wagner, 31 October 2008, LJ2738/R2479.

CSIRO (2007). *Climate change in Australia – technical report 2007.* Australian Government - Department of Climate Change.

BHP Billiton (2009). *Olympic Dam Expansion – Draft Environmental Impact Statement 2009.*

Clelia L. Marti, Jason P. Antenucci, David Luketina, Patricia Okely, and Jörg Imberger *Near Field Dilution Characteristics of a Negatively Buoyant Hypersaline Jet Generated by a Desalination Plant.* Journal of Hydraulic engineering, in press 2010.

DSE (2008) *Victorian Desalination Project Environment Effects Statements, Volume 2.*

IPCC (2007) *General guidelines on the use of scenario data for climate impact and adaptation assessment.* Available from http://www.ipcc-data.org/guidelines/index.html

Johnson, J.E. (1981) *Fisheries Research Paper Number 3, Hydrological data for Upper Spencer Gulf 1975 – 1978*. Department of Fisheries, South Australia, October 1981.

Jones, P.D., M. New, and D.E. Parker (1999) Surface air temperatures and its changes over the past 150 years. *Reviews of Geophysics*, **37**(2), 173-199.

Lauer, P.R. (2005) *Benthic metabolism adjacent to southern bluefin tuna (Thunnus maccoyil) pontoons in South Australia*. PhD Thesis, School of Biological Sciences, Faculty of Science and Engineering, Flinders University of South Australia.

Nunes, R.A. (1985) *Catalogue of data from a systematic programme of oceanographic measurements in Northern Spencer Gulf from 1982 to 1985.* Cruise Report No. 9. School of Earth Sciences, Flinders University of South Australia.

Nunes-Vaz, R.A., G.W. Lennon, and D.G. Bowers (1990) Physical behaviour of a large, negative or inverse estuary. *Cont. Shelf Res.,* **10**(3): 277-304.

Okely, P., P.S. Yeates, J.P. Antenucci, J. Imberger and M.R. Hipsey (2006) *Modelling of the impact of the Perth seawater desalination plant discharge on dissolved oxygen in Cockburn Sound.* Centre for Water Research document WP2136PO.

Okely, P., J.P. Antenucci, P.S. Yeates, C.L. Marti and J. Imberger (2007a) *Summary of investigations into the impact of the Perth seawater desalination plant discharge on Cockburn Sound.* Centre for Water Research document WP2160PO.

Okely, P., J.P. Antenucci, J. Imberger and C.L. Marti (2007b) *Field investigations into the impact of the Perth seawater desalination plant discharge on Cockburn Sound*., Centre for Water Research document WP2150PO.

Hipsey, M.R., J.P. Antenucci, and D. Hamilton (2009) *Computational Aquatic Ecosystem Dynamics Model: CAEDYM v3. v3.2 Science Manual (DRAFT)*.

Riley, J.P. and Skirrow, G. (1974) *Chemical Oceanography*. Academic Press, London.

Roberts, P. J. W., and Toms, G. (1987). "Inclined dense jets in a flowing current." J. Hydr. Engrg., ASCE, 113(3), 323-341.

Roberts, P. J. W., et.al. (1997). "Mixing in inclined dense jets." J. Hydr. Engrg., ASCE, 123(8), 693-699.

Roberts Phillip J.W., Ferrier Adrian and Daviero Greg(1997) *Mixing in Inclined Dense Jets*. Journal of Hydraulic Engineering, August 1997 pp95-108.

SA Water (2008) *Proposed Adelaide Desalination Plant Environmental Impact Statement*, *Chapter 7*.

SA Water (2009) *Proposed Adelaide Desalination Plant – Environmental Impact Statement. Response Document January 2009.*

Steffen (2009) *Climate change 2009 faster change & more serious risks.* Australian Government - Department of Climate Change.

Suppiah et al. (2006) *Climate change under enhanced greenhouse conditions in South Australia*. South Australian Government.

Swinbank, W C (1963) Longwave radiation from clear skies. *Quarterly Journal of Royal Meteorological Society.* 89: 339-348.

Wanninkhof, R. (1992). *Relationship between windspeed and gas exchange over the ocean.* J. Geophys. Res. (Oceans) **97(C5),** pp. 7373-7382.

BMT WBM Brisbane
Level 11, 490 Upper Edward Street Brisbane 4000
PO Box 203 Spring Hill QLD 4004
Tel +61 7 3831 6744 Fax +61 7 3832 3627
Email wbm@wbmpl.com.au
Web www.wbmpl.com.au

BMT WBM Denver
14 Inverness Drive East, #B132
Englewood Denver Colorado 80112 USA
Tel +1 303 792 9814 Fax +1 303 792 9742
Email wbmdenver@wbmpl.com.au
Web www.wbmpl.com.au

BMT WBM Mackay
Suite 1, 138 Wood Street Mackay 4740
PO Box 4447 Mackay QLD 4740
Tel +61 7 4953 5144 Fax +61 7 4953 5132
Email wbmmackay@wbmpl.com.au
Web www.wbmpl.com.au

BMT WBM Melbourne
Level 5, 99 King Street Melbourne 3000
PO Box 604 Collins Street West VIC 8007
Tel +61 3 8620 6100 Fax +61 3 8620 6105
Email wbmmelbourne@wbmpl.com.au
Web www.wbmpl.com.au

BMT WBM Newcastle
126 Belford Street Broadmeadow 2292
PO Box 266 Broadmeadow NSW 2292
Tel +61 2 4940 8882 Fax +61 2 4940 8887
Email wbmnewcastle@wbmpl.com.au
Web www.wbmpl.com.au

BMT WBM Perth
1 Brodie Hall Drive Technology Park Bentley 6102
Tel +61 8 9328 2029 Fax +61 8 9486 7588
Email wbmperth@wbmpl.com.au
Web www.wbmpl.com.au

BMT WBM Sydney
Level 1, 256-258 Norton Street Leichhardt 2040
PO Box 194 Leichhardt NSW 2040
Tel +61 2 9713 4836 Fax +61 2 9713 4890
Email wbmsydney@wbmpl.com.au
Web www.wbmpl.com.au

BMT WBM Vancouver
1190 Melville Street #700 Vancouver
British Columbia V6E 3W1 Canada
Tel +1 604 683 5777 Fax +1 604 608 3232
Email wbmvancouver@wbmpl.com.au
Web www.wbmpl.com.au